Study of structural, mechanical, elctronic and optical properties of different Heusler compounds

Roll: MS191303
Session: 2019-2020

Report submitted to the Department of Physics at
Jashore University of Science and Technology
in partial fulfillment of the requirements
for the degree of Masters of Science in Physics

March 2023

Abstract

The structural, electronic, elastic, magnetic and optical properties of transition metal-based full Heusler compounds Cu_2TiSi, Cu_2ZrGe, Ru_2TiSi, Ru_2VSi, Rh_2TiSi and Rh_2VSi have been investigated by utilizing self-consistent full potential linearized augmented plane wave (FP-LAPW) method within density functional theory. The calculation has been performed in WEIN2k by Perdew-Burke-Ernzerhof-generalized gradient approximations (PBE-GGA). We get the stable structure for ferromagnetic minimum energy calculations of these compounds. The symmetric behavior in the DOS at the Fermi level of both spin channels shows Cu_2TiSi and Cu_2ZrGe true metallic nature. Also, the direct band gap and zero value of the indirect band gap of Ru_2TiSi with minimum DOS in both spin channels at the fermi level indicate the antiferromagnetic behavior. Ru_2TiSi alloys can be used as future material for optoelectronics. In the band structure of Ru_2VSi, there has been band overlapping across the fermi level in the majority spin channel denotes metallic nature and direct band gap at the gamma point in the down spin channel denotes the semicondutor behaviour but it is not true half metal. The Rh_2TiSi, Rh_2VSi system has paramagnetic and ferromagnetic properties respectively from their density of states which shows metallic nature. As low magnetic moments of all compounds that do not obey the Slater-Pauling rule. However, the bulk modulus (B), Young's modulus (E), the shear modulus (G) and Poisson's ratio (v) have been obtained. The optical parameters that are complex dielectric tensor, refractive index, extinction coefficient, reflectivity, absorption coefficient, Electron energy loss and optical conductivity has been calculated.

Acknowledgements

Especially all my qualitative excellence of potential over this work is smooth by the grace of almighty Allah, the Lord of the worlds, the Most Merciful, the Guider of hearts, the Provider of sustenance, the Owner of life and death.

The work has been done under the supervision of my supervisor Dr. Mohammad Abdur Rashid. This work can not be accomplished exactly without his help. I am very thankful to him for his immense support regarding this work. Especially I am grateful to the author of many publications, books who indirectly help me to complete this work with accuracy.

I am also grateful to different scientific journals from where I have got answers of my question about this work. I have learned many things related to this work. My appreciation goes to all faculty members of the department of physics who inspire me to go forward in physics.

Contents

Study of structural, mechanical, elctronic and optical properties of different Heusler compounds

List of Figures

LIST OF FIGURES

List of Tables

Study of structural, mechanical, elctronic and optical properties of different Heusler compounds

Chapter 1

Introduction

Heusler alloys are important for magnetic data storage in our modern science. It has also the utilization in various fields like absorption, electricity production, energy storage and, in optoelectronics. We calculate properties for some metallic system, which exhibits the metallic behavior in the density of states and the band structure of these compounds. The antiferromagnetic semiconductor and half-metal have indicated extensive attention in spintronics [1, 2]. Half-metallicity was first inferred by de Groot and collaborators in a half-Heusler alloy in 1983 [3]. However, Heusler alloys are divided into two main categories; the full heusler which has stoichiometric formula X_2YZ and the half-heusler [4] that stoichiometric formula XYZ alloys, where X and Y are transitional metals and Z is group III, IV and, V element [5]. The full Heusler X_2YZ alloys with FCC lattices are characterized as the positions X_1(1/4, 1/4, 1/4), X_2(3/4, 3/4, 3/4), Y(1/2, 1/2, 1/2) and Z(0, 0, 0). These configurations mainly are affected by valence electrons of X and Y atoms [6–8]. Full-Heuslor alloys are of two types of structure. The first of these is the Hg_2CuTi structure is X_2YZ which forms when the nuclear charge of X is lesser than Y and the second is the Cu_2MnAl structure which forms under the condition when the nuclear charge of Y is less than of X [9]. The Hg_2CuTi structure which has the space group (216, $F4\bar{3}m$) and Cu_2MnAl structure which has the space group (225, $Fm\bar{3}m$). The

Cu_2TiSi and Cu_2ZrGe compounds have a greater impact from the theoretical point of view. Concerning to their applications; they are less affected by external fields due to their low magnetic moment. Thus, they do not generate annoying strong magnetic field much. In the present work, we explore the structural, elastic, electronic, magnetic and optical properties of Copper, Ruthenium and Rhodium base heusler alloys. Semiconductors which are too fragile and weak for structural applications are repeatedly used in computers and other electronic devices and ceramics, polymers and batteries. The application is just about everything computerized, for instance, phones, computers, printers, gaming devices calculators and semiconductor integrated circuits [10]. Although half-Heusler alloys like XYZ structure have attracted a lot of interest. The second family of Heusler compounds, the so-called full-Heusler alloys have been studied much more extensively due to the existence of diverse magnetic phenomena, [11]. In this paper, the electronic structures and the Cu_2MnAl type space group (225, $Fm\bar{3}m$) of Cu_2TiSi, Cu_2ZrGe, Rh_2TiSi, Rh_2VSi are metallic nature and semiconductor properties of Ru_2TiSi as well as down spin channel of Ru_2VSi is studied via the first principles method, based on the fact that the number of 3d valence electrons in the Rh, Ru, Cu atoms is higher than that in the Ti, V, Zr atoms [12–17]. The basic thing of these electronic devices is to inject the spin-polarized electrical current into semiconductors [18] in spintronics.

There are varieties of full heusler alloys for their unique characteristics under spin injection to the antiferromagnetic semiconductor and non-magnetic materials for using it in Hard disk drive read head and producing spin-polarised electrons in antiferromagnetic materials in spintronics. Usually, in this thesis, there is a try to search for those type of material that helps us to produce materials that can store a vast amount of electrical data. Antiferromagnetic Heusler alloys are fully compatible with other ferromagnetic and non-magnetic Heusler alloys, with small lattice mess up, large conduction band overlap, and similar interfacial properties. Therefore, antiferromagnetic Heusler compounds are perfect for a wide range of applications, such as antiferromagnetic spintronics devices. The metallic compound is suitable for producing energy storage such as parallel plate capacitors and it is very useful for optoelectronics. When it is necessary for self-polarization by the

electromagnetic wave then these metallic alloys are used. Heusler alloys have high ductile and strength than Iron or from some single elements; it should be made for bringing high mechanical strength within the metal alloys even individually they were less strength. It is used where it needs high tensile stress. This material can be used for future energy storage and speedy transmission of data in spintronics. To predict good reflectors and pefect strengths in metal alloys.

This thesis has arranged in a way that Basic Quantum Mechanics is in chapter 2, Density functional theory is in chapter 3 and Computational details is in chapter 4. The result has been given in chapter 5 for copper-based system and finally chapter 6 and 7 have arranged with the result of Ruthenium and Rhodium-based heusler compound respectively. Finally conclusion has given in chapter 8.

Chapter 2

Basic Quantum Mechanics

2.1 Schrödingers groundbreaking equation

Erwin Schrödinger's attempt to describe the so-called 'matter waves' in 1926, where he used de Broglie's relations to describe hypothetical plane waves, led to the most general form of the famous equation named after him, the time-dependent Schrödinger equation [19]

$$i\hbar\frac{\partial}{\partial t}\Psi(\vec{r},t) = \hat{H}\Psi(\vec{r},t) \tag{2.1}$$

It is often impracticable to use a complete relativistic formulation of the formula; therefore Schrödinger himself postulated a non-relativistic approximation which is nowadays often used, especially in quantum chemistry.

Using the Hamiltonian for a single particle

$$\hat{H} = \hat{T} + \hat{V} = -\frac{\hbar^2}{2m}\vec{\nabla}^2 + V(\vec{r},t) \tag{2.2}$$

leads to the (non-relativistic) time-dependent single-particle Schrödinger equation

$$i\hbar\frac{\partial}{\partial t}\Psi(\vec{r},t) = \left[-\frac{\hbar^2}{2m}\vec{\nabla}^2 + V(\vec{r},t)\right]\Psi(\vec{r},t). \tag{2.3}$$

In this thesis, from now on only non-relativistic cases are considered.

For N particles in three dimensions, the Hamiltonian is

$$\begin{aligned}\hat{H} = \sum_{i=1}^{N}\frac{\hat{p}_i^2}{2m_i} + V\left(\vec{r}_1,\vec{r}_2,\ldots,\vec{r}_N,t\right) = \\ -\frac{\hbar^2}{2}\sum_{i=1}^{N}\frac{1}{m_i}\nabla_i^2 + V\left(\vec{r}_1,\vec{r}_2,\ldots,\vec{r}_N,t\right).\end{aligned} \tag{2.4}$$

The corresponding Schrödinger equation reads

$$\begin{aligned}i\hbar\frac{\partial}{\partial t}\Psi\left(\vec{r}_1,\vec{r}_2,\ldots,\vec{r}_N,t\right) = \\ \left[-\frac{\hbar^2}{2}\sum_{i=1}^{N}\frac{1}{m_i}\nabla_i^2 + V\left(\vec{r}_1,\vec{r}_2,\ldots,\vec{r}_N,t\right)\right]\Psi\left(\vec{r}_1,\vec{r}_2,\ldots,\vec{r}_N,t\right)\end{aligned} \tag{2.5}$$

2.2 Time-independent equation

Special cases are the solutions of the time-independent Schrödinger equation, where the Hamiltonian itself has no time-dependency (which implies a time-independent potential $V\left(\vec{r}_1,\vec{r}_2,\ldots,\vec{r}_N,\right)$, and the solutions therefore describe standing waves which are called stationary states or orbitals). The time-independent Schrödinger equation is not only easier to treat, but the knowledge of its solutions also provides crucial insight to handle the corresponding time-dependent equation.

The time-independent equation is obtained by the approach of separation of variables, i.e. the spatial part of the wave function is separated from the temporal part via [20]

$$\Psi\left(\vec{r}_1,\vec{r}_2,\ldots,\vec{r}_N,t\right) = \psi\left(\vec{r}_1,\vec{r}_2,\ldots,\vec{r}_N\right)\tau(t) = \psi\left(\vec{r}_1,\vec{r}_2,\ldots,\vec{r}_N\right).e^{-i\omega t}. \tag{2.6}$$

Furthermore, the l.h.s. of the equation reduces to the energy eigenvalue of the Hamiltonian multiplied by the wave function, leading to the general eigenvalue equation

$$E\psi\left(\vec{r}_1, \vec{r}_2, \ldots, \vec{r}_N\right) = \hat{H}\psi\left(\vec{r}_1, \vec{r}_2, \ldots, \vec{r}_N\right) \tag{2.7}$$

Again, using the many-body Hamiltonian, the Schrödinger equation becomes

$$\begin{aligned} &E\psi\left(\vec{r}_1, \vec{r}_2, \ldots, \vec{r}_N\right) = \\ &\left[-\frac{\hbar^2}{2}\sum_{i=1}^{N}\frac{1}{m_i}\nabla_i^2 + V\left(\vec{r}_1, \vec{r}_2, \ldots, \vec{r}_N\right)\right]\psi\left(\vec{r}_1, \vec{r}_2, \ldots, \vec{r}_N\right). \end{aligned} \tag{2.8}$$

2.3 The wave function

In the last section, the term wave function was repeatedly used. Therefore, and for a better understanding of the following a closer look at the wave function is taken. The first and most important postulate is that the state of a particle is completely described by its (time-dependent) wave function, i.e.the wave function contains all information about the particle's state. For the sake of simplicity the discussion is restricted to the time-independent wave function. A question always arising with physical quantities is about possible interpretations as well as observations. The Born probability interpretation of the wave function, which is a major principle of the Copenhagen interpretation of quantum mechanics, provides a physical interpretation for the square of the wave function as a probability density [21, 22]

$$\left|\psi\left(\vec{r}_1, \vec{r}_2, \ldots, \vec{r}_N\right)\right|^2 d\vec{r}_1 d\vec{r}_2 \ldots d\vec{r}_N. \tag{2.9}$$

Equation(2.9) describes the probability that particles 1,2,...,N are located simultaneously in the corresponding volume element $d\vec{r}_1 d\vec{r}_2 \ldots d\vec{r}_N$ [23]; What happens if the positions of two particles are exchanged, must be considered as well. Following merely logical reasoning, the overall probability density cannot depend on such an exchange, i.e.

$$|\psi(\vec{r}_1, \vec{r}_2, \ldots, \vec{r}_i, \vec{r}_j, \ldots, \vec{r}_N)|^2 = |\psi(\vec{r}_1, \vec{r}_2, \ldots, \vec{r}_j, \vec{r}_i, \ldots, \vec{r}_N)|^2 \tag{2.10}$$

There are only two possibilities for the behavior of the wave function during a particle exchange. The first one is a symmetrical wave function, which does not change due to such an exchange. This corresponds to bosons (particles with integer or zero spin). The other possibility is an anti-symmetrical wave function, where an exchange of two particles causes a sign change, which corresponds to fermions (particles which half-integer spin) [24, 25]. In this text only electrons are from interest, which are fermions. The anti-symmetric fermion wave function leads to the Pauli principle, which states that no two electrons can occupy the same state, whereas state means the orbital and spin parts of the wave function [26](the term spin coordinates will be discussed later in more detail). The an-tisymmetry principle can be seen as the quantum-mechanical formalization of Pauli's theoretical ideas in the description of spectra (e.g. alkaline doublets) [27]. Another consequence of the probability interpretation is the normalization of the wave function. If equation (2.9) describes the probability of finding a particle in a volume element,setting the full range of coordinates as volume element must result in a probability of one, i.e. all particles must be found somewhere in space. This corresponds to the normalization condition for the wave function.

$$\int d\vec{r}_1 \int d\vec{r}_2 \ldots \int d\vec{r}_N \, |\psi(\vec{r}_1, \vec{r}_2, \ldots, \vec{r}_N)|^2 = 1 \tag{2.11}$$

Equation (2.11) also gives insight on the requirements a wave function must fulfill in order to be physical acceptable. Wave functions must be continuous over the full spatial range and square-integratable [28]. Another very important property of the wave function is that calculating expectation values of operators with a wave function provides the expectation value of the corresponding observable for that wave function [29]. For an observable $O(\vec{r}_1, \vec{r}_2, \ldots, \vec{r}_N)$, this can generally be written as

$$O = \langle O \rangle = \int d\vec{r}_1 \int d\vec{r}_2 \ldots \int d\vec{r}_N \psi^* \left(\vec{r}_1, \vec{r}_2, \ldots, \vec{r}_N\right) \hat{O} \psi \left(\vec{r}_1, \vec{r}_2, \ldots, \vec{r}_N\right) \tag{2.12}$$

2.4 Atoms and molecules

All atomic and molecular systems deal with charged particles.The single electron Schrödinger equation where the electron moves in a Coulomb potential,

$$i\hbar \frac{\partial}{\partial t} \psi(\vec{r}) = \left[-\frac{\hbar^2}{2m} \vec{\nabla}^2 - \frac{e^2}{4\pi\epsilon_0} \cdot \frac{1}{|\vec{r}|} \right] \psi(\vec{r}) \tag{2.13}$$

marks and good starting point.

For the sake of simplicity, the so-called atomic units are introduced at this point for subsequent usage. That means the electron mass m_e,the reduced Planck constant (Dirac constant) $\hbar$ as well as the vacuum permitivity factor $4\pi\epsilon_0$ are all set to unity [30].

The Schrödinger equation for the single electron simplifies to

$$E\psi(\vec{r}) = \left[-\frac{1}{2} \vec{\nabla}^2 - \frac{1}{|\vec{r}|} \right] \psi(\vec{r}) \tag{2.14}$$

This form of the Schrödinger equation is analytically solvable. Although for the description of matter, even atoms, the Schrödinger equation exceeds analytical accessibility soon.Usage of (2.8) allows a construction of a generalized many-body Schrödinger equation for a system composed of N electrons and M nuclei, where external magnetic and electric fields are neglected.

$$E_i \psi_i \left(\vec{r}_1, \vec{r}_2, \ldots, \vec{r}_N, \vec{R}_1, \vec{R}_2, \ldots, \vec{R}_N\right) = \hat{H} \psi \left(\vec{r}_1, \vec{r}_2, \ldots, \vec{r}_N, \vec{R}_1, \vec{R}_2, \ldots, \vec{R}_N\right) \tag{2.15}$$

Equation (2.15) doesn't seem overly complicated on the first look, but an examination of the corresponding molecular Hamiltonian

$$\hat{H} = -\frac{1}{2}\sum_{i=1}^{N}\nabla_i^2 - \frac{1}{2}\sum_{k=1}^{M}\nabla_k^2 - \sum_{i=1}^{N}\sum_{k=1}^{M}\frac{Z_k}{r_{ik}} + \sum_{i=1}^{N}\sum_{j>i}^{N}\frac{1}{r_{ij}} + \sum_{k=1}^{M}\sum_{l>k}^{M}\frac{Z_k Z_l}{R_{kl}} \tag{2.16}$$

more generally ,it can be written as

$$\begin{aligned}\hat{H} = &\sum_{i} -\frac{\hbar^2}{2m_e}\nabla_i^2 + \sum_{I} -\frac{\hbar^2}{2m_I}\nabla_I^2 + \sum_{iI} -\frac{Z_I e^2}{\left|\vec{r}_i - \vec{R}_I\right|} \\ &+ \frac{1}{2}\sum_{i\neq j}\frac{e^2}{|\vec{r}_i - \vec{r}_j|} + \frac{1}{2}\sum_{I\neq J}\frac{Z_I Z_J e^2}{\left|\vec{R}_I - \vec{R}_J\right|}\end{aligned} \tag{2.17}$$

reveals the real complexity of the equation.

In equation (2.16), M_k repsresents the nuclear mass in atomic units (i.e. in units of the electron mass), Z_k and Z_l represents the atomic numbers,and $\vec{r}_{ij} = \left|\vec{i} - \vec{j}\right|, r_{ik} = \left|\vec{i} - \vec{R}_k\right|$ and $R_{kl} = \left|\vec{R}_k - \vec{R}_l\right|$ reperesents the distances between the particles (electron-electron nucleus and nucleus-nucleus).

A term by term interpretation of the right hand side in (2.16) reveals that the first two terms correspond to the kinetic energies of the electrons and nuclei. The latter three terms denote the potential part of the Hamiltonian in terms of electrostatic particle-particle interactions. This is reflected by the corresponding signs, where the negative sign denotes an attractive potential between electrons and nuclei, whereas the positive signs denote repulsive potentials between electrons and electrons as well as the nuclei among themselves [23]. Taking advantage of the fact, that the mass of a proton is approximately 1800 times larger than the mass of an electron, which is the minimum mass ratio of electron to nucleus (hydrogen atom) and becomes even higher for heavier atoms, another simplification can be introduced. The so called Born-Oppenheimer approximation states that due to the mass difference the nucleus can be, in comparison to the electrons, considered non-moving, i.e. spatially fixed. One can say that the core movement can be neglected on the timescale of electronic transitions which means the core movement has no influence on them [21, 31, 32].

As a consequence, the general Hamiltonian is replaced by the so-called electronic

Hamil-tonian

$$\hat{H} = -\frac{1}{2}\sum_{i=1}^{N}\nabla_i^2 - \sum_{i=1}^{N}\sum_{k=1}^{M}\frac{Z_k}{r_{ik}} + \sum_{i=1}^{N}\sum_{j>i}^{N}\frac{1}{r_{ij}} \tag{2.18}$$

. or in terms of operators

$$H_{el} = \hat{T} + \hat{U} + \hat{V} = \hat{T} + \hat{V}_{tot}. \tag{2.19}$$

Especially the electronic Schrödinger equation is of major interest for problems of molecular physics and quantum chemistry. But despite all simplifications a simple look at equations (2.15) to (2.19) indicates that there are still a few more crucial points left to deal with until a useful solution can be obtained.

Inspection of equations (2.18) and (2.19) shows that the kinetic energy term $\vec{T}$ doesn't depend on the nuclear coordinates R_{kl}, or in other words, it is only a function of the electron number. Also the electron-electron repulsion $\vec{U}$ is the same for every system with only Coulomb interactions. Therefore the only part of the electronic Hamiltonian which depends on the atomic respectively molecular system is the external potential V caused by the nucleus-electron repulsion. Subsequently this also means that $\vec{T}$ and $\vec{U}$ only need the electron number N as input and will therefore be denoted as 'universal', whereas $\vec{V}$ is system dependent. The expectation value of $\vec{V}$ is also often denoted as the external potential V_{ext}, which is consistent as long as there are no external magnetic or electrical fields [29]. As soon as the external potential is known, the next step is the determination of the wave functions ψ_i which contain all possible information about the system. As simple as the sounds, that exact knowledge of the external potentials ,i.e. in similarity to classical mechanics, the largest system which can be solved analytically is a 2-body-system, which corresponds to a hydrogen atom. Using all approximations introduced up to now it is possible to calculate a problem similar to H_2^+ a single ionized hydrogen molecule. To get results for larger systems, further approximations have to be made.

2.5 The Hartree-Fock approcah

In order to find a suitable strategy to approximate the analytically not accessible solutions of many-body problems, a very useful tool is variational calculus, similar to the least-action principle of classical mechanics.By the use of variational calculus, the ground state wave function ψ_0,which corresponds to the lowest energy of the system E_0,can be approached. A useful literature source for the principles of variational calculus has been provided by T.Flieÿbach [33].

Hence, for now only the electronic Schrödinger equation is of interest, therefore in the following sections we set $H \equiv H_{el}$, $E \equiv E_{el}$, and so on.

Observables in quantum mechanics are calculated as the expectation values of operators [21, 34]. The energy as observable corresponds to the Hamilton operator, therefore the energy corresponding to a general Hamiltonian can be calculated as

$$\begin{aligned} E &= \langle \hat{H} \rangle \\ &= \int d\vec{r}_1 \int d\vec{r}_2 \ldots \int d\vec{r}_N \psi^* \left(\vec{r}_1, \vec{r}_2, \ldots, \vec{r}_N\right) \hat{H} \psi \left(\vec{r}_1, \vec{r}_2, \ldots, \vec{r}_N\right) \end{aligned} \tag{2.20}$$

The central idea of the Hartree-Fock approach is that the energy obtained by any (normalized) trial wave function, different from the actual ground state wave function, is always an upper bound, i.e. higher than the actual ground state energy.If the trial function happens to be the desired ground state wave function, the energies are equal

$$E_{trial} \geq E_0, \tag{2.21}$$

with

$$\begin{aligned} &E_{trial} = \\ &\int d\vec{r}_1 \int d\vec{r}_2 \ldots \int d\vec{r}_N \psi^*_{trial} \left(\vec{r}_1, \vec{r}_2, \ldots, \vec{r}_N\right) \hat{H} \psi_{trial} \left(\vec{r}_1, \vec{r}_2, \ldots, \vec{r}_N\right) \end{aligned} \tag{2.22}$$

and

$$E_0 = \int d\vec{r}_1 \int d\vec{r}_2 \ldots \int d\vec{r}_N \psi_0^* (\vec{r}_1, \vec{r}_2, \ldots, \vec{r}_N) \hat{H} \psi_0 (\vec{r}_1, \vec{r}_2, \ldots, \vec{r}_N) \tag{2.23}$$

The expressions above are usually inconvenient to handle. For the sake of a compact notation, in the following the bra-ket notation of Dirac is introduced.For a detailed description of this notation, the reader is referred to the original publication [35] In this notation, equations (2.21) to (2.22) are expressed as

$$\left\langle \psi_{\text{trial}} | \hat{H} | \psi_{\text{trial}} \right\rangle = E_{\text{trial}} \geq E_0 = \left\langle \psi_0 | \hat{H} | \psi_0 \right\rangle \tag{2.24}$$

Proof: The eigenfunctions ψ of the Hamiltonian $\hat{H}$(each corresponding to an energy eigenvalue E_i) form a complete basis set, therefore any normalized trial wave function ψ_{trial} can be expressed as linear combination of those eigenfunctions [36].

$$\psi_{\text{trial}} = \sum_i \lambda_i \psi_i \tag{2.25}$$

The assumption is made that the eigenfunctions are orthogonal and normalized. Hence it is requested that the trial wave function is normalized, it follows that

$$\langle \psi_{\text{trial}} | \psi_{\text{trial}} \rangle = 1 = \left\langle \sum_i \lambda_i \psi_i \mid \sum_j \lambda_j \psi_j \right\rangle = \sum_i \sum_j \lambda_i^* \lambda_j \langle \psi_i \mid \psi_j \rangle = \sum_j |\lambda_j|^2 \tag{2.26}$$

On the other hand,following (2.24) and (2.26)

$$E_{\text{trial}} = \left\langle \psi_{\text{trial}} | \hat{H} | \psi_{\text{trial}} \right\rangle = \left\langle \sum_i \lambda_i \psi_i | \hat{H} | \sum_j \lambda_j \psi_j \right\rangle = \sum_j E_j |\lambda_j|^2 \tag{2.27}$$

Together with the fact that the ground state energy E_0 is per definition the lowest possible energy, and therefore has the smallest eigenvalue ($E_0 \leq E_i$),it is found that

$$E_{\text{trial}} = \sum_j E_j |\lambda_j|^2 \geq E_0 \sum_j |\lambda_j|^2 \tag{2.28}$$

what resembles equation (2.24).

The mathematical framework used above, i.e. rules which assign numerical values to functions, so called functionals, is also one of the main concepts in density functional theory. A function gets a numerical input and generates a numerical output whereas a unctional gets a function as input and generates a numerical output [37]. Equations (2.20) to (2.28) also include that a search for the minimal energy value while applied on all allowed (physically possible, cf. 2.4 N-electron wave-functions will always provide the ground-state wave function (or wave functions, in case of a degenerate ground state where more than one wave function provides the minimum energy). Expressed in terms of functional calculus, where $\psi \to N$ addresses all allowed N-electron wave functions, this mean [23]

$$E_0 = \min_{\psi \to N} E[\psi] = \min_{\psi \to N} \langle \psi | \hat{H} | \psi \rangle = \min_{\psi \to N} \langle \psi | \hat{T} + \hat{V} + \hat{U} | \psi \rangle \tag{2.29}$$

For N-electron systems this search is, due to the large number of possible wave functions on the one hand and limitations in computational power and time, practically impossible. What is possible is the restriction of the search to a smaller subset of possible wave function, as it is done in the Hartree-Fock approximation. In the Hartree-Fock approach, the search is restricted to approximations of the N-electron wave function by an antisymmetric cf.chapter product of N (normalized) one-electron wave-functions, the so called spin-orbitals $\chi_i(\vec{x}_i)$ [38]. A wave function of this type is called Slater-determinant, and reads [23, 38].

$$\psi_0 \approx \phi_{SD} = (N!)^{-\frac{1}{2}} \begin{vmatrix} \chi_1(\vec{x}_1) & \chi_2(\vec{x}_1) & \cdots & \chi_N(\vec{x}_1) \\ \chi_1(\vec{x}_2) & \chi_2(\vec{x}_2) & \cdots & \chi_N(\vec{x}_2) \\ \vdots & \vdots & \ddots & \vdots \\ \chi_1(\vec{x}_N) & \chi_2(\vec{x}_N) & \cdots & \chi_N(\vec{x}_N) \end{vmatrix} \tag{2.30}$$

It is important to notice that the spin-orbitals $\chi_1(\vec{x}_i)$ are not only depending on spatial coordinates but also on a spin coordinate which is introduced by a spin function, $\vec{x}_i = \vec{r}_i, s$. A detailed discussions of the spin orbitals and their (necessary) properties is omitted in this text, a detailed treatise is provided in the books by Szabo [26] and Holthausen [23]. As spin orbitals e.g. hydrogen-type orbitals (for atomic calculations) and linear combinations of them are used [39].

Returning to the variational principle and equation (2.29), the ground state energy approximated by a single slater determinant becomes

$$\begin{aligned} E_0 = &\min_{\phi_{SD}\to N} E\left[\phi_{SD}\right] = \\ &\min_{\phi_{SD}\to N} \left\langle \phi_{SD}|\hat{H}|\phi_{SD}\right\rangle = \min_{\phi_{SD}\to N} \left\langle \phi_{SD}|\hat{T}+\hat{V}+\hat{U}|\phi_{SD}\right\rangle \end{aligned} \tag{2.31}$$

A general expression for the Hartree-Fock Energy is obtained by usage of the Slater determinant as a trial function

$$E_{HF} = \left\langle \phi_{SD}|\hat{H}|\phi_{SD}\right\rangle = \left\langle \phi_{SD}|\hat{T}+\hat{V}+\hat{U}|\phi_{SD}\right\rangle \tag{2.32}$$

For the sake of brevity, a detailed derivation of the final expression for the Hartree-Fock energy is omitted.It is a straightforward calculation found for example in the Book by Schwabl [34]. The final expression for the Hartree-Fock energy contains three major parts [23].

$$E_{HF} = \left\langle \phi_{SD}|\hat{H}|\phi_{SD}\right\rangle = \sum_i^N (i|\hat{h}|i) + \frac{1}{2}\sum_i^N\sum_j^N [(ii \mid jj) - (ij \mid ji)] \tag{2.33}$$

with

$$\left(i\left|\hat{h}_i\right|i\right) = \int \chi_i^*\left(\vec{x}_i\right)\left[-\frac{1}{2}\vec{\nabla}_i^2 - \sum_{k=1}^M \frac{Z_k}{r_{ik}}\right]\chi_i\left(\vec{x}_i\right)d\vec{x}_i \tag{2.34}$$

$$(ii \mid jj) = \iint \left|\chi_i\left(\vec{x}_i\right)\right|^2 \frac{1}{r_{ij}} \left|\chi_j\left(\vec{x}_j\right)\right|^2 d\vec{x}_i d\vec{x}_j \tag{2.35}$$

$$(ii \mid jj) = \iint \chi_i\left(\vec{x}_i\right)\chi_j^*\left(\vec{x}_j\right)\frac{1}{r_{ij}}\chi_j\left(\vec{x}_j\right)\chi_i^*\left(\vec{x}_i\right)d\vec{x}_i d\vec{x}_j \tag{2.36}$$

The first term corresponds to the kinetic energy and the nucleus-electron interactions, $\hat{h}$ denoting the single particle contribution of the Hamiltonian, whereas the latter two terms correspond to electron-electron interactions. They are called Coulomb and exchange integral, respectively [23,26]. Examination of equations (2.33) to (2.36) furthermore reveals, that the Hartree-Fock energy can be expressed as a functional of the spin orbitals $E_{HF} = E[\chi_i]$. Thus,variation of the spin orbitals leads to the minimum energy [23]. An important point is that the spin orbitals remain orthonormal during minimization. This restriction is accomplished by the introduction of Lagrangian multipliers λ_i in the resulting equations, which represent the Hartree-Fock equations. For a detailed derivation, the reader is referred to the book by Szabo and Ostlund [23, 26, 33].

Finally, one arrives at

$$\hat{f}\chi_i = \lambda_i \chi_i \qquad i = 1, 2, \ldots, N \tag{2.37}$$

$$\hat{f}_i = -\frac{1}{2}\vec{\nabla}_i^2 - \sum_{k=1}^{M} \frac{Z_k}{r_{ik}} + \sum_{i}^{N} \left[\hat{J}_j(\vec{x}_i) - \hat{K}_j(\vec{x}_i)\right] = \hat{h}_i + \hat{V}^{HF}(i), \tag{2.38}$$

the Fock operator for the $i-th$ electron. In similarity to (2.33) to (2.36), the first two terms represent the kinetic and potential energy due to nucleus-electron interaction,collected in the core Hamiltonian $\hat{h}_i$, whereas the latter terms are sums over the Coulomb operators $\hat{J}_j$ and the exchange operators $\hat{K}_j$ with the other j electrons, which form the Hartree-Fock potential $\hat{V}^{HF}$. There the major approximation of Hartree-Fock can be seen. The two electron repulsion operator from the original Hamiltonian is exchanged by a one-electron operator $\hat{V}^{HF}$ which describes the repulsion in average [23].

2.6 Limitations and failings of the Hartree-Fock approach

Atoms as well as molecules can have an even or odd number of electrons. If the number of electrons is even and all of them are located in double occupied spatial orbitals ϕ_i, the compound is in a singlet state. Such systems are called *closed* −

shell systems.Compounds with an odd number of electrons as well as compounds with single occupied orbitals, i.e. species with triplet or higher ground state, are called *closed-shell systems* respectively. These two types of systems correspond to two different approaches of the Hartree-Fock method. In the restricted HF-method (RHF), all electrons are considered to be paired in orbitals whereas in the unrestricted HF (UHF)-method this limitation is lifted totally. It is also possible to describe open-shell systems with a RHF approach where only the single occupied orbitals are excluded which is then called a restricted open-shell HF(ROHF) which is an approach closer to reality but also more complex and therefore less popular than UHF [23].

There are also closed-shell systems which require the unrestricted approach in order to get proper results. For instance, the description of the dissociation of H_2 (i.e. the behavior at large internuclear distance), where one electron must be located at one hydrogen atom, can logically not be obtained by the use of a system which places both electrons in the same spatial orbital. Therefore the choice of method is always a very important point in HF calculations [38]. The size of the investigated system can also be a limiting factor for calculations. Kohn tates a number of $M = p^5$ with $3 \leq p \leq 10$ parameters for a result with sufficient accuracy in the investigation of the H_2 systems [40]. For a system with N=100 (active) electrons the number of parameters rises to

$$M = p^{3N} = 3^{300} \quad to \quad 10^{300} \approx 10^{150} \quad to \quad 10^{300}. \tag{2.39}$$

Equation (2.39) states, that the minimization of the energy would have to be performed in a space of at least 10^{150} dimension which exceeds the computational possibilities nowadays by far. HF-methods are therefore restricted to systems with a small number of involved electrons ($N \approx 10$). Referring to the exponential factor in (2.39) this limitation is sometimes called *exponential wall* [40]. Since a many electron wave function cannot be described entirely by a single Slater determinant, the energy obtained by HF calculations is always larger than the exact ground state energy. The most accurate energy obtainable by HF-methods is called the *Hartree-*

Fock-limit [23]. The difference between E_{HF} and E_{exact} is called correlation energy and can be denoted as [41]

$$E_{corr}^{HF} = E_{min} - E_{HF}. \tag{2.40}$$

Despite the fact that E_{corr} is usually small against E_{min}, as in the example of a N_2 molecule where

$$E_{corr}^{HF} = 14.9eV < 0.001.E_{min}, \tag{2.41}$$

it can have a huge influence [42]. For instance, the experimental dissociation energy of the N_2 molecule is

$$E_{diss} = 9.9eV < E_{corr} \tag{2.42}$$

which corresponds to a large contribution of the correlation energy to relative energies such as reaction energies which are of particular interest in quantum chemistry [42]. The main contribution to the correlation energy arises from the mean field approximation used in the HF-method. That means one electron moves in the average field of the other ones, an approach which completely neglects the intrinsic correlation of the electron movements. To get a better understanding what that means, one may picture the repulsion of electrons at small distances which clearly cannot be covered by a mean-field approach like the Hartree-Fock-method [23].

Chapter 3

Density functional theory

3.1 A new base variable - the electron density

In the 2.4 about the wave function ψ, a general statement about the calculation of observables has been provided. A quantity calculated in a very similar way is the topic of this section. The electron density (for N electrons) as the basic variable of density functional theory is defined as [23, 43].

$$n(\vec{r}) = N \sum_{s_1} \int d\vec{x}_2 \ldots \int d\vec{x}_N \psi^* \left(\vec{x}_1, \vec{x}_2, \ldots, \vec{x}_N\right) \psi \left(\vec{x}_1, \vec{x}_2, \ldots, \vec{x}_N\right) \tag{3.1}$$

What has to be mentioned is that the notation in (3.1) considers a wave function dependent on spin and spatial coordinates. In detail, the integral in the equation gives the probability that a particular electron with arbitrary spin is found in the volume element $d\vec{r}_1$. Due to the fact that the electrons are indistinguishable, N times the integral gives the probability that any electron is found there. The other electrons represented by the wave function $\psi(\vec{r}_1, \vec{r}_2, \ldots, \vec{x}_N)$ have arbitrary spin and spatial coordinates [23]. If additionally the spin coordinates are neglected, the electron density can even be expressed as measurable observable only dependent on spatial

coordinates [40, 43].

$$n(\vec{r}) = N \int d\vec{r}_2 \ldots \int d\vec{r}_N \psi^* \left(\vec{r}_1, \vec{r}_2, \ldots, \vec{r}_N\right) \psi \left(\vec{r}_1, \vec{r}_2, \ldots, \vec{r}_N\right) \tag{3.2}$$

which can e.g. be measured by X-ray diffraction [23].

Before presenting an approach using the electron density as variable, it has to be ensured that it truly contains all necessary informations about the system. In detail that means it has to contain information about the electron number N as well as the external potential characterized by $\hat{V}$ [23]. The total number of electrons can be obtained by integration the electron density over the spatial variables [23]

$$N = \int d\vec{r} n(\vec{r}). \tag{3.3}$$

What is left to proof is that also the external potential is characterized uniquely by the electron density, where uniquely means up to an additive constant

3.2 The Hohenberg-Kohn theorems

The "basic lemma of Hohenberg-Kohn"[4] states that not only $n(\vec{r})$ is a functional of $v(\vec{r})$ but that also $(\vec{r})$ is up to a constant determined by $n(\vec{r})$ uniquely [23, 40, 43]. Since the original publication of Hohenberg and Kohn deals with an electron gas, the Hamiltonian is resembled by the electronic Hamilton operator introduced in equation (2.18) $\hat{H}_{el} = \hat{T} + \hat{V} + \hat{U}$ with the one difference that the non-universal contribution $\hat{V}$ in this case represents a general external potential (which in case of the electronic Hamilton approximated by Born-Oppenheimer contains a nuclear field contribution) [23, 29, 43].

Following the original approach of Hohenberg and Kohn, accompanied by their proof via reductio ad absurdum, the discussion in this thesis is restricted to non-degenerate ground states [43]. This restriction nevertheless doesn't affect the presented proof for the second theorem and can be lifted as well for the first theorem [44, 45].

The energy of the system can be denoted as

$$E = \langle\psi|\hat{H}|\psi\rangle = \langle\psi|\hat{T} + \hat{V} + \hat{U}|\psi\rangle = \int v(\vec{r})n(\vec{r})d\vec{r} + \langle\psi|\hat{T} + \hat{U}|\psi\rangle \tag{3.4}$$

which will be used for the proof of Hohenberg and Kohn's first theorem.

3.2.1 Theorem I

The external potential $v(\vec{r})$ is a functional of the electron density $n(\vec{r})$ and, up to an unimportant constant, uniquely determined by it. [43]

Proof. It is assumed that there exist two external potentials $v(\vec{r})$ and $v'(\vec{r})$ which differ by more than just a trivial constant. Furthermore, the assumption is made, that both potentials give rise to the same electron density $n(\vec{r})$. Clearly, arising from the nature of $\hat{V}$ n that case there have to be two different Hamiltonians $\hat{H}$ and $\hat{H}'$. Furthermore ψ and ψ' have to be different, since they fulfill different Schrödinger equations. Finally also the energies E and E' associated with the particular wave function differ [40, 46].

Now the two wave functions ψ and ψ' are used as trial functions assuming the other wave function is the ground state wave function. Then the expressions

$$\begin{aligned} &E_0' = \langle\psi'|\hat{H}'|\psi'\rangle < \langle\psi|\hat{H}'|\psi\rangle = \\ &\langle\psi|\hat{H} + \hat{V}' - \hat{V}|\psi\rangle = \langle\psi|\hat{H}|\psi\rangle + \langle\psi|\hat{V}' - \hat{V}|\psi\rangle \end{aligned} \tag{3.5}$$

and

$$\begin{aligned} &E_0 = \langle\psi|\hat{H}|\psi\rangle < \langle\psi'|\hat{H}|\psi'\rangle = \\ &\langle\psi'|\hat{H}' + \hat{V} - \hat{V}'|\psi'\rangle = \langle\psi'|\hat{H}'|\psi'\rangle + \langle\psi'|\hat{V} - \hat{V}'|\psi'\rangle \end{aligned} \tag{3.6}$$

are obtained. By the use of (3.4), this can be rewritten as

$$E_0' < E_0 + \int \left[v'(\vec{r}) - v(\vec{r})\right] n(\vec{r})d\vec{r} \tag{3.7}$$

and

$$E_0 < E_0' + \int \left[v(\vec{r}) - v'(\vec{r})\right] n(\vec{r})d\vec{r} \tag{3.8}$$

By summation of (3.7) and (3.8) the inequality

$$E_0' + E_0 < E_0 + E_0' \tag{3.9}$$

is obtained, which represents an inconsistency and therefore provides by *reduction to absurdity* the proof $v(\vec{r})$ is truly a unique functional of $n(\vec{r})$.

The first Hohenberg-Kohn theorem can also be written in another form which is some-times called the "strong form" of the Hohenberg-Kohn theorem [47]. Here $\Delta v(\vec{r})$ and $\Delta n(\vec{r})$ correspond to the change in potential and electron density respectively:

$$\int \Delta v(\vec{r}) \Delta n(\vec{r}) < 0 \tag{3.10}$$

Whereas equation (3.10) can be derived from the original proof [48] it can also be derived perturbatively. The importance of this proof lies in the fact, that it not only implies the first Hohenberg Kohn theorem (if $\Delta v(\vec{r}) \neq 0$ clearly also $\Delta n(\vec{r})$ must not vanish) but also provides an assertion about the signs of $\Delta v(\vec{r})$ and $\Delta n(\vec{r})$, i.e. a (mostly) positive potential $\Delta v(\vec{r})$ requires a (mostly) negative electron density $\Delta n(\vec{r})$ to ensure the negativity of the integral in (3.10) [47].

From the first Hohenberg Kohn theorem it is obvious that also the ground state wave function is a unique functional of the ground state electron density

$$\psi_0 \left(\vec{r}_1, \vec{r}_2, \ldots, \vec{r}_N\right) = \psi \left[n_0(\vec{r})\right]. \tag{3.11}$$

Furthermore, recalling (2.12), the ground state expectation value of any observable is a functional of $n_0(\vec{r})$ too, i.e.

$$O_0 = O\left[n_0(\vec{r})\right] = \left\langle \psi \left[n_0(\vec{r})\right] | \hat{O} | \psi \left[n_0(\vec{r})\right] \right\rangle. \tag{3.12}$$

Among these observables is the ground state energy, the expectation value of the Hamil-tonian, which is of great importance. Recalling equation (3.4), the ground

state energy corresponding to an potential $v(\vec{r})$ can be denoted as

$$E_{v,0} = E_v\left[n_0(\vec{r})\right] = \left\langle \psi\left[n_0(\vec{r})\right] \mid \hat{H}\psi\left[n_0(\vec{r})\right]\right\rangle = \int v(\vec{r})n_0(\vec{r})d\vec{r} + \left\langle \psi\left[n_0(\vec{r})\right]|\hat{T}+\hat{U}|\psi\left[n_0(\vec{r})\right]\right\rangle \tag{3.13}$$

To obtain a more convenient handling of equation (3.13), the Hohenberg-Kohn functional $F_{HK}[n(\vec{r})]$ and subsequently, the energy functional $E_v[n(\vec{r})]$ are defined: [43]

$$F_{HK}[n(\vec{r})] \equiv \left\langle \psi\left[n_0(\vec{r})\right]|\hat{T}+\hat{U}|\psi\left[n_0(\vec{r})\right]\right\rangle \tag{3.14}$$

$$E_v[n(\vec{r})] \equiv \int v(\vec{r})n_0(\vec{r})d\vec{r} + F_{HK}[n(\vec{r})] \tag{3.15}$$

In similarity to the terminology introduced in the section about the Hartree-Fock method, the Hohenberg-Kohn functional represents the system-independent or universal part. Equation (3.13) furthermore leads to another crucial finding of the original paper by Hohenberg and Kohn, which is often addressed as the second theorem of Hohenberg and Kohn [43].

3.2.2 Theorem II

The ground state energy can be derived from the electron density by the use of variational calculus. The electron density, which provides a minimum of the ground state energy, is therefore the exact ground state density. The second Hohenberg-Khon Theorem states the energy variational principle. It implyes that for any trial density which is not ground state density in a condition $n'(\mathbf{r}) \geq 0$ and $\int n'(\mathbf{r})dr =$ N [49]. That is

$$E_0 \leq E_v[n']. \tag{3.16}$$

where $E_v[n']$ is the energy functional of next equation (3.18)

Originally this second theorem has been proved by variation calculus, [43] the proof pro-vided subsequently is a different one, namely the so called *constrained-search* approach, introduced by Levy and Lieb [50, 51] and subsequently thoroughly examined in the books by Parr, Yang as well as Kryachko and Ludena [52, 53]. Since the

wave function is a unique functional of the electron density, every trial wave function ψ' corresponding to a trial density $n'(\vec{r})$ following equation (3.2). According to the Rayleigh-Ritz principle, the ground state energy is obtained as

$$E_{v,0} = \min_{\psi'} \left\langle \psi' | \hat{H} | \psi' \right\rangle . \tag{3.17}$$

Proof. In principle, the minimization can be carried out in two steps. In the first step, a trial electron density $n'(\vec{r})$ is fixed. The class of trial functions corresponding to that electron density is then denoted by $\psi'^{\alpha}_{n'}$ [40] Then, the constrained energy minimum is defined as

$$E_v\left[n'(\vec{r})\right] \equiv \min_{\alpha} \left\langle \psi'^{\alpha}_{n'} | \hat{H} | \psi'^{\alpha}_{n'} \right\rangle = \int v(\vec{r}) n'(\vec{r}) d\vec{r} + F\left[n'(\vec{r})\right] \tag{3.18}$$

In that notation, $F\left[n'(\vec{r})\right]$ is the universal functional

$$F\left[n'(\vec{r})\right] \equiv \min_{\alpha} \left\langle \psi'^{\alpha}_{n'} | \hat{T} + \hat{U} | \psi'^{\alpha}_{n'} \right\rangle \tag{3.19}$$

which is clearly related to the Hohenberg-Kohn functional in (3.13). What is important to notice at this point is that the universal functional $F\left[n'(\vec{r})\right]$ requires no explicit knowledge of $v(\vec{r})$.

In the second step, equation (3.5) is minimized over all trial densities $n'(\vec{r})$:

$$E_{v,0} = \min_{n'(\vec{r})} E_v\left[n'(\vec{r})\right] = \min_{n'(\vec{r})} \left\{ \int v(\vec{r}) n'(\vec{r}) d\vec{r} + F\left[n'(\vec{r})\right] \right\} \tag{3.20}$$

Now, for a non-degenerate ground state,the energy in (3.20) is attained, if $n'(\vec{r})$ is the actual ground state density.

Furthermore, the constrained search approach finally lifts the restriction to non-degenerate ground states. If a ground state density corresponding to a number of wave functions is selected, only one of the wave functions connected with the energy of the degenerate ground state is found [23] Recapitulating, it has been shown that density functional theory provides a clear and mathematical exact framework for the use of the electron density as base variable. Nevertheless, nothing of what has

been derived is of practical use. Or in other words, the Hohenberg-Kohn theorems, as important as they are, do not provide any help for the calculation of molecular properties and also don't provide any information about ap-proximations for functionals like $F\left[n(\vec{r})\right]$. In the direct comparison to the variational approach of the Hartree-Fock method, the variational principle introduced in the sec-ond theorem of Hohenberg and Kohn is even more tricky. Whereas in wave-function based approaches like Hartree-Fock or configuration interaction [23] (CI) the obtained energy value provides information about the quality of the trial wave function (the lower E, the better the wave function), this is not the case in the variational principle based on the electron density. More than that, it can even happen that some functionals provide energies lower than the actual ground state energy in particular calculations [23]

Also important to mention is that there are certain functions $n(r)$ which would fulfill the requirements [40] and therefore possible ground state densities, but do not correspond to a potential $v(\vec{r})$. Therefore another requirement on the electron density is its v-representability, i.e. it must correspond to some potential [40]

3.3 The Kohn-Sham equations

It is indeed appealing that the ground-state energy of a many-electron system can be obtained as the minimum of the energy functional

$$E[n] = \int n(\mathbf{r})v(\mathbf{r})d\mathbf{r} + F[n] \tag{3.21}$$

where

$$F[n] = T[n] + V_{\mathrm{ee}}[n] \tag{3.22}$$

The ground-state electron density is the density that minimizes $E[n]$ and hence satisfies the Euler equation

$$\mu = v(\mathbf{r}) + \frac{\delta F[n]}{\delta n(\mathbf{r})} \tag{3.23}$$

where μ is the Lagrange multiplier associated with the constraint

$$\int n(\mathbf{r})d\mathbf{r} = N \tag{3.24}$$

Among all possible solutions of (3.23), one takes that which minimizes $E[n]$.

Thomas-Fermi and related models constitute a direct approach, whereby one constructs explicit approximate forms for $T[n]$ and $V_{\text{ee}}\,[n]$. This produces a nice simplicity-the equations involve electron density alone. There are seemingly insurmountable difficulties in going beyond the crude level of approximation. In a trade of simplicity for accuracy, Kohn and Sham (1965) invented an ingenious indirect approach to the kinetic-energy functional $T[n]$, the Kohn-Sham (KS) method. They thereby turned density functional theory into a practical tool for rigorous calculations.

Kohn and Sham proposed introducing orbitals into the problem in such a way that the kinetic energy can be computed simply to good accuracy, leaving a small residual correction that is handled separately. To understand what is involved and what Kohn and Sham did, it is convenient to begin with the exact formula for the ground-state kinetic energy,

$$T = \sum_i^N n_i \left\langle \psi_i \left| -\frac{1}{2}\nabla^2 \right| \psi_i \right\rangle \tag{3.25}$$

where the ψ_i and n_i are, respectively, natural spin orbitals and their occupation numbers. The Pauli principle requires that $0 \leqslant n_i \leqslant 1$; we are assured from the Hohenberg-Kohn theory that this T is a functional of the total electron density

$$n(\mathbf{r}) = \sum_i^N n_i \sum_s |\psi_i(\mathbf{r}, s)|^2 \tag{3.26}$$

For any interacting system of interest, there are an infinite number of terms in (3.25) or (3.26), which is ponderous at best. Kohn and Sham (1965) showed that one can build a theory using simpler formulas, namely

$$T_s[n] = \sum_i^N \left\langle \psi_i \left| -\frac{1}{2}\nabla^2 \right| \psi_i \right\rangle \tag{3.27}$$

and

$$n(\mathbf{r}) = \sum_{i}^{N} \sum_{s} |\psi_i(\mathbf{r}, s)|^2 \tag{3.28}$$

Equations (3.27) and (3.28) are the special case of (3.25) and (3.26) having $n_i = 1$ for N orbitals and $n_i = 0$ for the rest; this representation of kinetic energy and density holds true for the determinantal wave function that exactly describes N noninteracting electrons.

We know that any nonnegative, continuous, and normalized density n is N representable and always can be decomposed according to (3.28). But given a $n(\mathbf{r})$, how can we have a unique decomposition in terms of orbitals so as to give a unique value to $T_s[n]$ through (3.27)? In analogy with the Hohenberg-Kohn definition of the universal functional $F_{\mathrm{HK}}[n]$, Kohn and Sham invoked a corresponding noninteracting reference system, with the Hamiltonian

$$\hat{H}_s = \sum_{i}^{N} \left(-\frac{1}{2}\nabla_i^2 \right) + \sum_{i}^{N} v_s(\mathbf{r}) \tag{3.29}$$

in which there are no electron-electron repulsion terms, and for which the ground-state electron density is exactly n. For this system there will be an exact determinantal ground-state wave function

$$\Psi_s = \frac{1}{\sqrt{N!}} \det\left[\psi_1 \psi_2 \cdots \psi_N\right] \tag{3.30}$$

where the ψ_i are the N lowest eigenstates of the one-electron Hamiltonian $\hat{h}_s$:

$$\hat{h}_s \psi_i = \left[-\frac{1}{2}\nabla^2 + v_s(\mathbf{r}) \right] \psi_i = \varepsilon_i \psi_i \tag{3.31}$$

The kinetic energy is $T_s[n]$, given by (3.27),

$$\begin{aligned} T_s[n] &= \left\langle \Psi_s \left| \sum_{i}^{N} \left(-\frac{1}{2}\nabla_i^2 \right) \right| \Psi_s \right\rangle \\ &= \sum_{i=1}^{N} \left\langle \psi_i \left| -\frac{1}{2}\nabla^2 \right| \psi_i \right\rangle \end{aligned} \tag{3.32}$$

and the density is decomposed as in (3.28). The foregoing definition of $T_s[n]$ leaves an undesirable restriction on the density-it needs to be noninteracting v-representable; that is, there must exist a noninteracting ground state with the given $n(\mathbf{r})$. This restriction on the domain of definition of $T_s[n]$ can be lifted, and $T_s[n]$ of the form equation (3.27) can be defined for any density derived from an antisymmetric wave function.

The quantity $T_s[n]$, although uniquely defined for any density, is still not the exact kinetic-energy functional $T[n]$. The very clever idea of Kohn and Sham (1965) is to set up a problem of interest in such a way that $T_s[n]$ is its kinetic-energy component, exactly. The resultant theory turns out, as we shall immediately see, to be of independent-particle form. Nevertheless, it is exact.

To produce the desired separation out of $T_s[n]$ as the kinetic energy component, rewrite (3.22) as

$$F[n] = T_s[n] + J[n] + E_{xc}[n] \tag{3.33}$$

where

$$E_{xc}[n] = T[n] - T_s[n] + V_{ee}[n] - J[n] \tag{3.34}$$

The defined quantity $E_{xc}[n]$ is called the exchange-correlation energy; it contains the difference between T and T_s, presumably fairly small, and the nonclassical part of $V_{ee}[n]$. The Euler equation (3.23) now becomes

$$\mu = v_{\text{eff}}\left(\mathbf{r}\right) + \frac{\delta T_s[n]}{\delta n(\mathbf{r})} \tag{3.35}$$

where the KS effective potential is defined by

$$v_{\text{eff}}(\mathbf{r}) = v(\mathbf{r}) + \frac{\delta J[n]}{\delta n(\mathbf{r})} + \frac{\delta E_{xc}[n]}{\delta n(\mathbf{r})} = v(\mathbf{r}) + \int \frac{n\left(\mathbf{r}'\right)}{|\mathbf{r} - \mathbf{r}'|} d\mathbf{r}' + v_{xc}(\mathbf{r}) \tag{3.36}$$

with the exchange-correlation potential

$$v_{xc}(\mathbf{r}) = \frac{\delta E_{xc}[n]}{\delta n(\mathbf{r})} \tag{3.37}$$

We do not at first attempt the direct solution of equation (3.35), for equation (3.35)

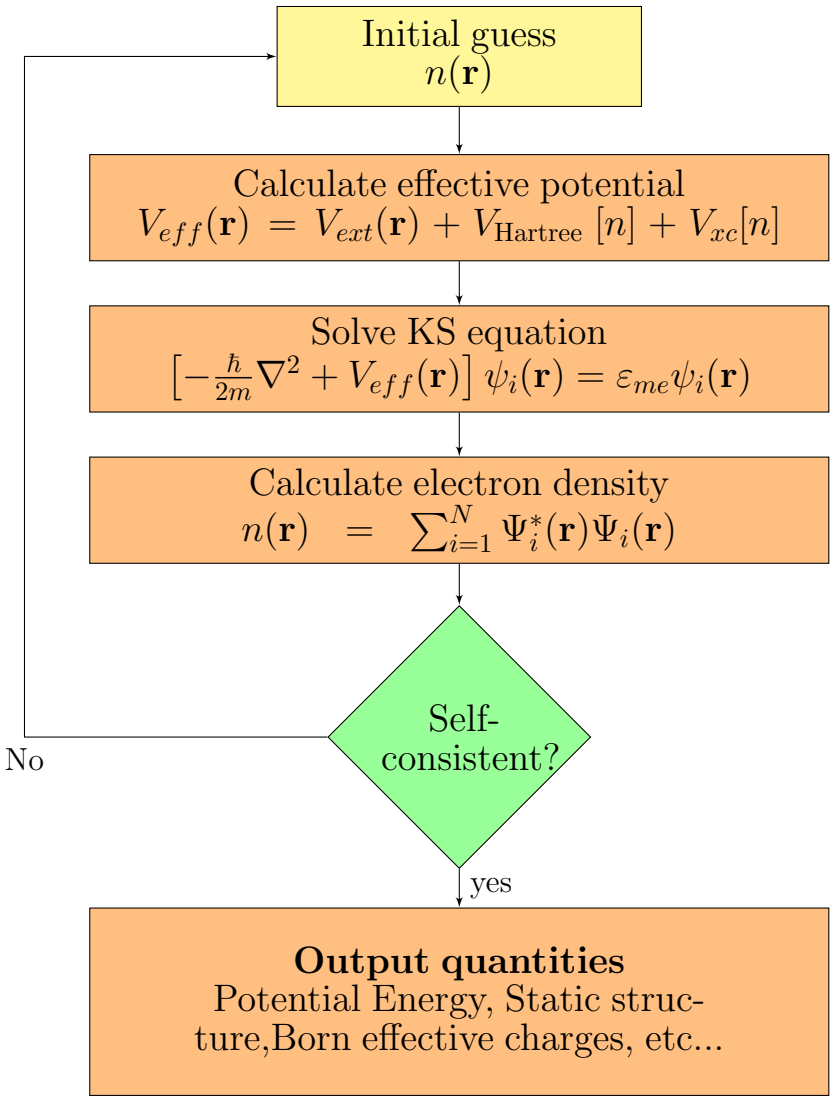

Figure 3.1: Flow chart of solving the Kohn-Sham equation

is merely a rearrangement of (3.23) and the explicit form of $T_s[n]$ in terms of density is as yet unknown. Rather, we follow the indirect approach designed by Kohn and Sham;

The Kohn-Sham treatment runs as follows. Equation (3.35) with the constraint (3.24) is precisely the same equation as one obtains from conventional density-functional theory when one applies it to a system of noninteracting electrons moving in the external potential $v_s(\mathbf{r}) = v_{\text{eil}}(\mathbf{r})$. Therefore, for a given $v_{\text{erf}}(\mathbf{r})$, one obtains the $\rho(\mathbf{r})$ that satisfies (3.35) simply by solving the N one-electron equations

$$\left[-\frac{1}{2}\nabla^2 + v_{\text{eff}}(\mathbf{r})\right]\psi_i = \varepsilon_i\psi_i \tag{3.38}$$

and setting

$$n(\mathbf{r}) = \sum_{i}^{N} \sum_{s} |\psi_i(\mathbf{r}, s)|^2 \tag{3.39}$$

Here, v_{eff} depends on $n(\mathbf{r})$ through (3.37); hence, (3.36), (3.38) and (3.39) must be solved self-consistently. One begins with a guessed $n(\mathbf{r})$, constructs $v_{\text{eff}}(\mathbf{r})$ from (3.36), and then finds a new $n(\mathbf{r})$ from (3.38) and (3.39). The total energy can be computed directly from (3.21) with (3.22). Equations (3.36)-(3.39) are the celebrated Kohn-Sham equations. They deserve our careful derivation and analysis, to which we proceed.

3.4 The Exchange-Correlation Functional in the Kohn Schemes

We should also clarify at this stage that there are inherent differences between the ex-change-correlation energy that appears in the Kohn-Sham formalism and their namesakes, the exchange and correlation energies.

In Hohenberg Kohn theorem the functional is

$$E[n] = \int n(\mathbf{r}) v(\mathbf{r}) d\mathbf{r} + F[n] \tag{3.40}$$

where

$$F[n] = T[n] + V_{ee}[n] \tag{3.41}$$

so Hohenberg Kohn modify the external potential of electron due to nucleus but there has a limitation of How the density will be decomposed into wave function. Another limitation is, there is no specific description of electron and electron interaction. In electron and electron interaction, there is classical term that means Hartree term and non-classical term. The non-classical term is regarded which comes out from solving the many body system. In many body system there is a corelation among electrons. And thus generates corelation energy. But In Hohenberg Kohn theorem there is no description about this.

Now we see that in Kohn-Sham equations they define the approximate kinetic energy in terms of wave function and they did it for individual electron orbital which occupies electrons. Finally they did summation over all individuals electron orbital that is N electron orbital which occupies $n_i = 1$

So the Hamilton has build for approximate kinetic energy and effective potential energy of individual electron from non-interacting system to calculate the interaction in interacting system. Finally the hamiltonian has been made by summing each hamiltonian made from single electron. By solving Schrödinger equation we get wave function for each electron and by which we can construct ground state wave function and ground state energy for many body system. But in externational potential, there is no clear description about electron and electron interaction.

In Kohn-Sham scheme the univeral Functional equation (3.33), there is non-classical term as it is for the exchange correlation of exchange of fermions (electrons) in many body system. In khon-sham theorem, they can not determine the accurate kinetic energy of electrons and all the electron-electron interraction (V_{ee} potential term. So in equation (3.34) $E_{xc}[n]$ is defined in such a way that there is the difference between exact kinetic energy of electrons and approximate (in non interacting reference frame) kinetic energy plus the difference between electron-electron interaction term and classical Hartree term. Only we can calculate $T_n]$ approximately and classical coulomb interaction and thus the exchange correlation energy has contained difficulties till now.

The local density approximation (LDA) is the first effort to estimate the exchange-correlation functional in DFT computations. The second well-known class of approximations to the Kohn-Sham exchange-correlation functional is the generalized gradient approximation (GGA). In the GGA approximation, the local electron density and local gradient in the electron density are included in the exchange and correlation energies [54].

3.4.1 Local Density Approximation (LDA)

The local density approximation is the simplest approximation to the exchange-correlation functional (LDA). The energy density of a homogeneous electron gas with the same electron density $n(\mathbf{r}$ at every site in the molecule has the value that would be supplied by a homogeneous electron gas with the same electron density $n(\mathbf{r}$ at that point, according to the local density approximation. The term "local" was coined to distinguish the technique from those in which the functional is reliant not only on r but also on the gradient (first derivative) of r, with the distinction arising from the assumption that a derivative is a nonlocal characteristic.

When the density is slowly changing, the local approximation is only valid in a theoretical sense. LDA delivers very good results even though atom and molecule densities are often highly inhomogeneous. LDA has been found to produce relatively satisfying findings for equilibrium structures, harmonic frequencies, and dipole moments in molecules [55].

The KS equations (3.36), (3.38) and (3.39) while exactly incorporating the kinetic energy $T_s[n]$, still leave the exchange-correlation functional $E_{xc}[n]$ of (3.33) unsettled. An explicit form for $E_{xc}[n]$ is needed to specify the KS equations. The search for an accurate $E_{xc}[n]$ has encountered tremendous difficulty and continues to be the greatest challenge in the density-functional theory. We describe in this section the simplest approximation, the local approximation proposed by Kohn and Sham (1965).

The uniform-electron-gas formula was used locally to obtain the Thomas-Fermi functional for kinetic energy and the Dirac functional for exchange energy. Now that the kinetic energy $T_s[n]$ is rigorously treated in the KS scheme, we can use the uniform-electron-gas formula solely for the unknown part of the rest of the energy functional. Thus we introduce the local-density approximation (LDA) for exchange and correlation energy,

$$E_{x\varepsilon}^{LDA}[n] = \int n(\mathbf{r})\varepsilon_{xc}(n)d\mathbf{r} \tag{3.42}$$

where $\varepsilon_{x\varepsilon}(n)$ indicates the exchange and correlation energy per particle of a uniform electron gas of density n. The corresponding exchange correlation potential of (3.36) then becomes

$$v_{xc}^{\mathrm{LDA}}(\mathbf{r}) = \frac{\delta E_{xc}^{\mathrm{LDA}}}{\delta n(\mathbf{r})} = \varepsilon_{xc}(n(\mathbf{r})) + n(\mathbf{r})\frac{\delta \varepsilon_{xc}(n)}{\delta n} \tag{3.43}$$

and the KS orbital equations read

$$\left[-\frac{1}{2}\nabla^2 + v(\mathbf{r}) + \int \frac{n\left(\mathbf{r}'\right)}{|\mathbf{r}-\mathbf{r}'|}d\mathbf{r}' + v_{xc}^{\mathrm{LDA}}(\mathbf{r})\right]\psi_i = \varepsilon_i\psi_i \tag{3.44}$$

The self-consistent solution of (3.44) defines the Kohn-Sham localdensity approximation (KS-LDA), which in the literature is usually simply called the LDA method.

3.4.2 Generalized-Gradient Approximations

The LSDA neglects inhonogeneities of real charge density which could be defferent from the Homogeneous Electron Gas(HEG). The exchange correlation energy density has significantly defferent result from HEG. This gives rise to the various Generalized-Gradient Approximations (GGA) which include density gradient correlation and higher spatial dertiviatives of electron density and gives better result than LDA in many cases. Three most widely used GGA'S are the from propeosed by Becke [56], Perdew et al. [57] and Perdew, Burke and Enzerhof [58]. From spin polarized system [59] we know that:

$$E_{XC}^{LSDA} \quad [n_{\uparrow}(r), n_{\downarrow}(r)] = \int n(r) \quad \epsilon_{XC}^{hom}\left(n_{\uparrow}(r), n_{\downarrow}(r)\right) dr \tag{3.45}$$

Where XC energy density $\epsilon_{XC}^{hom}(n(r))$ is a function of the density alone and is decomposed into exchange energy density $\epsilon_{X}^{hom}(n(r))$ and correlation energy density $\epsilon_{C}^{\mathrm{hom}}\left(n(r)\right)$. So that the XC energy functional is decomposed into exchange energy functional $E_X^{LDA}\left[n_(r)\right]$ and correlation energy functional $E_C^{LDA}\left[n_(r)\right]$ linearly.

From density gradient $\nabla n(r)$,

$$E_{XC}^{GGA} \quad [n_\uparrow(r), n_\downarrow(r)] = \int n(r) \quad \epsilon_{XC}^{hom}\left(n_\uparrow(r), n_\downarrow(r), |\nabla n_\uparrow(r)|, |\nabla n_\downarrow(r)|, \ldots\right) dr$$
$$= \int n(r) \quad \epsilon_X^{hom} n(r)\Big) F_{XC}\left(n_\uparrow(r), n_\downarrow(r), |\nabla n_\uparrow(r)|, |\nabla n_\downarrow(r)|, \ldots\right) dr \tag{3.46}$$

Where F_{XC} is dimensionless and $\epsilon_X^{hom} n(r)\big)$ is the exchange energy density of the unpolarized HEG. F_{XC} can be decomposed linearly into exchange contribution F_c as $F_{XC} = F_x + F_{\mathrm{c}}$. Generally GGA works better than LDA, in pridicting binding energy of molecules and bond length, crystall lattice constants, especially the system where charge density varried rapidly.

In case of ionic crystall, GGA overcorrects LDA results where the lattice constants of LDA fit well than GGA. But in case of transition metal oxides and rare-earth element, both LDA and GGA parform badly. This drawback leads to approximations beyond LDA and GGA.

3.4.3 Local Spin Density Approximation (LSDA)

Spin DFT is important in the theory of atoms amd molecules with net spins, as well as solids with magnetic order. The relevent example for our purpose is the Zeeman term that is different Fermions with up and down spin. According to this model the particle density,

$$n(r) = n(r, \sigma = \uparrow) + n(r, \sigma = \downarrow) \tag{3.47}$$

and the spin density

$$s(r) = n(r, \sigma = \uparrow) - n(r, \sigma = \downarrow) \tag{3.48}$$

This results the energy density as

$$E = E_{HK}[n, s] \equiv E'_{HK}[n] \tag{3.49}$$

Where [n] denotes the functionl of the density which depends both on space and spin. In absance of external Zeeman fields, the soluton of lowest energy may be spin

polarized. That is,

$$n(r, \sigma = \uparrow) \neq n(r, \sigma = \downarrow) \tag{3.50}$$

which is anologous to the broken symmetry solution of unrestricted Hartree-Fock theorem. The usefulness of spin Density Functional Theory is in these cases as well. The original Hartree-Fock theorem are valid and the ground state is determined by total ground state density $n(r, \sigma = \uparrow) + n(r, \sigma = \downarrow)$ for the system where there is no spin dependent external potential.

3.4.4 LDA+U Method

The systems which are strongly correlated contain rare-earth metal (transition metal) having partially filled d or f shells. L(S)DA and GGA can not explain them properly. In this method, electrons are considered into two classes: delocalized s, p electron and localized d or f electrons. The total energy in L(S)DA+U [60] method is given by,

$$E_{tot}^{LDA+U}\left[\rho_\sigma(r), n_\sigma\right] = E^{LSDA}\left[\rho_\sigma(r)\right] + E^{U}\left[n_\sigma\right] - E_{dc}\left[n_\sigma\right] \tag{3.51}$$

where, σ=spin indexes $\rho_\sigma(r)$=electron density for spin-σ electrons n_σ= density matrix of f or d electron for spin-σ electrons $E^{LSDA}\left[\rho_\sigma(r)\right]$= standard LSDA energy functional $E^{U}\left[n_\sigma\right]$electron-electron coulomb interaction energy . The last term is double counting term which remove the average LDA energy contribution of d or f electrons from the LDA energy

$$E_{dc}\left[n_\sigma\right] = \frac{1}{2}UN(N-1) - \frac{1}{2}J\left[N_\uparrow(N_\uparrow - 1) + N_\downarrow(N_\downarrow - 1)\right] \tag{3.52}$$

where, $N = N_\uparrow + N_\downarrow$. U and J are coulomb and exchange parameters. If exchange and non sphericity is neglected then,

$$E_{tot}^{LDA+U} = E_{LDA} + \frac{1}{2}U\sum_{i \neq j} n_i n_j - \frac{1}{2}UN(N-1) \tag{3.53}$$

The orbital energies ε_i are derivative of above equation with respect to orbital oc-

cupations n_i :

$$\varepsilon_i = \frac{\partial E}{\partial n_i} = \varepsilon_{LDA} + U(\frac{1}{2} - n_i) \tag{3.54}$$

For$n_i = 1$, LDA orbital energiesare shifted by $-\frac{U}{2}$ and by $\frac{U}{2}$ for unoccupied orbitals ($n_i = 0$), resulting the upper and lower Hubbard bands, which opens a gap at the Fermi energy in transition metal oxides. In case of double counting term, it has two different tretement: AMF and FLL. The former is most suitable for small U system [61] and the letter for large U system [62]. The energies for double counting is given by [63],

$$E^{dc}_{AMF} = \frac{1}{2}UN^2 - \frac{U + 2lJ}{2l+1}\frac{1}{2}\sum_{\sigma} N_\sigma^2 \tag{3.55}$$

and

$$E^{dc}_{AMF} = \frac{1}{2}UN(N-1) - \frac{1}{2}J\sum_{\sigma} N_\sigma(N_{\sigma-1}) \tag{3.56}$$

where,

$\frac{N}{2(2l+1)}$=average occupation of the correlated orbitals, $\frac{N_\sigma}{2l+1}$=average occupation of a single spin of the correlated orbital

3.5 Problems and limitations of DFT

In summary, both the Hohenberg-Kohn formulation as well as the approach by Kohn-Sham are formally exact and therefore allow in principle an exact solution provided that the functional $E_{xc}\,[n(\vec{r})]$ is exactly known. In practice this is never the case, which reveals the crucial point in (ground state) density functional theory. Every calculatory approach in DFT stands and falls with the quality of the approximation for the unknown functionals $F\,[n(\vec{r})]$ and $E_{xc}\,[n(\vec{r})]$ [23,40]. As stated in the introduction, possible approximations of the fuctional $E_{xc}[n(\vec{r})]$ are not discussed in this thesis but can be found in several literature sources [23, 47, 64, 65].

There are also a few other points which have to be taken into consideration. In 3.1 about the electron density, the term v -representability has been introduced, accompanied by the fact that there do exist particle densities which do not correspond to a potential $v(\vec{r})$ [23, 40].

The same question for an antisymmetric N-body wave function $\psi(\vec{r}_1, \vec{r}_2, \ldots, \vec{r}_N)$ can also be asked. How can it be assured that a given density $n(\vec{r})$ corresponds to such a wave function? Both of these questions are very important, because an energy calculated from a "physically impossible density" would provide a useless solution [23, 47].

Nevertheless, the problem of N -representability has been solved and it has been proofed that every nonnegative function can be written in the form (3.1) by the use of some anti-symmetric wave function $\psi(\vec{r}_1, \vec{r}_2, \ldots, \vec{r}_N)$ [66, 67]. The v-representability problem on the other hand lacks of a solution.But instead of a solution, it is referred to the proof which has been presented for the second HK-theorem (Levy and Lieb) and the subsequent statement that a knowledge of $v(\vec{r})$ and therefore v -representability of the density is not a a necessity [50, 51, 68].

Another problem arises as soon as information about excited states is required. Recalling that the minimum of the functional $E_v[n'(\vec{r})]$ in (3.18) corresponds to the ground state energy, it could be assumed that the other extrema of the functional correspond to excited state densities as well, even if the variational principle is in general only valid for the ground state. This is in fact the case, but on the other hand not every excited state density corresponds to an extremum of the functional [29, 69]. Therefore, to obtain trustful information about the excited states of a system, other methods have to be found. A variety of different methods [70–73] have been investigated one of the most prominent among them is the so called time-dependent DFT, [23, 29, 74] to which the final part of this thesis is assigned.

3.6 Basis functions

In practice, numerical solution of the KS differential equation (3.31) typically proceeds by expanding the KS orbitals in a suitable set of basis functions and solving the resulting secular equation for the coefficients in this expansion and or for the eigenvalues for which it has a solution. The construction of suitable basis functions is a major enterprise within electronic-structure theory (with relevance far beyond

DFT), and the following lines do little more than explaining some acronyms often used in this field.

In physics much is known about the construction of basis functions for solids due to decades of experience with band-structure calculations. This includes many calculations that predate the widespread use of DFT in physics. There is a fundamental dichotomy between methods that work with fixed ba-sis functions that do not depend on energy, and methods that employ energy- dependent basis functions. Fixed basis functions are used e.g., in plane-wave expansions, tight-binding or LCAO (linear combination of atomic orbitals) approximations, or the OPW (orthogonalized plane wave) method. Examples for methods using energy-dependent functions are the APW (augmented plane wave) or KKR (Korringa-Kohn-Rostoker) approaches. This distinction became less clear-cut with the introduction of 'linear methods' [75], in which energy-dependent basis functions are linearized (Taylor expanded) around some fixed reference energy. The most widely used methods for solving the Kohn-Sham equation in solid-state physics, LMTO (linear muffin tin orbitals) and LAPW (linear augmented plane waves), are of this latter type [76].

Development of better basis functions is an ongoing enterprise [77, 78]. The situation is quite similar in chemistry. Due to decades of experience with Hartree-Fock and CI calculations much is known about the construction of basis functions that are suitable for molecules. Almost all of this continues to hold in DFT — a fact that has greatly contributed to the recent popularity of DFT in chemistry. Chemical basis functions are classified with respect to their behaviour as a function of the radial coordinate into Slater type orbitals (STOs), which decay exponentially far from the origin, and Gaussian type orbitals (GTOs), which have a gaussian behaviour. STOs more closely resemble the true behaviour of atomic wave functions [in particular the cusp condition of Kato's theorem for Coulomb potentials] [79, 80] but GTOs are easier to handle numerically because the product of two GTOs located at different atoms is another GTO located in between, whereas the product of two STOs is not an STO. The so-called 'contracted basis functions', in which STO basis functions are reexpanded in a small number of GTOs, represent a compromise between the

accuracy of STOs and the convenience of GTOs. The most common methods for solving the Kohn-Sham equations in quantum chemistry are of this type [64, 81]. Very accurate basis functions for chemical purposes have been constructed by Dunning [82] and, more recently, by da Silva and collaborators [83, 84]. More details on the development of suitable basis functions can be found, e.g., in these references and Ref. [64]

A very popular approach to larger systems in DFT, in particular solids, is based on the concept of a pseudopotential (PP). The idea behind the PP is that chemical binding in molecules and solids is dominated by the outer (valence) electrons of each atom. The inner (core) electrons retain, to a good approximation, an atomic-like configuration, and their orbitals do not change much if the atom is put in a different environment. Hence, it is possible to approximately account for the core electrons in a solid or a large molecule by means of an atomic calculation, leaving only the valence density to be determined self-consistently for the system of interest.

In the original Kohn-Sham equation the effective potential $v_s[n] = v_{ext} + v_H[n] + v_{xc}[n]$ is determined by the full electronic density $n(\mathbf{r})$, and the selfconsistent solutions are single-particle orbitals reproducing this density. In the PP approach the Hartree and xc terms in $v_s[n]$ are evaluated only for the valence density n_v, and the core electrons are accounted for by replacing the external potential v_{ext} by a pseudopotential v_{ext}^{PP}. Hence $v_s^{PP}[n_v] = v_{ext}^{PP} + v_H[n_v] + v_{xc}[n_v]$[43] The PP v_{ext}^{PP} is determined in two steps. First, one determines, in an auxiliary atomic calculation, an effective PP, v_s^{PP}, such that for a suitably chosen atomic reference configuration the single-particle orbitals resulting from v_s^{PP} agree - outside a cut-off radius r_c separating the core from the valence region - with the valence orbitals obtained from the all-electron KS equation for the same atom. As a consequence, the valence densities n_v^{at} obtained from the atomic KS and the atomic PP equation are the same. Next, one subtracts the atomic valence contributions $v_H[n_v^{at}]$ and $v_{xc}\lfloor n_v^{at} \rfloor$ from $v_s^{PP}\lfloor n_v^{at} \rfloor$ to obtain the external PP v_{ext}^{PP} which is then used in the molecular or solid-state calculation, together with $v_H[n_v]$ and $v_{xc}[n_v]$ taken at the proper valence densities for these systems.

The way ${v_s}^{PP}$ is generated from the atomic calculation is not unique. Common pseudopotentials are generated following the prescription of, e.g. Bachelet, Hamann and Schlüter [85], Kleinman and Bylander [86], Vanderbilt [87] or Troullier and Martins [88]. Useful reviews are Refs. [89–91]. The pseudopotential approach is very convenient because it reduces the number of electrons treated explicitly, making it possible to perform density-functional calculations on systems with tens of thousands of electrons. Moreover, the PP pseudopotentials ${v_{ext}}^{PP}$ are much smoother than the bare nuclear potentials v_{ext}. The remaining valence electrons are thus well described by plane-wave basis sets.

Some of the choices one has to make in a practical Kohn-Sham calculation are illustrated schematically in the equation below.

$$\left[-\frac{\nabla^2}{2m} + v_{ext}(\mathbf{r}) + v_H(\mathbf{r}) + v_{xc}(\mathbf{r})\right]\phi_n(\mathbf{r}) = \mathcal{E}_n\phi_n(\mathbf{r})$$

The first term $-\frac{\nabla^2}{2m} \rightarrow$ in bracket is; non relativistic:Schrodinger, scalar relativistic relativistic:Dirac. Second term $v_{ext}(\mathbf{r}) \rightarrow$ is nuclei,pseudopotential. Third term $v_H(\mathbf{r}) \rightarrow$ is poisson eq, integral. Fourth term $v_{xc}(\mathbf{r}) \rightarrow$ is L(S)DA, GGA, hybrids, MGGA. $\phi_n(\mathbf{r}) \rightarrow$ is for mesh/basis, GTO/STO/.., LMTO/LAPW/PW/..and the Eigen value is $\mathcal{E}_n \rightarrow$ is Lagrange multipliers, Band structure.

Chapter 4

Computational details

In this thesis the structural properties, volume optimization, electronic properties (band structure, density of states), magnetic, optical and mechanical properties have been determined using the self-consistent full potential linearized augmented plane wave (FP-LAPW) [92] method as implemented in WIEN2k [93] code within the density functional theory (DFT) [94]. We have optimized the structure of Cu_2TiSi, Cu_2ZrGe, Ru_2TiSi, Ru_2VSi, Rh_2TiSi and Rh_2VSi through energy minimization where we calculate the lattice parameters for each compound respectively. These values of lattice parameter have been fixed so that the further calculations can be carried out with the use of these values. The energy convergence criterion was set to 10^{-5} Ry. In the FP-LAPW method [95], the unit cell is divided into two parts: non-overlapping atomic spheres centered at the atomic sites and the interstitial region. The Perdew–Burke Ernzerhof generalized gradient approximation (GGA) had been utilized for the exchange and correlation potential energy in Kohn-Sham equation.

we set $RK_{max} = 8.5$ for all calculation and the convergence of the basis set was controlled by the cut-off parameter -6 Ry(Rydberg). The R_{MT} is the smallest of the MT (muffin-tin) sphere radius and K_{max} is the largest reciprocal lattice vector used in the plane wave expansion. The charge density and the potential in the interstitial

region had been expanded as a Fourier series with the largest wave vectors up to $G_{max} = 12$. The maximum value of angular momentum $l_{max} = 6$ is selected for the wave function elongation inside the atomic sphere. The cutoff energy, which defines the separation of valence and core states, was chosen as -6 Ry. The charge convergence is selected as 0.0001 e and energy convergence 0.00001 Ry(Rydberg) during self-consistency cycles. Number of k-points in the brillouin zone 1000 for SCF, Band structure and mechanical calculation and 5000 for both DOS and optical properties calculation. $Emax$ is selected as 3.0 electron volt for the optical property calculations. The effect of spin–orbit coupling is neglected.

The material behavior under zero pressure is defined by calculating elastic constants. All these constants have the effective significant indication of mechanical properties, structural stability, bond indexes of solids and anisotropy. On aspects of the symmetry of cubic lattice, the elastic constants reduce to three independent constants, as like C_{11}, C_{12} and C_{44} have been calculated by IRelast package. The .struct and .outputeos files have been kept in a directory and applied the command for calculating elastic constant. Conventionally the stability conditions of the elastic constants for cubic crystal are $C_{11} - C_{12} > 0$, $C_{11} > 0$, $C_{44} > 0$, $C_{11} + 2C_{12} > 0$, $C_{12} > B > C_{11}$ [96–98] and the elastic anisotropy factor, 'A' that gives vital particularities on structural stability is obtained from [96, 99]

$$A = \frac{2C_{44}}{C_{11} - C_{12}}$$

Regarding full isotropic materials, 'A' is equal to one. That makes deviation from the anisotropy of crystal. In spite of having the significance that elastic constants are calculated by the first principle study of mono-crystals, the abundance received tremendous interest. Usually, PBE-GGA potential is used for the calculation that the bulk modulus B and the shear modulus G have made as follows

$$G = \frac{(G_V + G_R)}{2}$$

and

$$B = B_V = B_R = \frac{C_{11} + C_{12}}{3}$$

Here,

$$G_V = \frac{(C_{11} - C_{12} + 3C_{44})}{5} \quad \text{and} \quad G_R = \frac{5C_{44}\,(C_{11} - C_{12})}{[4C_{44} + 3\,(C_{11} - C_{12})]}$$

and anisotrophy constant can be defined by [100, 101]

$$A_G = \frac{(G_V - G_R)}{(G_V + G_R)}$$

When G_V= G_R, the A_G= 0, which impiles the full isotropy, since A_G obtains from zero, we get higher anisotropy. In the elastic part, stress to strain ratio, young's modulus E, indicates the stiffness of material that is obtained from

$$E = \frac{9BG}{(3B + G)}$$

When E increases, the crystal becomes stiffer and more covalent. The ductility index proposed by Pugh, $\frac{B}{G}$ for soft materials, the value would be greater than 1.75. The Poisson's ratio $\nu > 0.26$ for materials act like as ductile fashion and otherwise brittle fashion. For perfectly elastic isotropic regions and perfectly incompressible material takes the ν values 0.25, 0.5 correspondingly.

Chapter 5

Investigation of Cu_2TiSi and Cu_2ZrGe

5.1 Structural properties

The structure of Cu_2TiSi and Cu_2ZrGe are the full-heusler alloys are shown in Figure 5.1. For the Copper based heusler alloys the four FCC latices are inserted into each other. The space group is (225, $Fm\bar{3}m$), for that structure. The Figure 5.2 shows the Calculated total energy of Cu_2TiSi and Cu_2ZrGe compounds as functions of the unit cell volume.

The Cu atom has two positions one at X_1(1/4, 1/4, 1/4) and another is far from the first position at X_2(3/4, 3/4, 3/4). The Titanium and Zirconium position at Y(1/2, 1/2, 1/2) and the Silicon and Germanium positions are at Z(0, 0, 0). Graphically, the lattice constants can also be obtained from the energy vs volume diagram with the help of the equation $a_o = \sqrt[3]{4V} \times (0.529)(\text{Å})$. Where V is equilibrium volume and the equilibrium lattice parameter a_o. The optimized Volume is clearly indicated in the Energy vs Volume curve. It is evident that the minimization of energy is held at the lowest point of Figure 5.2, where the equilibrium lattice parameter is also

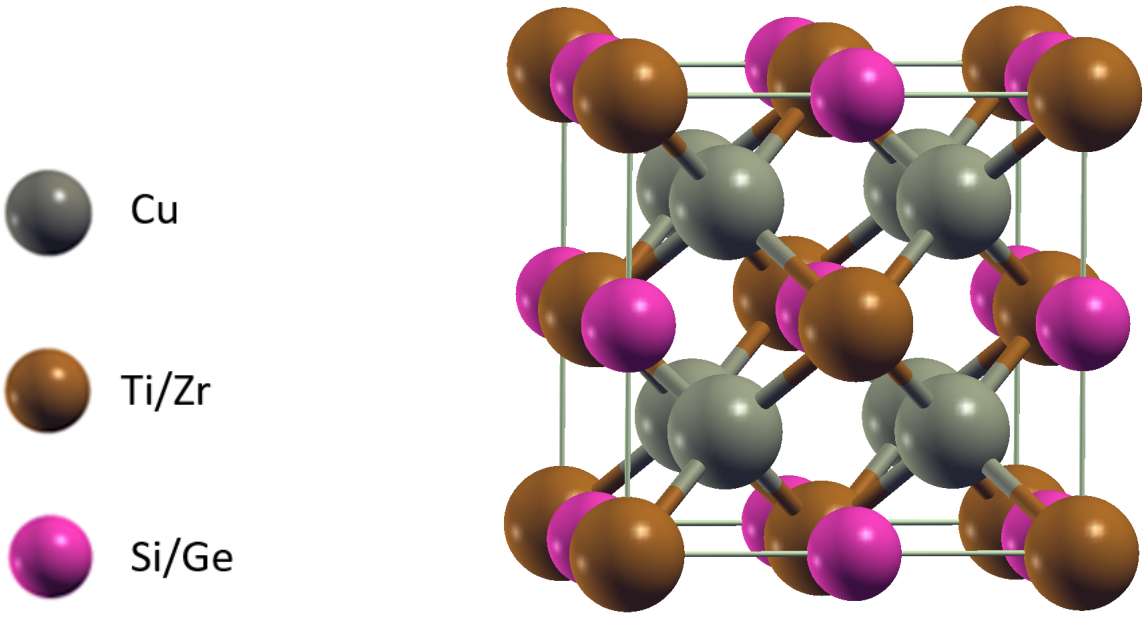

Figure 5.1: Structure of Cu_2TiSi and Cu_2ZrGe

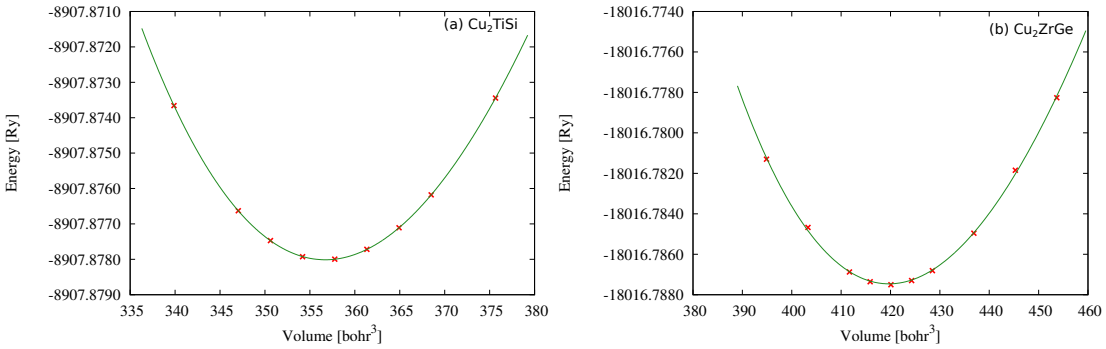

Figure 5.2: Volume optimization of Cu_2TiSi and Cu_2ZrGe

extracted.

5.2 Elastic properties

After having the structure file and energy minimization, the elastic constants C_{11}, C_{12} and C_{44} give the prediction of the mechanical and molecular behavior properties of these systems. The isotropic and anisotropic scheme of copper-based full heusler alloys can be seen from elastic anisotropy factor A, anisotropy percentage A_G. Also Cauchy's Pressure, Young's modulus E, ductility modulus G, Poisson's ratio v, B/G ratio and bulk modulus B has been calculated in Table 5.1.

Cu_2TiSi has B/G ratio of 3.776 which means a high ratio of bulk and shear modulus

Table 5.1: Lattice constants a_0, Band gap, The obtained value of Fermi energy E_f, the calculated elastic constants C_{11}, C_{12} and C_{44}, the bulk modulus (B), the elastic anisotropy factor (A), the percentage of anisotropy A_G, Cauchy's Pressure, Young's modulus (E), the shear modulus (G), B/G ratio and Poisson's ratio ν of Cu_2TiSi and Cu_2ZrGe

Specification	Cu_2TiSi	Cu_2ZrGe
a_0(Å)	5.9633	6.2891
Band gap (ev)	0.0	0.0
Fermi energy(eV)	0.7021580886	0.6859454548
C_{11}(GPa)	173.5554	95.0609
C_{12}(GPa)	166.7748	115.4802
C_{44}(GPa)	84.5710	32.1863
B(GPa)	113.4434	70.18
A	24.945	−3.153
A_G	0.734	−1.910
Cauchy's Pressure	82.204	83.294
E(GPa)	82.828	−54.529
G(GPa)	30.047	−16.732
B/G	3.776	−4.194
ν	0.378	0.629

indicate the metal has good mechanical strength and ductile behavior [102] from the elastic limit under applied load on it. It also evident that the materials capable of plastically deform able. So this material can be used for engineering purposes. Whereas (B/G) ratio of -4.194 for Cu_2ZrGe indicates more fragile nature [103, 104]. The Poisson's ratio ν of Cu_2TiSi and Cu_2ZrGe is 0.378, 0.629 respectively where the poisson's ratio $\nu > 0.26$ that first one is elastically deform able and the second one has high plasticity as the larger the Poisson's ratio ($\nu > 0.5$), the better the plasticity. Above the critical value 0.26 the materials is ductile. The cubic lattice conditions $C_{11} - C_{12} > 0$, $C_{12} < B < C_{11}$ has not satisfied by Cu_2ZrGe system which implies the mechanically unstable structure due to it's molecular behavior in this alloy. For Cu_2TiSi all conditions $C_{11} - C_{12} > 0$, $C_{11} > 0$, $C_{44} > 0$, $C_{11} + 2C_{12} > 0$ and

$C_{12} < B < C_{11}$ [96–98] are satisfied which indicate elastically stable material. The value of Anisotropy constant for Cu_2TiSi and Cu_2ZrGe system is 24.945, -3.153 is largly deviate from 1. A_G is 0.734, -1.910 correspondingly for the systems that shows the anisotropy. The softness behavior can be seen by Cauchy's pressure greater than zero and $B/G > 0$. The desired Poisson's ratio (-1 to +0.5) is satisfied with the positive value of Young's modulus (E), Bulk modulus (B), and shear modulus (G) for Cu_2TiSi better than Cu_2ZrGe where Young's modulus and shear modulus is negative for this system.

5.3 Electronic Properties

From the Figure 5.3 (a) it is pointed out that the band is overlapped in the Fermi level. So the band gap is 0 eV and shows metallic nature. In Figure 5.3(b) at the Fermi level, the band overlapping [105],

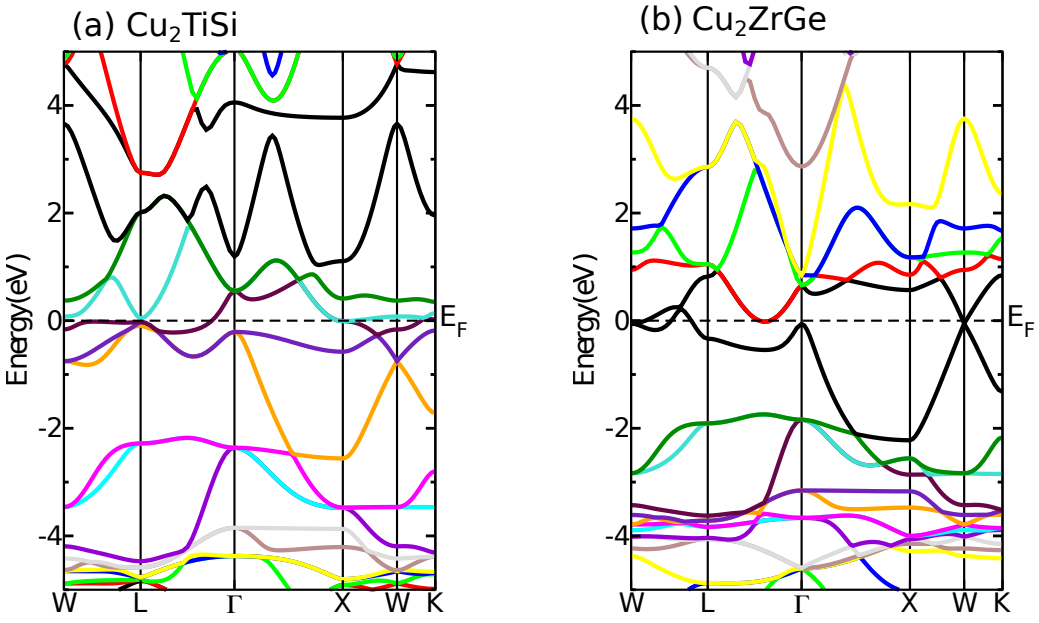

Figure 5.3: The band structures along the high symmetry directions in the Brillouin zone of (a) Cu_2TiSi and (b) Cu_2ZrGe at their predicted equilibrium lattice constants.

bands crossing [106], intraband transition are occurred. For the two system, the 3d orbital contribution of copper in the band structure is more than the other atoms

orbital contain in the system [107]. The low energy region is due to the s orbital of Si and Ge atoms for the alloys [6, 108]. The first energy region below Fermi level mainly consists of the occupied 3d states of Cu with small contribution of 3d states of Ti atoms.

From the band structure of this two system, the gap between the valence band and conduction band is 0 eV. As there is no valence band maximum and conduction band minimum. Moreover, in both spin channel the band overlapped shows the two system is metallic in nature.

For understanding the density of states from the Figure 5.4 (a), there is well defined doss at the Fermi level for majority spin channel and minority spin channel of Cu_2TiSi. With the increasing of energy at 0.5 eV the corresponding DOS peaks at 3 eV, 2.5 eV, 0.8 eV, 0.1 eV of Cu_2TiSi, Ti, Cu and silicon Total DOS for both spin channel. However at point 0 eV in the Fermi level each atomic DOS curve has a definite value which shows the metallic behavior at the both spin channel. In the positive energy region after the energy 2 eV the DOS curve are flat like nature for filled 3d orbital of Copper. Then for Cu and Ti atom they are individually metallic nature from the partial density of state except silicon. The Total DOS of this system is higher than individual atomic DOS contribution in the energy interval -7.3 eV to 6.8 eV. So the Cu_2TiSi is metallic nature. The electron transport properties depend on the DOS near the Fermi level.

As It has DOS in the Fermi level for both up spin and down spin channel the band gap is zero. The significant symmetric DOS and PDOS curve for up spin and down spin channel accounts for zero magnetic moment of the mettalic system.

For the PDOS of Cu atom Figure 5.4 (b) and 5.4 (f) regarding Cu_2TiSi and Cu_2ZrGe, there has the difference of PDOS in lower energy region -4 eV. But at higher energy region there has no significant differences above the Fermi level. The Titanium atom has more available states above 0 eV which shows good conductor as the 3d orbital is partially filled [109] in the high energy region. So the available free electron is low. Also, as the upper shell s electron-orbital is filled by electron. Similarly for the Si and Ge, Figure 5.4 (d) and 5.4 (h) after 0 eV, the occupied electrons states is

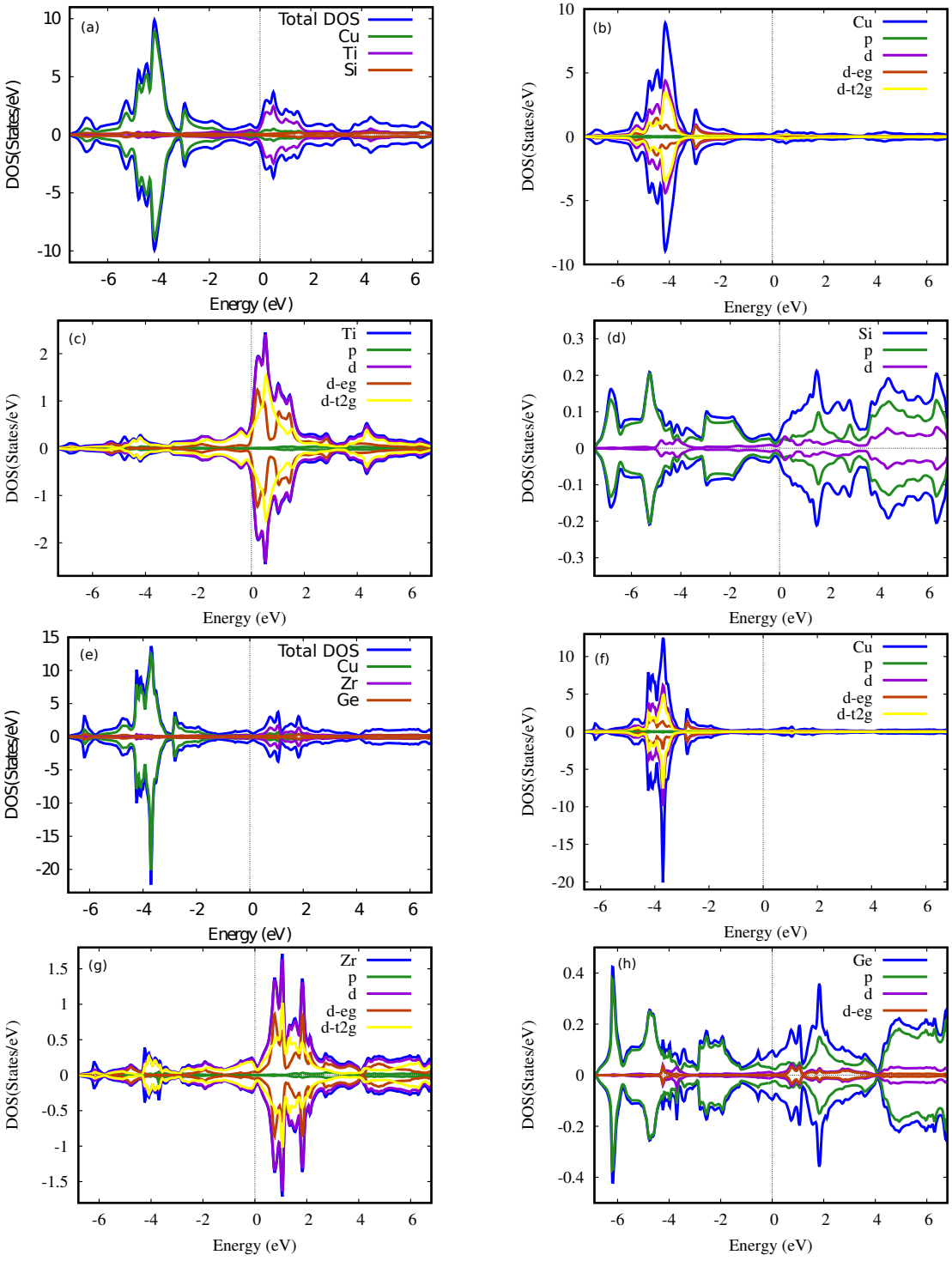

Figure 5.4: Total Density and partial density of states (a, h) of spin polarized Cu_2TiSi and Cu_2ZrGe system

high for Germanium and the electrons are tidily bonded in the Si and Ge, as a result for the conduction of electron is occurred at high energy region, that causes heat up the silicon and germanium semiconductor [110]. Moreover the total magnetic moment of Cu_2TiSi and Cu_2ZrGe is zero which shows antiferromagnetic nature, so

the net magnetization of these compounds are zero [111] for application of external magnetic field. The antiferromagnetic nature shows that the two system is metallic.

5.4 Optical Properties

The optical property of Cu_2TiSi and Cu_2ZrGe has also been calculated. For instance the Optical conductivity ($\sigma(\omega)$), Electron energy loss function ($L(\omega)$), Refractive index ($n(\omega)$), Absorption coefficient($I(\omega)$), Complex dielectric tensor $\varepsilon_{ij}(\omega)$, Extinction coefficient ($K(\omega)$), Optical reflectivity ($\rho(\omega)$), Real dielectric tensor ε'_{ij}, Imaginary dielectric tensor ε''_{ij} [112,113] are investigated With the help of FP-LAPW method and generalized gradient approximation (GGA).

The dielectric tensor is considered as real dielectric tensor and imaginary dielectric tensor. It is introduced as a significant characteristics of a specific crystallographic medium. The tensor component for face centered cubic crystal Cu_2TiSi and Cu_2ZrGe have illustrated in the Figure 5.5 (c) and Figure 5.5 (d) are shown real dielectric tensor and imaginary dielectric tensor respectively.

In Figure 5.5 (c) indicates the real part of $\varepsilon_{ij}(\omega)$, (Re$\varepsilon_{ij}(\omega)$) for both Cu_2TiSi and Cu_2ZrGe compounds. The static part of die-electric tensor goes to infinity for both of them; and Steep slope this implies two important facts: Firstly, both crystal have shows metallic behavior in this energy range 0 to 1 eV denotes the loss of light transit for both compounds. So Cu_2TiSi in IR region has high storage energy for polarization of charge. As the Cu_2ZrGe curve is not so high as Cu_2TiSi, so the Cu_2TiSi is seen clearly more responsive than Cu_2ZrGe. It is seen that (Re$\varepsilon_{ij}(\omega)$) has roots 0.6 eV and 1.2 eV for Cu_2TiSi, Cu_2ZrGe and the curves go down at 3.70 eV, 4.30 eV respectively. Where (Re$\varepsilon_{ij}(\omega)$)=0. At 0 value of real dielectric tensor, the compounds do not any effect to incident light, which this fact is mainly due to the plasmon oscillations. In contrast with the Figure 5.5 (e) (electron energy loss) one can declare that there is a pick arisen at point 1.4 eV and 1.9 eV. High polarization response occurred in infrared spectrum limit 1.77 eV to visible spectrum 3.7 eV for both compounds. For the values greater than 4.3 eV the (Re$\varepsilon_{ij}(\omega)$) is negative for

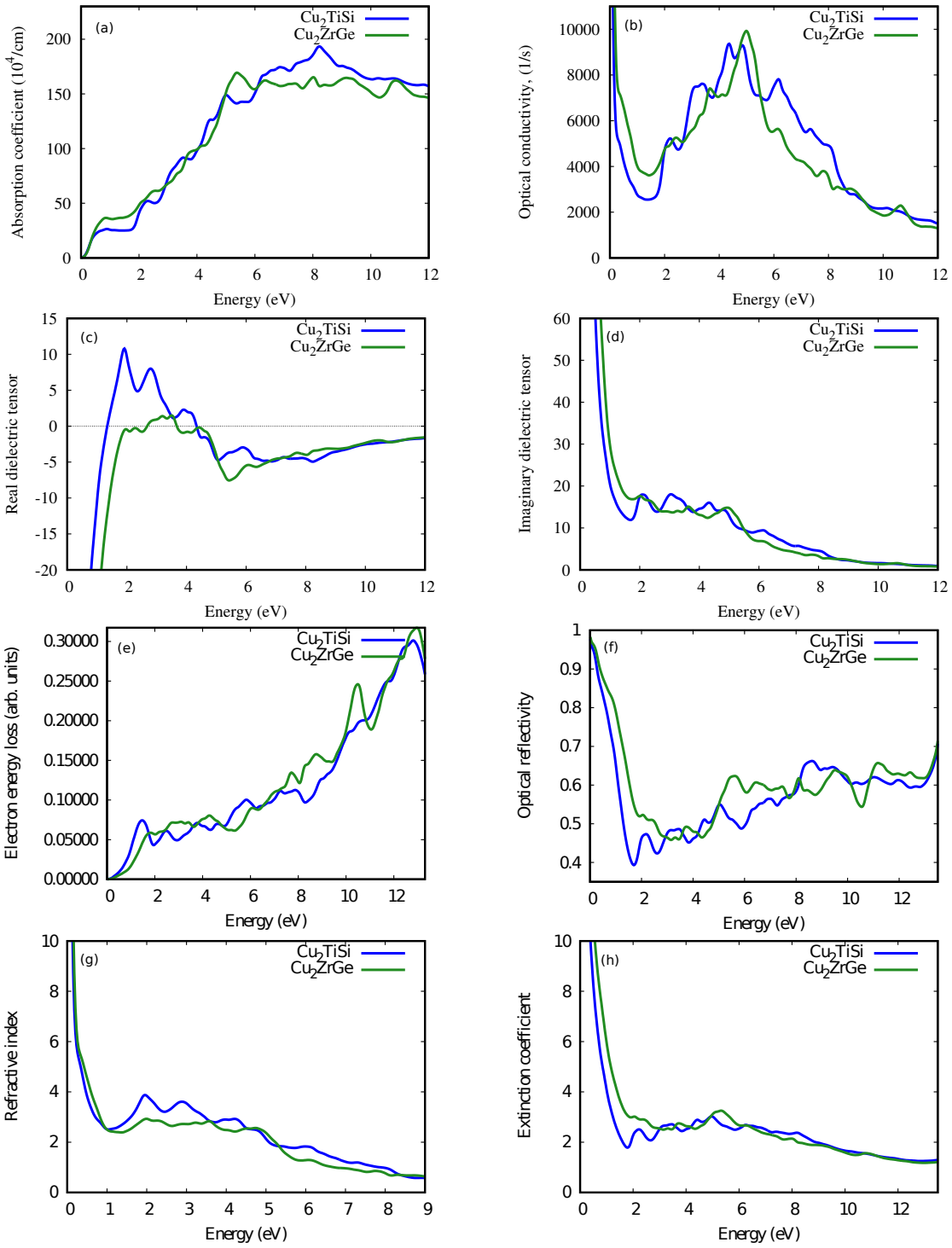

Figure 5.5: Absorption coefficient ($I(\omega)$), Optical conductivity ($\sigma(\omega)$), the real and imaginary part of dielectric tensor; $\varepsilon_{ij}(\omega)$, Electron energy loss function ($L(\omega)$), Optical reflectivity ($\rho(\omega)$), Refractive index and Extinction coefficient for Cu_2TiSi and Cu_2ZrGe compounds.

both compounds; after that these element would be opaque. The peak in electron energy loss right after 4.8 eV is the evidence of opaqueness of the compounds as

real dielectric tensor is negative value. As the dielectric constant is infinity for metal [114], so the electric field does not exist inside the conductor as it resist to formation of electric field [115]. Since the ability of a metal to store energy compared to those with low dielectric constants materials. In this case electric field permittivity is larger than dielectric materials [116]. As the permittivity is high [117], then tensor has sharp peak in the low energy infrared region, after this it remains constant with the increasing photon energy. This shows the metallic behavior of the compound.

In Figure 5.5 (d) shows the Im$\varepsilon_{ij}(\omega)$ curves for both compounds. Each curve implies the electron energy loss when electron pass through occupied level to unoccupied one. Electron moves largely in the infra-red domain (energies less than 0.6 eV) that exhibits the metal char-acteristic of these compounds. When the photon is incident on the compound, the electrons are transmitted in intra-band. But in the value of energy 1.5 eV, one sees the sudden decrease of Im$\varepsilon_{ij}(\omega)$ curves for both compounds which is the result of plasmon oscillation. As the response of passages occurred at large region (1.5 eV) it has the property of metals. The curve shows the electron energy loss. In high energy region electron transition is stopped, in this energy range. Figure 5.5 (a) shows the absorption curve of both compounds. Since the absorption of materials are depend on the energy of the incident photon. Initially in Low incident photon energy the absorption is ascending. The absorption curve which enhance almost linearly in the beginning (Infrared Region). In the visible region, one observes fast ascending of the absorption curve that maximizes in 3.10 eV energy region. The main part of absorbed light in the infrared and visible spectrum which help to electron transition.

Next to the real part of refractive index depicted in Figure 5.5 (g). It is clear that in the low energy limit, the curve tends to the large value. Which is metallic behavior. The decreasing of, extinction coefficient, $(K(\omega))$ in the high energy region denote the super-luminescence phenomenon. At the end, the reflectivity is shown in the Figure 5.5 (f) the static reflection index is high for denser medium. In optical reflectivity curve drop sharply from infrared region 1.77 eV to ultraviolet region because of inter band transitions [112, 118]. Which also the properties of metals.

It is comparable that for all diagrams in the infrared, visible and UV regimes, the Cu_2TiSi response to incident photons is higher than Cu_2ZrGe. This property of Cu_2TiSi origins from the electronic configuration.

To describe the refractive index of these typical metal compound, there is always two part; Real part of refractive index and the imaginary part of refractive index, which is so called the extinction coefficient. However the refractive index is related to the relative permittivity. So the refractive index is the square root of the dielectric constant $n(\omega) = \sqrt{\epsilon_r}$. The complex relation between real and imaginary part of the refractive index is $n_l(\omega, s) = n + ix$. Or $n(\omega) = n + k(\omega)$. However, s is the direction for index measurements. The optical conductivity has the highest value in the infrared region. With the increase of energy it is shown in the graph that at 1.7 eV for Cu_2TiSi reflectivity reaches slightly lower than Cu_2ZrGe. The lowest value of index occurred because of high energy photon rather than infrared region and here the absorption increases rapidly and also the refractive index decreases. As the absorption increasing with the increasing value of photon, the energy loss curve also increases. That is why the metal heated and the metal goes to slightly pass in the higher energy region.

Chapter 6

Characteristics of Ru_2TiSi and Ru_2VSi

6.1 Structural properties:

The total energy is calculated as a function of lattice constant for spin polarization calculations. The structure Figure 6.1 for this compounds where four FCC sub lattices are inserted each other, space group (225, $Fm\bar{3}m$), is stable for spin polarization calculations. The Calculated total energy curve of Ru_2TiSi and Ru_2VSi compounds are given in Figure 6.2 as a function of the unit cell volume.

The Ru atom has two positions one at X_1(1/4, 1/4, 1/4) and another is far from the first position at X_2(3/4, 3/4, 3/4). The Titanium and Vanadium position at Y(1/2, 1/2, 1/2) and the Silicon position are at Z(0, 0, 0) Figure 6.1. Graphically, the lattice constants can be obtained from the E-V, energy vs volume diagram with the help of equation $a_o = \sqrt[3]{4V} \times (0.529)(\text{Å})$. Where V is the equilibrium volume. The equilibrium lattice parameter a_o is extracted from volume optimized minimum energy curve of Ru_2TiSi and Ru_2VSi. The optimized Volume is observed from the Energy vs Volume curve. It is evident that the minimization of energy is held at the

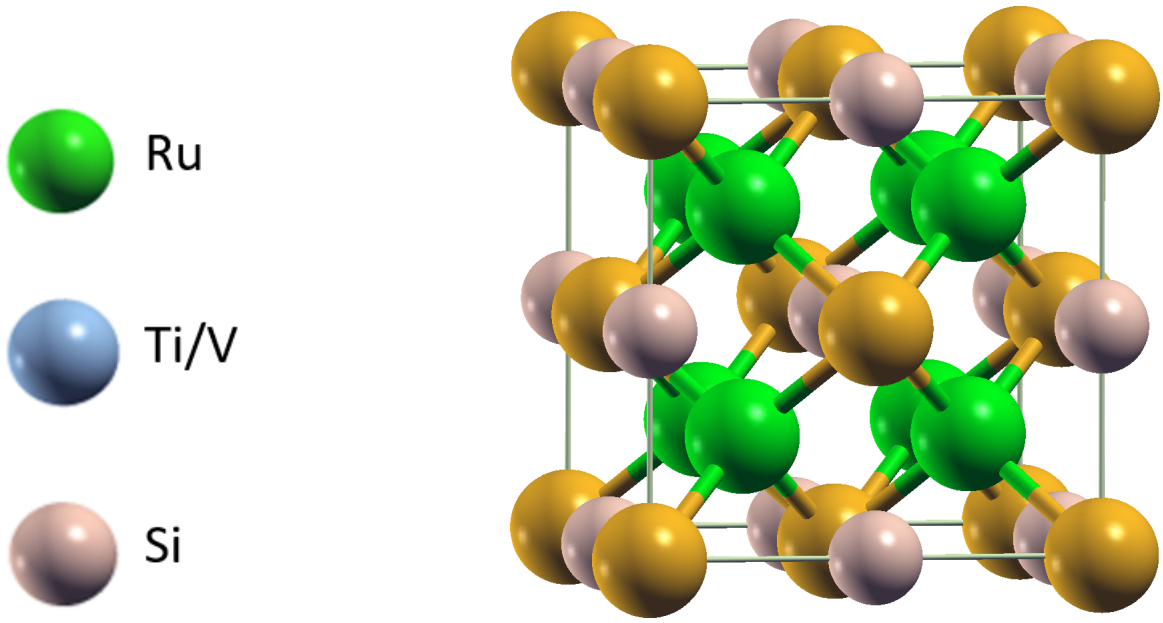

Figure 6.1: Structure of Ru_2TiSi and Ru_2VSi

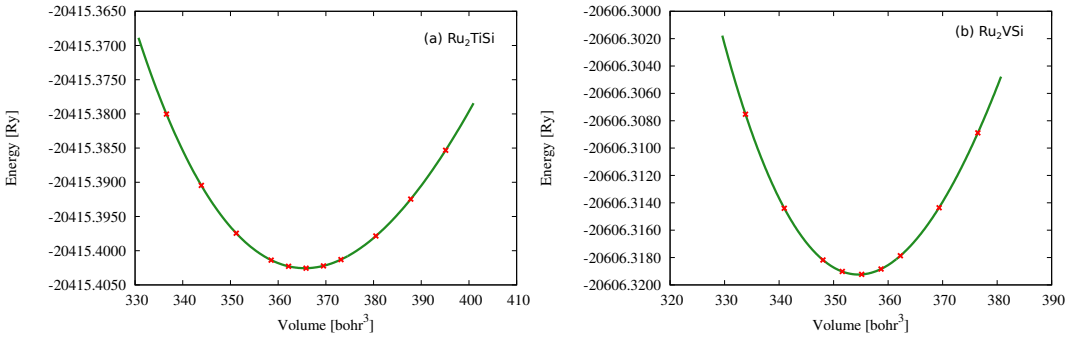

Figure 6.2: Volume optimization of Ru_2TiSi and Ru_2VSi

lowest point of the Figure 6.2, where the equilibrium lattice parameter is extracted.

6.2 Elastic properties

After energy minimization and by the software IRelast package, we have calculated elastic constants C_{11}, C_{12} and C_{44} that give connection between the mechanical and the dynamical properties of solids. In addition elastic anisotropy factor A, anisotropy percentage A_G, Cauchy's pressure, Young's modulus E, ductility modulus G, Poisson's ratio ν, B/G ratio and bulk modulus (B) are calculated and listed in Table 6.1

The two compounds satisfy the cubic lattice conditions $C_{11} - C_{12} > 0$, $C_{11} > 0$,

$C_{44} > 0$, $C_{11} + 2C_{12} > 0$ and $C_{12} < B < C_{11}$ [96–98]. That is the indication of the mechanical stability of the two material. Elastic anisotropy factor for Ru_2TiSi and Ru_2VSi has deflected from 1 as 0.772 and 0.935. So Ru_2VSi is nearly perfectly isotropic materials. As the value of A_G is 0.008 and 0.0005 that implies the two system is isotropic. From Poisson's ratio ν is 0.214, 0.244 for Ru_2TiSi and Ru_2VSi respectively that indicate Ru_2VSi is elastic up to the elastic limit. These materials has brittle nature as the poisson's ratio $\nu < 0.26$. The ratio B/G <1.75 for Ru_2TiSi and Ru_2VSi that's why these materials are brittle nature [103, 104]. For both compounds obey Cauchy's pressure greater than zero and $B/G > 0$ which indicate metallic bonding [119].

Table 6.1: Lattice constnats a_0, Band gap, Fermi energy E_f, the estimated elastic constants C_{11}, C_{12} and C_{44}, the bulk modulus (B), the elastic anisotropy factor (A), the percentage of anisotropy A_G, Cauchy's pressure, Young's modulus (E), the shear modulus (G), B/G ratio and Poisson's ratio ν for Ru_2TiSi and Ru_2VSi

Specification	Ru_2TiSi	Ru_2VSi
a_0	6.0065	5.9455
Band gap (ev)	0.0	0.0
Fermi energy(eV)	0.9400172065	0.9643782562
C_{11}(GPa)	447.2505	402.0528
C_{12}(GPa)	129.6341	160.6862
C_{44}(GPa)	122.6498	112.8782
B(GPa)	192.295	187.5796
A	0.772	0.935
A_G	0.008	0.0005
Cauchy's pressure	6.984	47.808
E(GPa)	330.215	288.397
G(GPa)	136.026	115.938
B/G	1.414	1.618
ν	0.214	0.244

6.3 Electronic properties

The electronic band structure of Ru_2TiSi Figure 6.3(a) and Figure 6.3(b) for up spin and down spin channel are semiconducting behavior. It is noticed that the band is not overlap between conduction band and valence band in the Fermi level for both spin channel in the Figure 6.3 (a) and b. So both of the up spin and down spin channel is semiconductor nature [120] type as there is a direct band gap and the indirect band gap is 0 eV. In up spin channel Figure 6.3(c) at least one conduction band hybridized with the valence band across the Fermi level absolutely which has been observed the nature of metallic behavior and down spin channel Figure 6.3(d) where conduction band minimum crosses the Fermi level for Ru_2VSi as there is a direct band gap and zero value of indirect band gap between the valence band maximum and conduction band minimum. So Ru_2VSi has semiconducting property [121, 122] property in the down spin channel. The energy bands ranging from -4 to -1 eV and 0 to +3 eV in both alloys are assigned to the strong hybridization of Ru, Ti and V d orbital with s and p orbital of Silicon. The d orbital contribution in the band structure at the Fermi level is more than the other atoms orbital contain in the system. The width of the energy gap can be calculated using the energies of the highest occupied band at the γ point and the lowest unoccupied band at the X point [123].

The contribution of density of states Figure 6.4 (a) at the Fermi level is low in both majority spin channel and minority spin channel of Ru_2TiSi. With the increasing of eV at 0.4 eV the corresponding DOS peaks of 4.4 eV for Ru_2TiSi Total DOS and 2.5 eV, 2.1 eV, 0.1 eV for Ti, Ru and silicon atomic DOS for up spin and down spin channel. At Fermi level each atomic DOS curve has a negligible value for up spin and down spin channel which shows antiferromagnetic semiconductor type [124].

The significant symmetric DOS curve for up spin and down spin channel in the Fermi level implies the zero magnetic moment of the Ru_2TiSi. The magnetic moment of Ru_2TiSi is low for all atom and the total magnetic moment is zero which shows antiferromagnetic nature. The total DOS contribution of Ru_2VSi Figure6.4(e) for up spin is high and down spin is low corresponding Ru_2VSi Total DOS and atomic

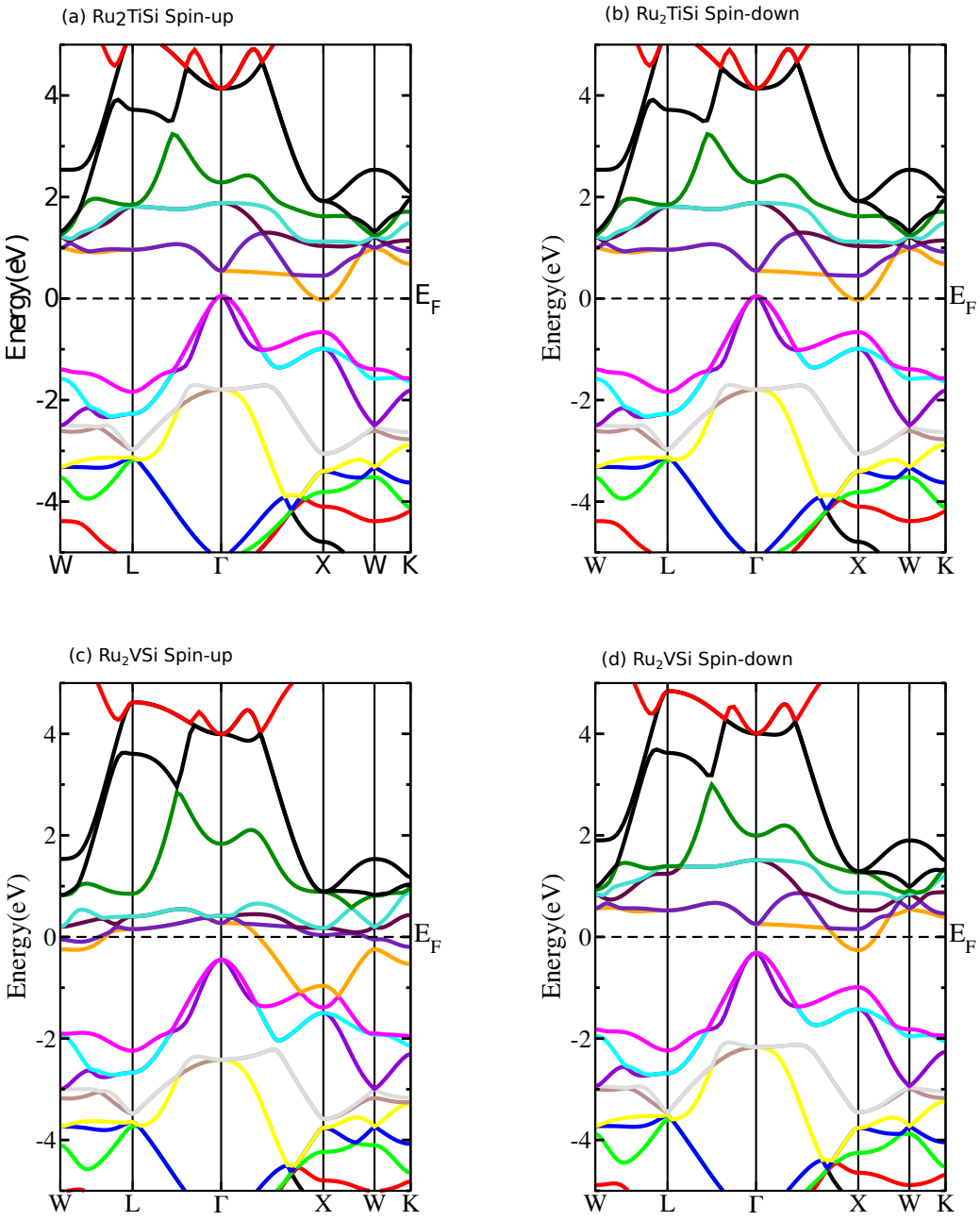

Figure 6.3: Spin-polarized band structures along the high symmetry directions in the Brillouin zone of (a, b) Ru_2TiSi and (c, d) Ru_2VSi at their predicted equilibrium lattice constants for the up and down spin.

DOS of Ru, V and silicon atom in the Fermi level Figure 6.4 (e), (f), (g) and (h). It is observed that there is unsymmetrical distributions of DOS figure 6.4 on both spin channels indicating magnetic characteristics. As the contribution of density of states in the majority spin channel is high and significantly low in the down spin channel so these compound is not completely spin polarized. The spin polarization

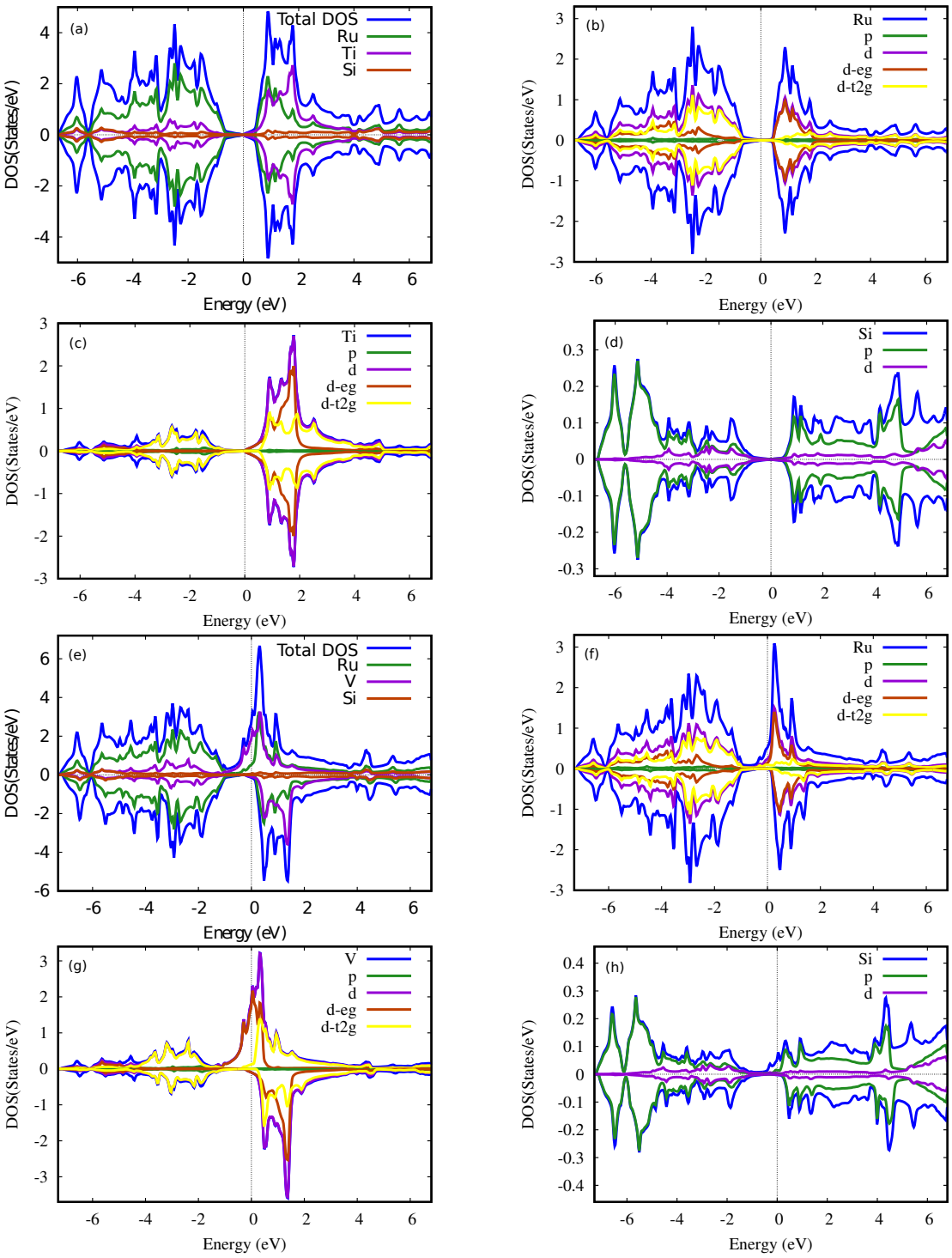

Figure 6.4: Total Density and partial density of states (a, h) of spin polarized Ru_2TiSi and Ru_2VSi system

(p) at Fermi energy (E_f) of a material [125] is defined by equation as follows

$$p = \frac{N\uparrow(E_f) - \downarrow N(E_f)}{N\uparrow(E_f) + N\downarrow(E_f)} \tag{6.1}$$

where N ↑ (E_f) and N ↓ (E_f) are the spin-dependent den-sity of states at E_f and ↑ and ↓ represent the majority and minority states, respectively. Whereas the value of (P) < 1 for these material, therefore these material is not completely spin polarized. But for true half-metal P=1, therefore 100% spin polarization. As the asymmetry of DOS that for up spin channel is maximum and down spin channel is minimum. This character is dominated by vanadium [126].

6.3.1 Magnetic moment

The magnet moment for Ru_2TiSi is zero that shows antiferromagnetic nature and the corresponding contribution of density of states in the Fermi level is very low. The magnetic moment of vanadium is 0.91477 Table 6.2 then the up spin channel changed with higher density of states with asymmetry Figure 6.4 (e). As the DOS is asymmetric nature in Fermi level for Ru_2VSi the net magnetization is not zero [127, 128]. The total magnetic moment 0.96991 for Ru_2VSi which shows ferromagnetic nature. This magnetic moment mainly originate from the d orbital hybridized with p orbital. The valence electron of Ru, Ti, V and Si is 8, 4, 5 and 4 respectively.

The full heusler alloys, the total magnetic moment illustrated with the formula $M_t = Z_t - 24$. In the case of half-heusler alloys the total magnetic moment is described with the formula $M_t = Z_t - 18$ (Slater Pauling rule). Where M_t is the total magnetic moment. Z_t is the total number of valence electron in the unit cell. In conventional antiferromagnets, the electronic band structures and DOS are identical for both spin channel [124]. We see that Ru_2TiSi there is no spin-polarization, while in the half-metallic antiferromagnet, the electronic structures are completely asymmetric, resulting in 100% spin-polarization [129–131]. The valence electron of the two system and experimental value from the table shows that they don't obey the Slater Pauling rule [132, 133].

Table 6.2: Magnetic Moment for the corresponding systems (Ru_2TiSi, Ru_2VSi) atoms

System	Magnetic moment (μ_B)				
	Sphere − 1	Sphere − 2	Sphere − 3	Interstitial	Total
Ru_2VSi	−0.02879	0.91477	0.00217	0.11054	0.96991

6.4 Optical properties

The complex dielectric tensor relation is [134]

$$\varepsilon_{ij}(\omega) = \varepsilon'_{ij}(\omega) + \varepsilon''_{ij}(\omega) \tag{6.2}$$

ε'_{ij} is the real part of complex dielectric tensor about polarization, dispersion, store energy and release energy of electromagnetic wave. ε''_{ij} is the imaginary part of complex dielectric tensor $\varepsilon_{ij}(\omega)$ which is associated with absorbed energy when electromagnetic wave penetrate into the compounds. In real dielectric tensor the store energy is high Figure 6.5 (c) at IR to visible range. So in this region the refractive index has been the highest value.

The imaginary part of dielectric tensor gives a high peak at visible spectrum (1.77-3.1 eV) after this it decreases in Ultraviolet region at 10 eV for both alloys Figure 6.5(d). This means the visible spectrum is absorbed in the compounds and extinction coefficient 6.5 (h) is also high in visible spectrum as the visible light gets weaker and absorbed. The complex refractive index of these metal is real part of refractive index ($n(\omega)$) and another is the imaginary part of refractive index, which is so called the extinction coefficient. However the refractive index is related to the relative permittivity $n(\omega) = n + k(\omega)$. The refractive index is vital importance in refractometer, solar cells, photonic crystal and telescope. In the Figure 6.5 (g) the energy range 0.3 eV, the real part of refraction index decreases drastically [122].

It has observed that, Real dielectric tensor ($\mathrm{Re}\varepsilon_{ij}(\omega)$) has roots at 0.4 eV for Ru_2VSi and the curves goes down at point 3.5 eV and 3.8 eV for Ru_2VSi, Ru_2TiSi respectively. Where ($\mathrm{Re}\varepsilon_{ij}(\omega)$)=0. At 0 value of real dielectric tensor, these compound Figure 6.5(c) does not respond to incident light, which is mainly due to the plasmon

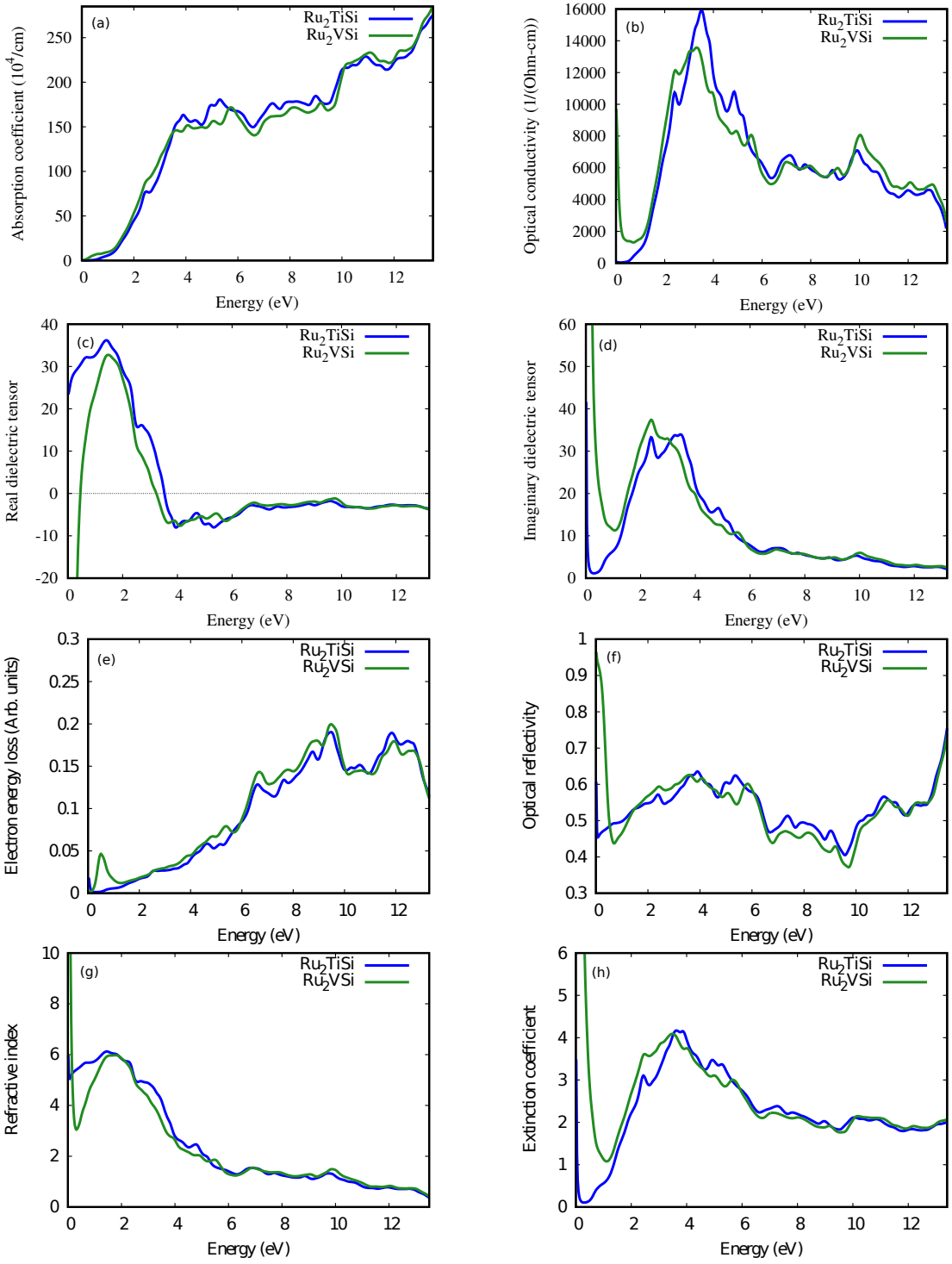

Figure 6.5: Absorption coefficient ($I(\omega)$), Optical conductivity ($\sigma(\omega)$), the real and imaginary part of dielectric tensor $\epsilon_{ij}(\omega)$, Electron energy loss function ($L(\omega)$), Optical reflectivity ($\rho(\omega)$), Refractive index, Extinction coefficient for Ru_2TiSi and Ru_2VSi compounds.

oscillations [135]. For the values greater than 3.8 eV the ($Re\varepsilon_{ij}(\omega)$) is negative for both compounds; thus the element would be opaque. The precise peak in Eloss

right after 6 eV is the evidence of opaqueness of the compounds Figure 6.5 (e). The polarization of electron also changed at high energy region.

The Imaginary dielectric tensor $\mathrm{Im}\varepsilon_{ij}(\omega)$ curves for the two alloys Figure 6.5(d) indicates the passage of electron from an occupied level to an unoccupied level. The absorption coefficient ($I(\omega)$) Figure 6.5 (a) represent the absorbed light in the infrared and visible region are rapidly high at 1 eV to 4 eV; the electron transition here is also rapid. In the UV limit the absorption get saturated value. The optical conductivity curve define the absorbed light spent to enhance the conductivity in the high energy limit 6.5 (b).

Since there is a production of electron and hole pair then the conductivity increases. The decreasing of extinction coefficient ($K(\omega)$) in the ultra-violet region clarifies the "super-luminescence" phe-nomenon. So the release and absorption of spectrum is also high. In infrared spectrum the reflectivity decrease sharply for Ru_2VSi. In optical reflectivity ($\rho(\omega)$) curve drop sharply and optical conductivity ($\sigma(\omega)$) curve arisen with sharp peak at point 10 eV because of inter band transitions 6.5 (b) and 6.5 (f). The all diagrams in the infrared, visible and UV regimes the Ru_2TiSi response to incident photons is higher than Rh_2VSi. The electron energy loss ($L(\omega)$) at high energy region is high as the crystal is excited and heat up. After 12.5 eV the electron energy loss curve decreases sharply.

Chapter 7

Exploration of Rh_2TiSi and Rh_2VSi

7.1 Structural properties

The Rhodium based heusler alloys space group (225, $Fm\bar{3}m$), where the four FCC sub lattices are inserted each other in Figure 7.1. The Figure 7.2 shows the Calculated energy of Rh_2TiSi and Rh_2VSi compounds as a function of the unit cell volume. The Rh atom has two positions one at X_2(1/4, 1/4, 1/4) and another is far from the first position at X_2(3/4, 3/4, 3/4). The Titanium and Vanadium position at Y(1/2, 1/2, 1/2) and the Silicon position are at Z(0, 0, 0).

The lattice constants are obtained from the Energy vs Volume diagram with the help of equation $a_o = \sqrt[3]{4V} \times (0.529)(\text{Å})$. Where V is equilibrium volume. It is evident that the minimization of energy is held at the lowest point in the volume optimized curve, where the equilibrium lattice parameter is also extracted. The lattice parameter of the Rh_2 TiSi and Rh_2VSi system is 6.0897 Å and 6.0177 Å respectively.

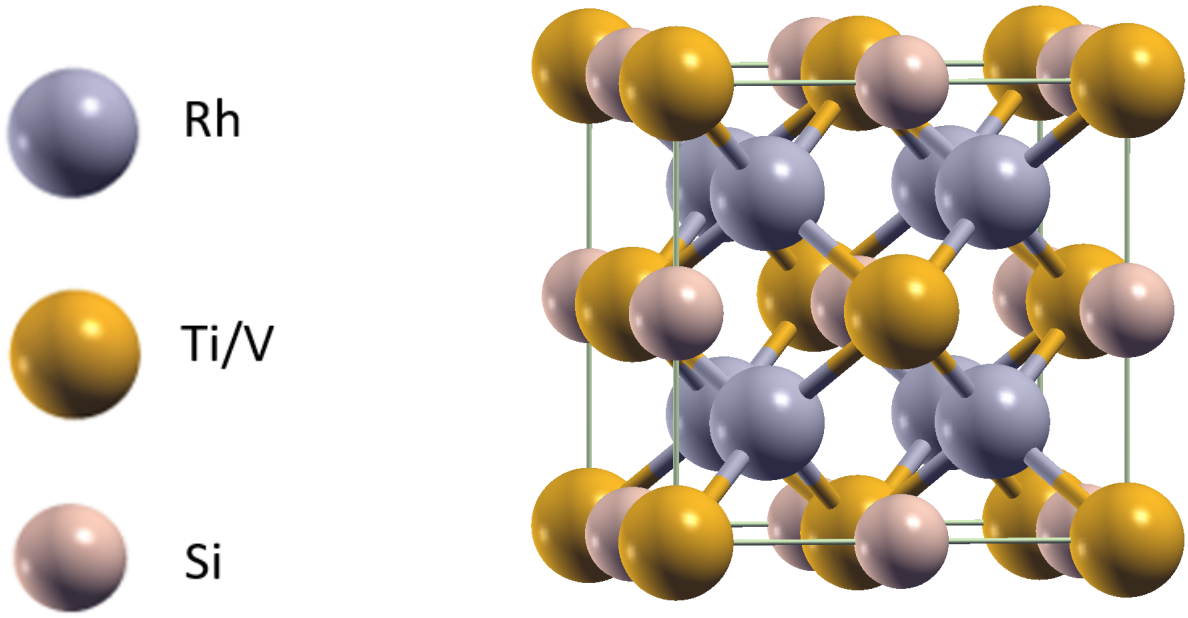

Figure 7.1: Structure of Rh_2TiSi and Rh_2VSi

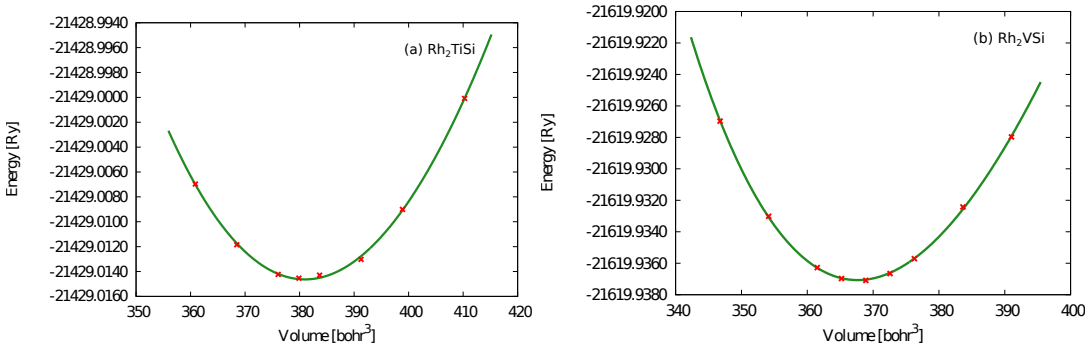

Figure 7.2: Volume optimization of Rh_2TiSi and Rh_2VSi

7.2 Elastic properties

The calculated elastic constants C_{11}, C_{12} and C_{44} that signifies about the mechanical stability and the atomic behavior of these two system. we also calculated elastic anisotropy factor A, anisotropy percent A_G, Cauchy's pressure, Young's modulus E, ductility modulus G, Poisson's ratio ν, B/G ratio and bulk modulus (B) (show Table 7.1). Rh_2TiSi and Rh_2VSi do not satisfy the stable cubic lattice conditions $C_{11} - C_{12} > 0$ and $C_{12} < B < C_{11}$ except $C_{11} > 0$, $C_{44} > 0$, $C_{11} + 2C_{12} > 0$ [96] therefore it indicates the mechanically unstable structure. Elastic anisotropy factor for Rh_2TiSi and Rh_2VSi is -0.414, -1.282 respectively has deviated from unity that indicate anisotropy of the materials. The percentage of anisotropy A_G is -1.379, -

0.951 correspondingly for the two system is highly anisotropic. For both compounds Cauchy's pressure greater than zero and $B/G > 0$ for metallic bonding [119]. It can be noted that poisson's ratio for Rh_2VSi is negative that the material has high energy absorber and gain resistance to fracture. Therefore Rh_2TiSi material has higher B/G ratio than the ductility condition $B/G > 1.75$ and it's Poisson's ratio $\nu > 0.26$ so this material is ductile behavior. The Rh_2VSi compound has $B/G < 1.75$ that is the exhibition of brittle nature [103, 104].

Table 7.1: Lattice constnats a_0, Band gap, Fermi energy E_f, the estimated elastic constants is C_{11}, C_{12}, C_{44}, the bulk modulus (B), Elastic anisotropy factor (A), the percentage of anisotropy A_G, Cauchy's pressure, Young's modulus (E), the shear modulus (G), B/G ratio and Poisson's ratio ν for Rh_2TiSi and Rh_2vSi

Specification	Rh_2TiSi	Rh_2VSi
a_0	6.0897	6.0177
Band gap (ev)	0.0	0.0
Fermi energy(eV)	0.8340274500	0.8712044174
C_{11}(GPa)	23.3461	115.1180
C_{12}(GPa)	263.5755	254.4935
C_{44}(GPa)	49.6839	89.3178
B(GPa)	95.641	123.204
A	-0.414	-1.282
A_G	-1.379	-0.951
Cauchy's pressure	213.892	165.176
E(GPa)	123.472	650.335
G(GPa)	48.05	524.256
B/G	1.99	0.235
ν	0.285	-0.379

7.3 Electronic properties

The electronic band structure of Rh_2TiSi for up spin and down spin channel are given in 7.3 (a) and Figure 7.3 (b) respectively. It is pointed out that the band is overlap

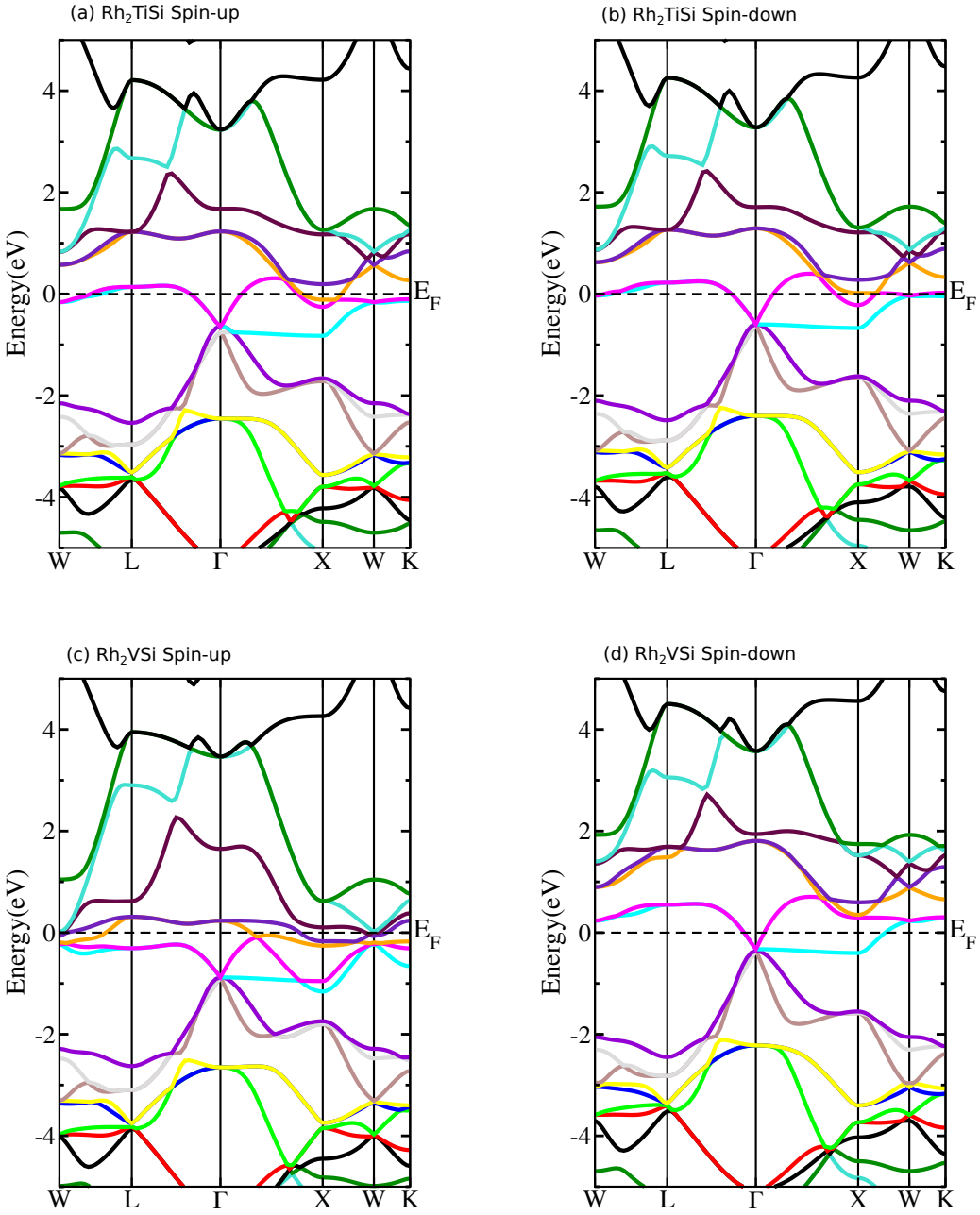

Figure 7.3: Spin-polarized band structures along the high symmetry directions in the Brillouin zone of (a, b) Rh_2TiSi and (c, d) Rh_2VSi at their predicted equilibrium lattice constants for the up and down spin channel.

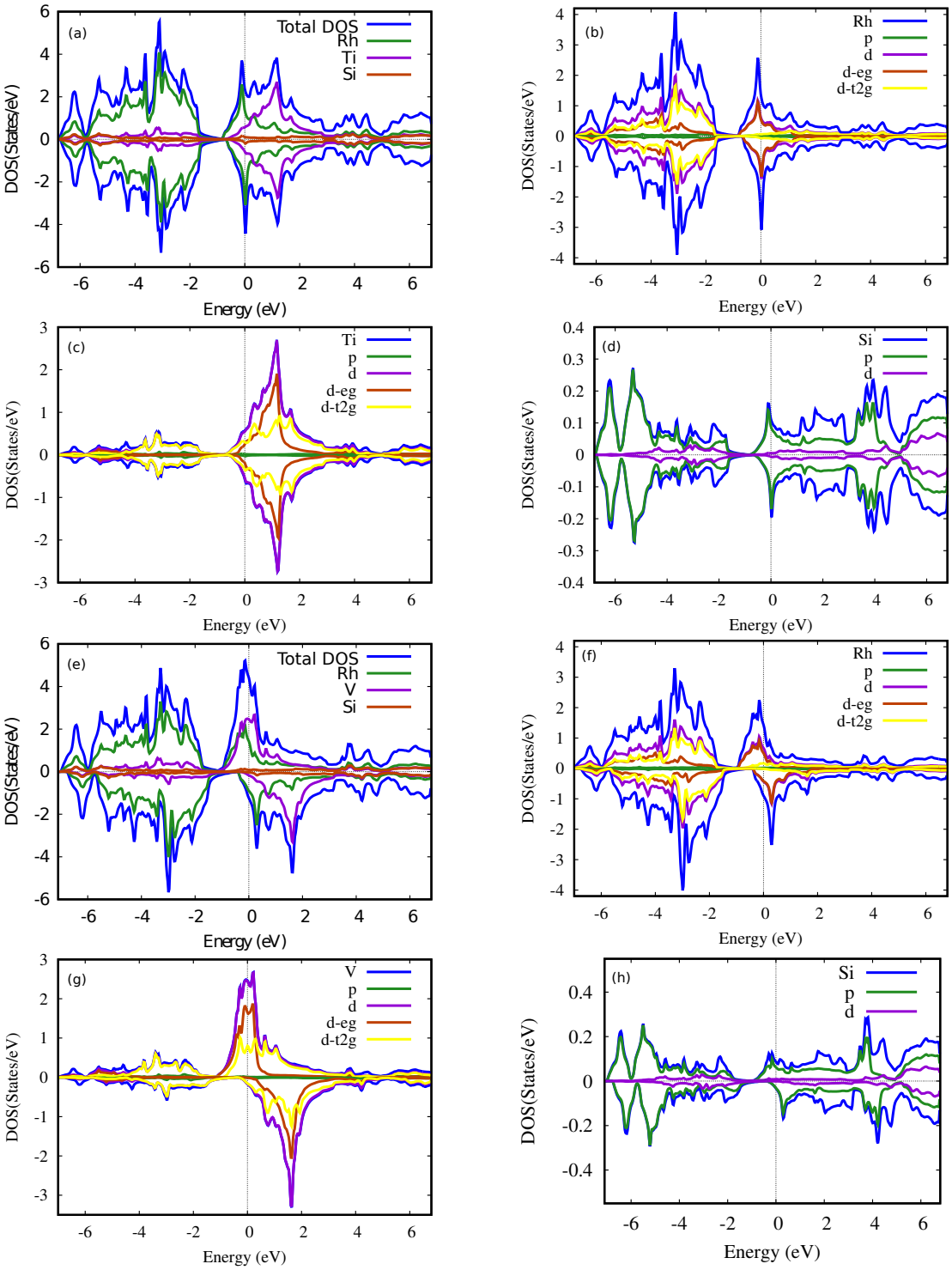

Figure 7.4: Total Density and partial density of states (a, h) of spin polarized Rh_2TiSi and Rh_2VSi system

in the Fermi level and the band intersection, intraband transition are occurred. So both of the up spin and down spin channel is metallic nature. In this band structure d orbital contribution is more than the other atoms orbital contain in the system

at the Fermi level. As the band gap 0 eV between the valence band maximum and conduction band minimum [136]. The bottom of the conduction band and the apex of the valence band touches each other below the fermi level.

With the increasing of energy at 1.3 eV the corresponding DOS peaks value arisen 3.8, 2.3, 1 and 0.1 (States/eV) of Rh_2TiSi total DOS and individual atomic DOS of Ti, Rh and silicon for up spin and down spin channel Figure 7.4(a). However the slightly asymmetric DOS behaviour in both spin channel shows the total magnetic moment of Rh_2TiSi has significant value.

The spin polarization (p) at Fermi energy (E_f) of a material is defined by equation as follows

$$p = \frac{N\uparrow(E_f) - \downarrow N(E_f)}{N\uparrow(E_f) + N\downarrow(E_f)} \tag{7.1}$$

where $N\uparrow(E_f)$ and $N\downarrow(E_f)$ are the spin-dependent density of states at E_f and $\uparrow$ and $\downarrow$ represent the majority and minority states respectively. When both spin channel has different definite DOS value, there is no complete spin-polarization. As we observed for the identical DOS of Rh_2TiSi and asymmetric DOS of Rh_2VSi for both spin channel, the spin polarization of Rh_2TiSi compound is close to zero. In Fermi level E_f for full spin-polarization (P =100%) the DOS $N\uparrow E_f$ or $N\downarrow E_f$ is equal to zero.

For the significant asymmetric DOS curve Figure 7.4 (f), (g) for both spin channels in the Fermi level, there is a net magnetization. After having the major DOS contribution in the Fermi level the above two systems is said to be metallic nature.

7.3.1 Magnetic moment

In the two system, it is evident that the magnetic moment has a variation given in Table 7.2. For the Rh_2TiSi the magnetic moment of is paramagnetic nature, as the magnetic moment is low, positive value [137]. Moreover the total magnetic moment of Rh_2VSi is ferromagnetic nature since the total magnetic moment 2.52978 for unsymmetrical DOS at the Fermi level [138]. This magnetic moments mainly originates from the d orbital of atoms. The valence electron of the two system and

experimental value from the table for the two system shows that they don't obey the Slater Pauling rule, for the full heusler alloys formula $M_t = Z_t - 24$. Since theoretically the total number of valence electron in Rh_2TiSi is 26 and the M_t value is 2. The total number of valence electron in Rh_2VSi is 27 and the M_t value is 3.

Table 7.2: Magnetic Moment for the corresponding systems (Rh_2TiSi, Rh_2VSi) atoms

System	Magnetic moment (μ_B)				
	Sphere − 1	Sphere − 2	Sphere − 3	Interstitial	Total
Rh_2TiSi	0.13156	0.03951	0.01454	0.02476	0.34193
Rh_2VSi	0.43437	1.45107	0.01627	0.19370	2.52978

7.4 Optical Properties

The optical property of Rh_2TiSi and Rh_2VSi has also been observed, for instance the Optical conductivity ($\sigma(\omega)$), Electron energy loss function ($L(\omega)$), Refractive index ($n(\omega)$), Absorption coefficient($I(\omega)$), Complex dielectric tensor $\varepsilon_{ij}(\omega)$ [139], Extinction coefficient ($K(\omega)$), Optical reflectivity ($\rho(\omega)$), Real dielectric tensor ε'_{ij}, Imaginary dielectric tensor ε''_{ij} are investigated With the help of FP-LAPW method and generalized gradient approximation (GGA).

The real part of $\varepsilon_{ij}(\omega)$ is (Re$\varepsilon_{ij}(\omega)$) for both Rh_2TiSi and Rh_2VSi compounds in Figure 7.5 (c). The fixed part of dielectric tensor arise to infinity which signifies the facts [140]. Firstly, both compounds have shown metallic behavior, in the energy range 0 to 0.6 eV denotes the loss of light in the crystal medium for both crystal compounds. It is seen that (Re$\varepsilon_{ij}(\omega)$) has roots 0.3 eV and 0.6 eV for Rh_2TiSi and Rh_2VSi respectively and the curves goes down at 3.80 eV, where (Re$\varepsilon_{ij}(\omega)$)=0. So for IR to visible energy region the absorption energy is high that is suitable for using self capacitance. At 0 value of real dielectric tensor, these compound does not respond to incident light, where the fact is mainly due to the plasmon oscillations and energy absorption. Comparing with the Figure 7.5 (e) (electron energy loss) one

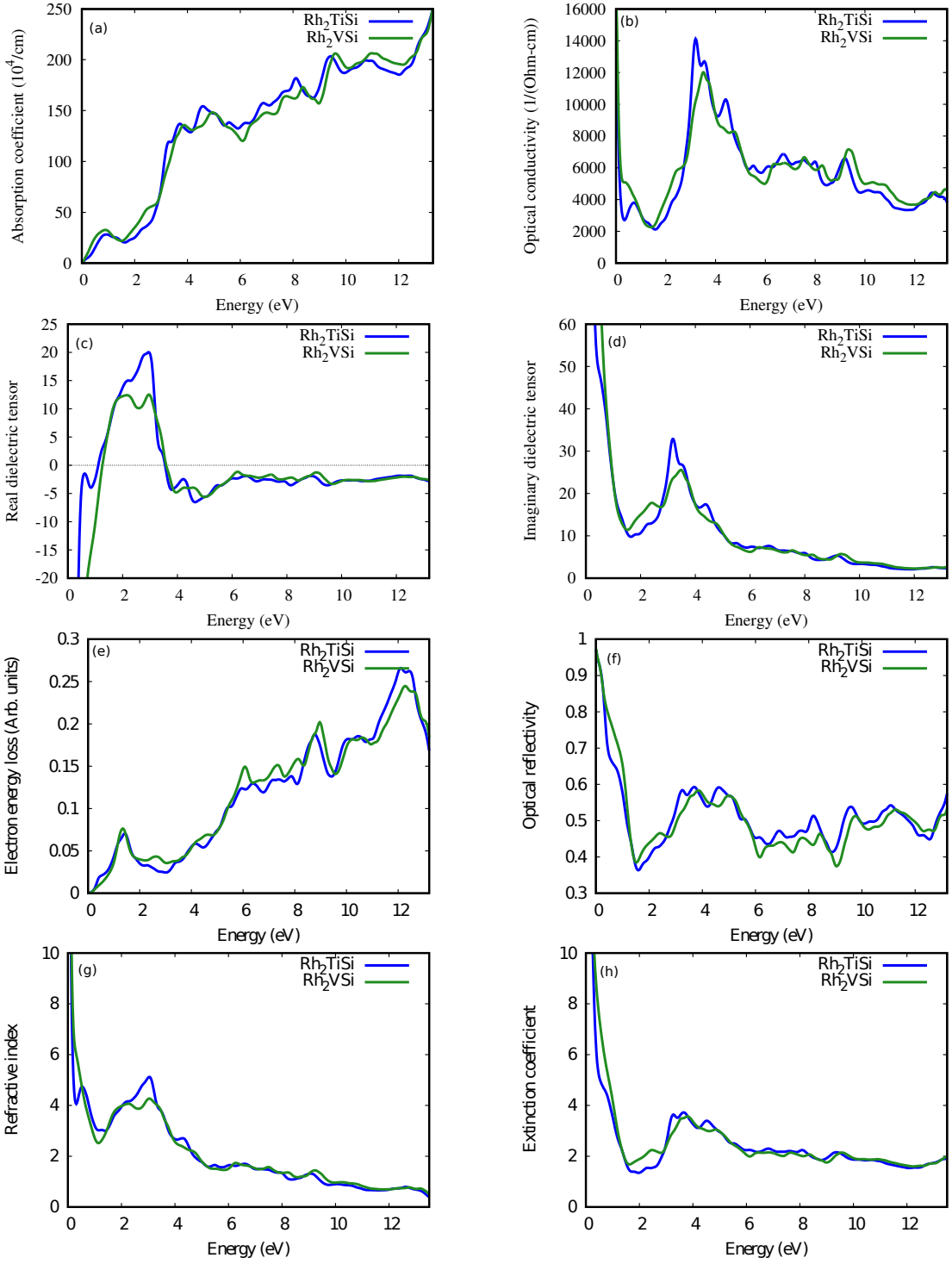

Figure 7.5: Absorption coefficient ($I(\omega)$), Optical conductivity ($\sigma(\omega)$), the real and imaginary part of dielectric tensor $\varepsilon_{ij}(\omega)$, Electron energy loss function ($L(\omega)$), Optical reflectivity ($\rho(\omega)$), Refractive index, Extinction coefficient for Rh_2TiSi and Rh_2VSi compounds.

can deduced that there is a pick arisen at point 1.6 eV and the relative permittivity is increasing from 1.6 eV. The fundamental positive response occurred in infrared

spectrum 1.77 eV and visible (1.77-3.1 eV) spectrum for both compounds. That means the polarization and store energy is increased Figure 7.5 (c) at visible region indicate high refractive index Figure 7.5 (g). For the values larger than 3.8 eV the ($Re\varepsilon_{ij}(\omega)$) is negative for both alloys; thus the crystal would be opaque. The intense peak in Eloss after 3.8 eV is the sign of opaqueness of the crystals.

Low energy state of incident photon, the electrons are transmitted in intra-band region shows $Im\varepsilon_{ij}(\omega)$ curves Figure 7.5 (d). But in the value of energy 1.4 eV, one observe the rapid decrease of $Im\varepsilon_{ij}(\omega)$ curves for both compounds which again indicates the plasmon oscillation. As the response of passages of electron occurred at at large region (1.4 eV) it has the property of metals. Moreover at high energy region the electron get scattered by atom so the electron energy loss is high in Figure 7.5 (e). With the increasing the energy of incident photons, the electron transition in visible spectrum range is significantly increased for both compounds, so that the electron transition peak of 3.5 eV and 3.8 eV for Rh_2TiSi and Rh_2VSi respectively is observed. Below IR region and at visible region $Im\varepsilon_{ij}(\omega)$ is high that shows the large wave and visible light gets attenuated during passing through it. So the extinction coefficient below 1.77 eV spectrum is high and absorbed energy is high at visible light.

In the visible range related to $Im\varepsilon_{ij}(\omega)$ and ($Re\varepsilon_{ij}(\omega)$) curves, the Rh_2TiSi response to incident photons is higher than Rh_2VSi alloy. As incident photon frequency higher at UV region (9.3 eV), there are another peaks arisen for both compounds. But for further stimulation, the amplitude of peaks reduces and stopped electron transition in this energy range.

Next to the real part of refraction index [141] are clarified in Figure 7.5 (g). In the low energy limit, the curve goes to the large value for compact atomic medium. The reflectivity is shown in the Figure 7.5 (f) with proper attention the refractive index is high for both strong metallic properties of these compounds. And decreases for plasmon oscillation. In optical reflectivity curve drop instantly from infrared region 1.77 eV to ultraviolet region because of inter band transitions. Which also the properties of metals. The refractive index of metal compound has real part

of refractive index and the imaginary part of refractive index, which is so called the extinction coefficient mainly the loss of electromagnetic wave in medium. The optical conductivity has the highest value at visible region 7.5 (b). The lowest value of refractive index occurred because of high energy spectrum rather than visible region and here the absorption increases rapidly and also the refractive index decreases.

Chapter 8

Conclusion

We calculated the structural, elastic, electronic, optical and magnetic properties of Copper based Cu_2TiSi and Cu_2ZrGe, Ruthenium based Ru_2TiSi and Ru_2VSi and Rhodium based Rh_2TiSi and Rh_2VSi full heusler alloys by computer simulations with generalized gradient approximation for exchange correlation functions. The FP-LAPW method by PBE-GGA approximation is used for ferromagnetic calculation to find the minimum or ground state energy for the compounds. From these result it is clear that the Cu_2TiSi and Cu_2ZrGe are antiferromagnetic in nature and significant DOS near the Fermi level clarifies the metallic property. The mechanical property of Cu_2TiSi shows elastically stable and Cu_2ZrGe shows fragile in nature. The Ru_2TiSi alloy is antiferromagnetic in nature as the magnetic moment is zero but the symmetrical density of states and direct band gap for both spin channel shows semiconductor property. The Ru_2VSi has positive high magnitude of magnetic moment so these metal shows ferromagnetic properties as the asymmetrical DOS at the Fermi level. As the perfect minimum DOS value in the down spin channel of Ru_2VSi, so which is why these material is not true half-metal. From the band structure of Ru_2VSi these metrial has no gap in up spin channel which indicate metallic property and there is a direct band gap in the down spin channel which shows shows semiconductor property. From the elastic constant other mechanical property is re-

solved. These materials has isotropic but brittle nature from their compound. As the poisson's ratio is lower than 0.26 and B/G ratio is less than 1.75 which denotes these materials has fragile nature. The magnetic moment for Rh_2TiSi is low and Rh_2VSi is high and they are paramagnetic and ferromagnetic nature respectively which are also evident from the density of states for these materials. For engineering purposes Rh_2TiSi can be used as it has high B/G, and poission's ratio. On the contrary Rh_2VSi is brittle nature and highly anisotropic. For all these materials the Cauchy's pressure greater than zero and has metallic bonding. The optical property for all the alloys shows metallic property. The refractive index and polarization in the IR and visible region is high.

List of Abbreviations

BZ	:	Brillouin Zone
DFT	:	Density Functional Theory
DOS	:	Density of States
GGA	:	Generalized Gradient Approximation
HK	:	Hohenberg-Kohn
KS	:	Kohn-Sham
SOC	:	Spin Orbit Coupling
XC	:	Exchange correlation
GMR	:	Giant Magnetoresistance
TMR	:	Tunnel Magnetoresistane
SGS	:	Spin Gapless Semiconductor
AF	:	Antiferromagnetic
NMR	:	Nuclear Magnetic Resonance

List of Abbreviations

EM	:	Electro Magnetic
HDD	:	Hard Disk Drive
NM	:	Non Magnetic
DOS	:	Density of States
PDOS	:	Partial Density of States

Bibliography

[1] Igor Žutić, Jaroslav Fabian, and S Das Sarma. Spintronics: Fundamentals and applications. *Reviews of modern physics*, 76(2):323, 2004.

[2] J De Boeck, Willem Van Roy, Johan Das, V Motsnyi, Zhiyu Liu, Lieven Lagae, H Boeve, K Dessein, and Gustaaf Borghs. Technology and materials issues in semiconductor-based magnetoelectronics. *Semiconductor Science and technology*, 17(4):342, 2002.

[3] RA De Groot and FM Mueller. Pg v. engen, and khj buschow. *Phys. Rev. Lett*, 50(25):2024–2027, 1983.

[4] J Pierre, RV Skolozdra, J Tobola, S Kaprzyk, C Hordequin, MA Kouacou, I Karla, R Currat, and E Lelievre-Berna. Properties on request in semi-heusler phases. *Journal of alloys and compounds*, 262:101–107, 1997.

[5] Friedrich Heusler. Über magnetische manganlegierungen. *Verhandlungen der Deutschen Physikalischen Gesellschaft*, 5:219, 1903.

[6] Nazmiye Kervan. Half-metallicity in the full-heusler co2scp compound: A density functional study. *Journal of magnetism and magnetic materials*, 324(23):4114–4117, 2012.

[7] Ali Bentouaf, Fouad H Hassan, Ali H Reshak, and Brahim Aïssa. First-principles study on the structural, electronic, magnetic and thermodynamic properties of full heusler alloys co2vz (z= al, ga). *Journal of Electronic Materials*, 46(1):130–142, 2017.

[8] A Birsan and V Kuncser. Theoretical investigations of electronic structure and magnetism in zr2cosn full-heusler compound. *Journal of Magnetism and Magnetic Materials*, 388:1–4, 2015.

[9] K Özdog, I Galanakis, et al. First-principles electronic and magnetic properties of the half-metallic antiferromagnet cr2mnsb. *Journal of magnetism and magnetic materials*, 321(15):L34–L36, 2009.

[10] P. W. Leech and P. Ressel. *Application to Semiconductor Devices*, pages 435–454. Springer Berlin Heidelberg, Berlin, Heidelberg, 2003.

[11] I Galanakis, PH Dederichs, and N Papanikolaou. Slater-pauling behavior and origin of the half-metallicity of the full-heusler alloys. *Physical Review B*, 66(17):174429, 2002.

[12] J Kübler, GH Fecher, and C Felser. Understanding the trend in the curie temperatures of co 2-based heusler compounds: Ab initio calculations. *Physical Review B*, 76(2):024414, 2007.

[13] Wei Zhang, Lei Zhao, Zhengnan Qian, Yu Sui, Yuqiang Liu, Wenhui Su, Ming Zhang, Zhuhong Liu, Guodong Liu, and Guangheng Wu. Magnetic properties of the heusler alloy co2tial synthesized by melt-spinning technique. *Journal of alloys and compounds*, 431(1-2):65–67, 2007.

[14] Tanja Graf, Gerhard H Fecher, Joachim Barth, Jürgen Winterlik, and Claudia Felser. Electronic structure and transport properties of the heusler compound co2tial. *Journal of Physics D: Applied Physics*, 42(8):084003, 2009.

[15] DP Rai and RK Thapa. A first principle calculation of full-heusler alloy co2tial: Lsda. *International Scholarly Research Notices*, 2012, 2012.

[16] R.Y. Umetsu, K. Kobayashi, R. Kainuma, Y. Yamaguchi, K. Ohoyama, A. Sakuma, and K. Ishida. Powder neutron diffraction studies for the l21 phase of co2yga (y=ti, v, cr, mn and fe) heusler alloys. *Journal of Alloys and Compounds*, 499(1):1–6, 2010.

[17] Hong Pei Han. Ferromagnetic material of the nearly half-metallic alloy co2tiga. In *Advanced Materials Research*, volume 690, pages 590–593. Trans Tech Publ, 2013.

[18] Jaroslav Fabian, Alex Matos-Abiague, Christian Ertler, Peter Stano, and Igor Zutic. Semiconductor spintronics. *arXiv preprint arXiv:0711.1461*, 2007.

[19] E. Schrödinger. An undulatory theory of the mechanics of atoms and molecules. *Phys. Rev.*, 28:1049–1070, Dec 1926.

[20] Matthias Bartelmann, Björn Feuerbacher, Timm Krüger, Dieter Lüst, Anton Rebhan, and Andreas Wipf. *Theoretische Physik 3— Quantenmechanik*. Springer, 2018.

[21] D.J. Griffiths and P.D.J. Griffiths. *Introduction to Quantum Mechanics*. Pearson international edition. Pearson Prentice Hall, 2005.

[22] Max Born. Quantum mechanics of collision processes. *Uspekhi Fizich*, 1926.

[23] Wolfram Koch and MC Holthausen. A chemist's guide to density functional theory, 2001, 1989.

[24] Wolfgang Pauli. The connection between spin and statistics. *Physical Review*, 58(8):716, 1940.

[25] Arthur Jabs. Connecting spin and statistics in quantum mechanics. *Foundations of Physics*, 40(7):776–792, 2010.

[26] Attila Szabo and Neil S Ostlund. Modern quantum chemistry: introduction to advanced electronic structure theory. Technical report, 1996.

[27] Wolfgang Pauli. On the connexion between the completion of electron groups in an atom with the complex structure of spectra. *Zeitschrift für Physik*, 31:765, 1925.

[28] Nouredine Zettili. Quantum mechanics: concepts and applications, 2003.

[29] Klaus Capelle. A bird's-eye view of density-functional theory. *arXiv preprint cond-mat/0211443*, 2002.

[30] Donald Allan McQuarrie and John Douglas Simon. *Physical chemistry: a molecular approach*, volume 1.

[31] Max Born and Robert Oppenheimer. Zur quantentheorie der molekeln. *Annalen der physik*, 389(20):457–484, 1927.

[32] Hubert Klar et al. The born-oppenheimer approximation revisited. *Journal of Applied Mathematics and Physics*, 8(08):1507, 2020.

[33] Torsten Fliesbach. *Mechanik: Lehrbuch Zur Theoretischen Physik I*. Spektrum Akademischer Verlag, 2009.

[34] F. Schwabl. *Quantenmechanik (QM I): Eine Einführung*. Springer-Lehrbuch. Springer Berlin Heidelberg, 2007.

[35] Paul Adrien Maurice Dirac. A new notation for quantum mechanics. In *Mathematical Proceedings of the Cambridge Philosophical Society*, volume 35, pages 416–418. Cambridge University Press, 1939.

[36] David J Griffiths and Darrell F Schroeter. *Introduction to quantum mechanics*. Cambridge university press, 2018.

[37] Christian B Lang and Norbert Pucker. *Mathematische methoden in der physik*, volume 2. Springer, 2005.

[38] Attila Szabo and Neil S Ostlund. *Modern quantum chemistry: introduction to advanced electronic structure theory*. Courier Corporation, 2012.

[39] Eva Pavarini, Erik Koch, and Ulrich Schollwöck. *Emergent Phenomena in Correlated Matter: Autumn School Organized by the Forschungszentrum Jülich and the German Research School for Simulation Sciences at Forschungszentrum Jülich 23-27 September 2013; Lecture Notes of the Autumn School Correlated Electrons 2013*, volume 3. Forschungszentrum Jülich, 2013.

[40] Walter Kohn. Nobel lecture: Electronic structure of matter—wave functions and density functionals. *Reviews of Modern Physics*, 71(5):1253, 1999.

[41] Per-Olov Löwdin. Scaling problem, virial theorem, and connected relations in quantum mechanics. *Journal of Molecular Spectroscopy*, 3(1-6):46–66, 1959.

[42] Björn O Roos. *Lecture notes in quantum chemistry*, volume 58. Springer, 1992.

[43] Pierre Hohenberg and Walter Kohn. Inhomogeneous electron gas. *Physical review*, 136(3B):B864, 1964.

[44] Jan Adriaan Berger. *Current-density functionals in extended systems*. University Library Groningen][Host], 2006.

[45] Walter Kohn. Density functional theory: Basic results and some observations. In *Density Functional Methods In Physics*, pages 1–9. Springer, 1985.

[46] Juan Carlos Cuevas. Introduction to density functional theory. *Universität Karlsruhe, Germany*, 2010.

[47] Klaus Capelle. A bird's-eye view of density-functional theory. *Brazilian journal of physics*, 36:1318–1343, 2006.

[48] OV Gritsenko and EJ Baerends. The spin-unrestricted molecular kohn–sham solution and the analogue of koopmans's theorem for open-shell molecules. *The Journal of chemical physics*, 120(18):8364–8372, 2004.

[49] Philip Peter Rushton. *Towards a non-local density functiona description of exchange and correlation*. PhD thesis, Durham University, 2002.

[50] Mel Levy. Universal variational functionals of electron densities, first-order density matrices, and natural spin-orbitals and solution of the v-representability problem. *Proceedings of the National Academy of Sciences*, 76(12):6062–6065, 1979.

[51] Elliott H Lieb. Density functionals for coulomb systems. In *Inequalities*, pages 269–303. Springer, 2002.

[52] Robert G Parr et al. W. yang density functional theory of atoms and molecules. *Oxford University Press*, 1:1989, 1989.

[53] Eugene S Kryachko and Eduardo V Ludeña. *Energy density functional theory of many-electron systems*, volume 4. Springer Science & Business Media, 2012.

[54] Zenebe Assefa Tsegaye. Density functional theory studies of electronic and optical properties of zns alloyed with mn and cr. Master's thesis, Institutt for fysikk, 2012.

[55] L. Mehdaoui, R. Miloua, M. Khadraoui, M.O. Bensaid, D. Abdelkader, F. Chiker, and A. Bouzidi. Theoretical analysis of electronic, optical, photo-voltaic and thermoelectric properties of agbis2. *Physica B: Condensed Matter*, 564:114–124, 2019.

[56] A. D. Becke. Density-functional exchange-energy approximation with correct asymptotic behavior. *Phys. Rev. A*, 38:3098–3100, Sep 1988.

[57] John P. Perdew, J. A. Chevary, S. H. Vosko, Koblar A. Jackson, Mark R. Pederson, D. J. Singh, and Carlos Fiolhais. Atoms, molecules, solids, and surfaces: Applications of the generalized gradient approximation for exchange and correlation. *Phys. Rev. B*, 46:6671–6687, Sep 1992.

[58] John P. Perdew, Kieron Burke, and Matthias Ernzerhof. Generalized gradient approximation made simple. *Phys. Rev. Lett.*, 77:3865–3868, Oct 1996.

[59] U von Barth and L Hedin. A local exchange-correlation potential for the spin polarized case. i. *Journal of Physics C: Solid State Physics*, 5(13):1629, jul 1972.

[60] Vladimir I Anisimov, F Aryasetiawan, and A I Lichtenstein. First-principles calculations of the electronic structure and spectra of strongly correlated systems: the lda+ u method. *Journal of Physics: Condensed Matter*, 9(4):767, jan 1997.

[61] Local-density functional and on-site correlations: The electronic structure of la2cuo4 and lacuo3, author = Czyzyk and G. A. Sawatzky, journal = Phys. Rev. B, volume = 49, issue = 20, pages = 14211–14228, numpages = 0, year = 1994, month = May, publisher = American Physical Society, doi = 10.1103/PhysRevB.49.14211, url = https://link.aps.org/doi/10.1103/PhysRevB.49.14211.

[62] Vlasdimir I Anisimov, IV Solovyev, MA Korotin, MT Czyzyk, and GA Sawatzky. Density-functional theory and nio photoemission spectra. *Physical Review B*, 48(23):16929, 1993.

[63] Erik R Ylvisaker, Warren E Pickett, and Klaus Koepernik. Anisotropy and magnetism in the lsda+ u method. *Physical Review B*, 79(3):035103, 2009.

[64] A Szabo and NS Ostlund. Modern quantum chemistry. macgraw-hill, 1989.

[65] John P Perdew and Stefan Kurth. Density functionals for non-relativistic coulomb systems in the new century. In *A primer in density functional theory*, pages 1–55. Springer, 2003.

[66] Thomas L Gilbert. Hohenberg-kohn theorem for nonlocal external potentials. *Physical Review B*, 12(6):2111, 1975.

[67] John E Harriman. Orthonormal orbitals for the representation of an arbitrary density. *Physical Review A*, 24(2):680, 1981.

[68] Elliott H Lieb. Density functionals for coulomb systems. In *Density Functional Methods In Physics*, pages 31–80. Springer, 1985.

[69] John P Perdew and Mel Levy. Extrema of the density functional for the energy: Excited states from the ground-state theory. *Physical Review B*, 31(10):6264, 1985.

[70] Ivan Andrejkovics and A Nagy. Excitation energies in density functional theory: comparison of several methods for the h2o, n2, co and c2h4 molecules. *Chemical physics letters*, 296(5-6):489–493, 1998.

[71] Mel Levy and Agnes Nagy. Variational density-functional theory for an individual excited state. *Physical review letters*, 83(21):4361, 1999.

[72] K Capelle. Variational calculation of many-body wave functions and energies from density functional theory. *The Journal of chemical physics*, 119(3):1285–1288, 2003.

[73] C-O Almbladh, U Von Barth, and R Van Leeuwen. Variational total energies from ϕ-and ψ-derivable theories. *International Journal of Modern Physics B*, 13(05n06):535–541, 1999.

[74] Erich Runge and Eberhard KU Gross. Density-functional theory for time-dependent systems. *Physical Review Letters*, 52(12):997, 1984.

[75] O Krogh Andersen. Linear methods in band theory. *Physical Review B*, 12(8):3060, 1975.

[76] Ch Seidel. Highlights of condensed-matter theory. proceedings of the international school of physics "enrico fermi", course lxxxix at varenna on lake como, 28 june-16 july 1983. hg. von f. bassani, f. fumi und mp tosi. isbn 0-444-86976-x. amsterdam/oxford/new york/tokyo: North holland physics publishing 1985. xviii, 916 s., lwd., dfl. 340.00. *Acta Polymerica*, 38(10):588–588, 1987.

[77] OK Andersen and T Saha-Dasgupta. Muffin-tin orbitals of arbitrary order. *Physical Review B*, 62(24):R16219, 2000.

[78] Eva Zurek, Ove Jepsen, and Ole Krogh Andersen. Muffin-tin orbital wannier-like functions for insulators and metals. *ChemPhysChem*, 6(9):1934–1942, 2005.

[79] Tosio Kato. On the eigenfunctions of many-particle systems in quantum mechanics. *Communications on Pure and Applied Mathematics*, 10(2):151–177, 1957.

[80] Norman Henry March. *Self-consistent fields in atoms: Hartree and Thomas–Fermi atoms*. Elsevier, 2016.

[81] John A Pople. Nobel lecture: Quantum chemical models. *Reviews of Modern Physics*, 71(5):1267, 1999.

[82] Thom H Dunning Jr. Gaussian basis sets for use in correlated molecular calculations. i. the atoms boron through neon and hydrogen. *The Journal of chemical physics*, 90(2):1007–1023, 1989.

[83] ABF da Silva and M Trsic. Universal gaussian and slater-type bases for h to xe based on the generator coordinate hartree–fock method. i. ground and certain low-lying excited states of the neutral atoms. *Mol Phys*, 68:433–445, 1989.

[84] FE Jorge, EVR De Castro, and ABF Da Silva. A universal gaussian basis set for atoms cerium through lawrencium generated with the generator coordinate hartree–fock method. *Journal of computational chemistry*, 18(13):1565–1569, 1997.

[85] Giovanni B Bachelet and M Schlüter. Relativistic norm-conserving pseudopotentials. *Physical Review B*, 25(4):2103, 1982.

[86] Leonard Kleinman and DM Bylander. Efficacious form for model pseudopotentials. *Physical Review Letters*, 48(20):1425, 1982.

[87] David Vanderbilt. Soft self-consistent pseudopotentials in a generalized eigenvalue formalism. *Physical review B*, 41(11):7892, 1990.

[88] Norman Troullier and José Luís Martins. Efficient pseudopotentials for plane-wave calculations. *Physical review B*, 43(3):1993, 1991.

[89] Warren E Pickett. Pseudopotential methods in condensed matter applications. *Computer Physics Reports*, 9(3):115–197, 1989.

[90] D Porezag, MR Pederson, and AY Liu. The accuracy of the pseudopotential approximation within density-functional theory. *Computer Simulation of Materials at Atomic Level*, pages 219–230, 2000.

[91] Mike C Payne, Michael P Teter, Douglas C Allan, TA Arias, and ad JD Joannopoulos. Iterative minimization techniques for ab initio total-energy

calculations: molecular dynamics and conjugate gradients. *Reviews of modern physics*, 64(4):1045, 1992.

[92] D Singh. Planes waves, pseudopotentials and the lapw, 1994.

[93] Peter Blaha, Karlheinz Schwarz, Georg KH Madsen, Dieter Kvasnicka, Joachim Luitz, et al. wien2k. *An augmented plane wave+ local orbitals program for calculating crystal properties*, 60, 2001.

[94] Aron J Cohen, Paula Mori-Sánchez, and Weitao Yang. Challenges for density functional theory. *Chemical reviews*, 112(1):289–320, 2012.

[95] I Galanakis. Surface properties of the half-and full-heusler alloys. *Journal of Physics: Condensed Matter*, 14(25):6329, 2002.

[96] Mahsa Afsari, Arash Boochani, and Mohammadreza Hantezadeh. Electronic, optical and elastic properties of cubic perovskite cspbi3: Using first principles study. *Optik*, 127(23):11433–11443, 2016.

[97] A. Akriche, H. Bouafia, S. Hiadsi, B. Abidri, B. Sahli, M. Elchikh, M.A. Timaoui, and B. Djebour. First-principles study of mechanical, exchange interactions and the robustness in co2mnsi full heusler compounds. *Journal of Magnetism and Magnetic Materials*, 422:13–19, 2017.

[98] Ju-Yong Jong, Jingchuan Zhu, Myong-Gil Jon, Yi Zhou, JinGuk Kim, and Jihong Yan. Theoretical investigation of stabilities and physical properties of low cost fe-based full-heusler materials. *Journal of Alloys and Compounds*, 693:462–467, 2017.

[99] A. Abada, K. Amara, S. Hiadsi, and B. Amrani. First principles study of a new half-metallic ferrimagnets mn2-based full heusler compounds: Mn2zrsi and mn2zrge. *Journal of Magnetism and Magnetic Materials*, 388:59–67, 2015.

[100] A. Hamidani, B. Bennecer, and B. Boutarfa. Structural and elastic properties of the half-heusler compounds irmnz (z=al, sn and sb). *Materials Chemistry and Physics*, 114(2):732–735, 2009.

[101] K. Benkaddour, A. Chahed, A. Amar, H. Rozale, A. Lakdja, O. Benhelal, and A. Sayede. First-principles study of structural, elastic, thermodynamic, electronic and magnetic properties for the quaternary heusler alloys corufez (z = si, ge, sn). *Journal of Alloys and Compounds*, 687:211–220, 2016.

[102] S.F. Pugh. Xcii. relations between the elastic moduli and the plastic properties of polycrystalline pure metals. *The London, Edinburgh, and Dublin Philosophical Magazine and Journal of Science*, 45(367):823–843, 1954.

[103] Ericmoore Jossou, Linu Malakkal, Barbara Szpunar, Dotun Oladimeji, and Jerzy A. Szpunar. A first principles study of the electronic structure, elastic and thermal properties of ub2. *Journal of Nuclear Materials*, 490:41–48, 2017.

[104] Volodymyr Ivashchenko, Patrice Turchi, and V. Shevchenko. Phase transformation b1 to b2 in tic, tin, zrc and zrn under pressure. *Condensed Matter Physics*, 16, 09 2013.

[105] J.-C. Charlier, X. Gonze, and J.-P. Michenaud. First-principles study of the electronic properties of graphite. *Phys. Rev. B*, 43:4579–4589, Feb 1991.

[106] AH Reshak and Sikander Azam. Theoretical study of the structural, electronic structure, fermi surface, electronic charge density and optical properties of the of lnvo4 (ln= sm, eu, gd and dy). *Int. J. Electrochem. Sci*, 8:10396–10423, 2013.

[107] R. E. Dietz, H. Kamimura, M. D. Sturge, and A. Yariv. Electronic structure of copper impurities in zno. *Phys. Rev.*, 132:1559–1569, Nov 1963.

[108] Cr R Brundle, M Be Robin, and Harold Basch. Electronic energies and electronic structures of the fluoromethanes. *The Journal of Chemical Physics*, 53(6):2196–2213, 1970.

[109] F Werfel and O Brümmer. Corundum structure oxides studied by xps. *Physica Scripta*, 28(1):92, 1983.

[110] Muhammed E Gulduren. *Fabrication and Characterization of Thermoelectric Nanolayer Thin Films Modified By MeV Si Ions*. The University of Alabama in Huntsville, 2014.

[111] Nzar Rauf Abdullah, Mohammad T Kareem, Hunar Omar Rashid, Andrei Manolescu, and Vidar Gudmundsson. Spin-polarised dft modeling of electronic, magnetic, thermal and optical properties of silicene doped with transition metals. *Physica E: Low-dimensional Systems and Nanostructures*, 129:114644, 2021.

[112] Mark Fox. Optical properties of solids. 2002.

[113] Frederick Wooten. *Optical properties of solids*. Academic press, 2013.

[114] AL Efros and Boris I Shklovskii. Critical behaviour of conductivity and dielectric constant near the metal-non-metal transition threshold. *Physica status solidi (b)*, 76(2):475–485, 1976.

[115] John Henry Poynting. Xv. on the transfer of energy in the electromagnetic field. *Philosophical Transactions of the Royal Society of London*, (175):343–361, 1884.

[116] Stephen Ducharme. An inside-out approach to storing electrostatic energy. *ACS nano*, 3(9):2447–2450, 2009.

[117] A Amudhavalli, R Rajeswarapalanichamy, K Iyakutti, and AK Kushwaha. First principles study of structural and optoelectronic properties of li based half heusler alloys. *Computational Condensed Matter*, 14:55–66, 2018.

[118] MS Dresselhaus et al. Solid state physics part ii optical properties of solids. *Lecture Notes (Massachusetts Institute of Technology, Cambridge, MA)*, 17:15–16, 2001.

[119] M. Eberhart and Travis Jones. Cauchy pressure and the generalized bonding model for nonmagnetic bcc transition metals. *Physical Review B*, 86, 10 2012.

[120] Xiaotian Wang, Zhenxiang Cheng, Jianli Wang, Xiao-Lin Wang, and Guodong Liu. Recent advances in the heusler based spin-gapless semiconductors. *Journal of Materials Chemistry C*, 4(30):7176–7192, 2016.

[121] Dibya Rai and R. Thapa. Author's personal copy an investigation of semiconducting behavior in the minority spin of co 2 crz (z = ga, ge, as): Lsda and lsda + u method. *Journal of Alloys and Compounds*, 542, 07 2013.

[122] Arash Anjami, Arash Boochani, Seyed Moahammad Elahi, and Hossein Akbari. Ab-initio study of mechanical, half-metallic and optical properties of mn2zrx (x= ge, si) compounds. *Results in physics*, 7:3522–3529, 2017.

[123] Selçuk Kervan and Nazmiye Kervan. Spintronic properties of the ti2cob heusler compound by density functional theory. *Solid state communications*, 151(17):1162–1164, 2011.

[124] Tariq Hadji, Hafid Khalfoun, Habib Rached, and Ahmed Azzouz-Rached. Spin gapless semiconductor and nearly spin semimetal antiferromagnets: The case of the inverse heusler compounds mn2liz (z = al and ga). *Materials Research Bulletin*, 143:111461, 2021.

[125] RJ Soulen Jr, JM Byers, MS Osofsky, B Nadgorny, T Ambrose, SF Cheng, Pr R Broussard, CT Tanaka, J Nowak, JS Moodera, et al. Measuring the spin polarization of a metal with a superconducting point contact. *science*, 282(5386):85–88, 1998.

[126] K Özdogan, I Galanakis, E Şaşioglu, and B Aktaş. Search for half-metallic ferrimagnetism in v-based heusler alloys mn2vz (z= al, ga, in, si, ge, sn). *Journal of Physics: Condensed Matter*, 18(10):2905, 2006.

[127] Arash Yari, Mahboubeh Yeganeh, Firouzeh Motamad Dezfuli, and Arash Boochani. Investigation of the stability, electronic structure, and magnetic properties of sc2vz (z= ge, si) heusler alloys: First-principles calculations. *Materials Science and Engineering: B*, 267:115096, 2021.

[128] Michelle E Jamer, Yung Jui Wang, Gregory M Stephen, Ian J McDonald, Alexander J Grutter, George E Sterbinsky, Dario A Arena, Julie A Borchers, Brian J Kirby, Laura H Lewis, et al. Compensated ferrimagnetism in the zero-moment heusler alloy mn 3 al. *Physical Review Applied*, 7(6):064036, 2017.

[129] H Van Leuken and RA De Groot. Half-metallic antiferromagnets. *Physical review letters*, 74(7):1171, 1995.

[130] I Galanakis, K Özdoğan, E Şaşıoğlu, and Bekur Aktaş. Doping of mn 2 v al and mn 2 v si heusler alloys as a route to half-metallic antiferromagnetism. *Physical Review B*, 75(9):092407, 2007.

[131] Li Guan-Nan and Jin Ying-Jiu. First-principles study on the half-metallicity of half-heusler alloys: Xyz (x= mn, ni; y= cr, mn; z= as, sb). *Chinese Physics Letters*, 26(10):107101, 2009.

[132] I. Galanakis, P. H. Dederichs, and N. Papanikolaou. Slater-pauling behavior and origin of the half-metallicity of the full-heusler alloys. *Phys. Rev. B*, 66:174429, Nov 2002.

[133] Iosif Galanakis and Peter H Dederichs. Half-metallicity and slater-pauling behavior in the ferromagnetic heusler alloys. pages 1–39, 2005.

[134] Vladimir M Agranovich and Vitaly Ginzburg. *Crystal optics with spatial dispersion, and excitons*, volume 42. Springer Science & Business Media, 2013.

[135] S Naderizadeh, SM Elahi, MR Abolhassani, F Kanjouri, N Rahimi, and J Jalilian. Electronic and optical properties of full-heusler alloy fe3- xmnxsi. *The European Physical Journal B*, 85(5):1–7, 2012.

[136] Gerhard H Fecher and Claudia Felser. Substituting the main group element in cobalt–iron based heusler alloys: Co2feal1- xsix. *Journal of Physics D: Applied Physics*, 40(6):1582, 2007.

[137] R Meenakshi, R Aram Senthil Srinivasan, A Amudhavalli, R Rajeswarapalanichamy, and K Iyakutti. Electronic structure, magnetic, optical and transport properties of half-heusler alloys rhfez (z= p, as, sb, sn, si, ge, ga, in, al)–a dft study. *Phase Transitions*, 94(6-8):415–435, 2021.

[138] Idris Hamid Bhat, Saleem Yousuf, Tahir Mohiuddin Bhat, and Dinesh C Gupta. Investigation of electronic structure, magnetic and transport properties of half-metallic mn2cusi and mn2znsi heusler alloys. *Journal of Magnetism and Magnetic Materials*, 395:81–88, 2015.

[139] Farhana Mostari, Md Atikur Rahman, and Rukayia Khatun. First principles study on the structural, elastic, electronic and optical properties of cubic 'half-heusler'alloy ruvas under pressure. *Int. J. Mat. Math. Sci*, 2(4):51–63, 2020.

[140] M Dadsetani, S Namjoo, and H Nejati. Optical study of filled tetrahedral compounds li3aln2 and li3gan2. *Journal of electronic materials*, 39(8):1186–1193, 2010.

[141] A Dhawan, JF Muth, DN Leonard, MD Gerhold, J Gleeson, T Vo-Dinh, and PE Russell. Focused ion beam fabrication of metallic nanostructures on end faces of optical fibers for chemical sensing applications. *Journal of Vacuum Science & Technology B: Microelectronics and Nanometer Structures Processing, Measurement, and Phenomena*, 26(6):2168–2173, 2008.

Appendix A

Complex dielectric function relation

As the complex dielectric function relation is [134],

$$\epsilon_{ij} = \epsilon'_{ij} + \epsilon''_{ij}$$

$$D_i = \epsilon_{ij} E_j$$

In this case ,it is taken into account of the frequency dispersion , so the much better approximation is.

$$\epsilon_{ij}(\omega) = \epsilon'_{ij}(\omega) + \epsilon''_{ij}(\omega)$$

ϵ'_{ij} is the real part of complex dielectric constant function.ϵ''_{ij} is the imaginary part of complex dielectric constant function which is associated with energy loss for passing the wave into the medium.

Then take spatial dispersion as well as frequency dispersion into account, within the limits of linear theory. This implies the validity of the equations

$$\epsilon_{ij}(\omega, K) = \epsilon'_{ij}(\omega, K) + \epsilon''_{ij}(\omega, K)$$

$$D_i(\omega, K) = \epsilon_{ij} E_j(\omega, K)$$

Moreover, the function $\epsilon_{ij}(\omega, K)$ determines the energy loss a particle is subject to when moving through matter, the molecular forces between bodies, and the fluctuations of the electromagnetie field. Thus, it characterizes the medium (crystal) very completely.

The behaviour of a dielectric material to an external electric field is characterized by three macroscopic vectors: The electric field strength ε; the polarization $\mathbf{P}$ and the electric displacement D. [112]

The microscopic report of the material is determined primarily by the polarization. As a result of this, the first attempt in all the examples treated by electromagnetism in this book is to calculate $\mathbf{P}$. The dielectric constant ϵ_r is then determined from $\mathbf{P}$, and the optical properties are deduced from ϵ_r.

The polarization is expressed as the net dipole moment per unit volume. The application of a field produces a polarization by the forces asserted on the positive and negative charges of the atoms that are apprehended within the medium. If the atoms have permanent dipole moments, the field will affect a torque to these randomly orientated dipoles and want to align them along the field direction. If there are no permanent dipoles, the field will push the positive and negative charges in opposite directions and induce a dipole parallel to the field. In either case, the ultimate result is the same: the application of the field tends to produce many microscopic dipoles aligned parallel to the direction of the external field. This generates a net dipole moment within the dielectric, and hence a polarization.

The microscopic dipoles will all tend to align along the field direction, and so the polarization vector will be parallel to $\boldsymbol{\varepsilon}$. This allows us to write:

$$\mathbf{P} = \epsilon_0 \times \mathcal{E} \tag{A.1}$$

where ϵ_0 is the electric permittivity of free space and χ is the electric susceptibility of the medium.

Equation A. 1 creates two assumptions that need a brief word of explanation.(1) We have assumed that the medium is isotropic, even though we know that some

materials are anisotropic. In particular, anisotropic crystals have preferred non-equivalent axes, and P will not necessarily be parallel 10& (2) We have assumed that **P** varies linearly with $\boldsymbol{E}$. This will not always be the case. In particular, if the optical intensity is very large, we can enter the dominion of nonlinear optics, in which eqn A. 1 is not valid.

Both of these qualifications introduce unnecessary complications at this stage, and are not considered further in this appendix. The electric displacement **D** of the medium is related to the electric field $\boldsymbol{E}$ and polarization **P** through:

$$\mathrm{D} = \epsilon_0 \boldsymbol{Q} + \mathbf{P} \tag{A.2}$$

This may be considered to be the definition of D. By combining eqns A.I and A.2, we can write:

$$\mathrm{D} = \epsilon_0 \epsilon_r \boldsymbol{\varepsilon} \tag{A.3}$$

where

$$\epsilon_r = 1 + x. \tag{A.4}$$

ϵ_r is the relative dielectric constant of the medium, and is an extremely important parameter in the explanation of the propagation of light through dielectrics. In electrostatic problems we are frequently interested in calculating the spatial dependence of electric field, and hence the electric potential V, from the free charge density ϱ. This calculation can be performed by using the Poisson equation:

$$\nabla^2 V = -\frac{Q}{\epsilon_r \epsilon_0} \tag{A.5}$$

Poisson's cquation is derived from Gauss's law of electrostatics:

$$\nabla - \boldsymbol{\varepsilon} = \frac{e}{\epsilon_r \epsilon_0} \tag{A.6}$$

We recall that the electric fteld strength is the gradient of the potential:

$$\varepsilon = -\nabla V \tag{A.7}$$

Equation A.5 follows directly by substituting for $\boldsymbol{E}$ in eqn A.6 using eqn A.7. Once we know V, we can then determine ε from eqn A. 7. This approach is also useful when we are considering devices in which the potential across the device is fixed by an external voltage source. The response of a material to external magnetic fields is treated in a similar way to the response of dielectrics to electric fields. The magnetization $\mathbf{M}$ of the medium is proportional to the magnetic field strength H through the magnetic susceptibility X_M :

$$\mathbf{M} = XM\mathbf{H} \tag{A.8}$$

The magnetic flux density $\mathbf{B}$ is related to $\mathbf{H}$ and $\mathbf{M}$ through:

$$\begin{aligned} \mathbf{B} &= \mu_0(\mathbf{H} + \mathbf{M}) \\ &= \mu_0 \left(1 + \chi_M\right) \mathbf{H} \\ &= \mu_0 \mu_r \mathbf{H} \end{aligned} \tag{A.9}$$

where μ_0 is the magnetic permeability of the vacuum and $\mu_r = 1 + \chi_M$ is the relative magnctic permeability of the medium. $\mu_0 = 4\pi \times 10^{-7}\mathrm{Hm}^{-1}$ in SI units. The laws that deduce the combined electric and magnetic response of a medium are summarized in Maxwell's equations of electromagnetism:

$$\nabla \cdot \mathbf{D} = e \tag{A.10}$$

$$\nabla \cdot \mathbf{B} = 0 \tag{A.11}$$

$$\nabla \times \boldsymbol{\varepsilon} = -\frac{\partial \mathbf{B}}{\partial t} \tag{A.12}$$

$$\nabla \times \mathbf{H} = \mathbf{j} + \frac{\partial \mathbf{D}}{\partial t} \tag{A.13}$$

where Q is the free charge density, and j is the current density. The first of these four equations is Gauss's law of electrostatics (equ A.6) written in terms of D rather than $\boldsymbol{E}$. The second is the equivalent of Gauss's law for magnetostatics with the assumption that free magnetic monopoles do not exist. The third equation combines

the Faraday and Lenz laws of electromagnetic induction. The fourth is a statement of Ampere's law, with the second term on the right hand side to account for the displacement current.

The second Maxwell equation naturally leads to the concept of the vector potential. This is defined through the equation

$$B = \nabla \times A \tag{A.14}$$

We see that the vector potential A automatically satisfies eqn A.11, because $\nabla \cdot (\nabla \times \mathbf{A}) = 0$ for all $\mathbf{A}$. However, this definition does not define $\mathbf{A}$ uniquely, We can add any vector of the form $\nabla\varphi$ to A without changing B. This follows because

$$\nabla \times (\mathbf{A} + \nabla\varphi) = \nabla \times \mathbf{A} + \nabla \times (\nabla\varphi) = \nabla \times \mathbf{A}. \tag{A.15}$$

$\varphi(\mathbf{r})$ can be any scalar function of $\mathbf{r}$. For this reason, we have to give an additional definition, which specifies the gauge in which we are working. The Coulomb gauge is defined by

$$\nabla \cdot \mathbf{A} = 0 \tag{A.16}$$

This gauge is a convenient one because it allows us to derive a simple relationship between $\boldsymbol{E}$ and $\mathbf{A}$. By substituting for $\mathbf{B}$ in the third Maxwell equation (eqn A.12) using eqn A.14, we see that:

$$\nabla \times \boldsymbol{E} = -\frac{\partial}{\partial t}(\nabla \times \mathbf{A}) = \nabla \times \left(-\frac{\partial \mathbf{A}}{\partial t}\right) \tag{A.17}$$

The solution is

$$\varepsilon = -\frac{\partial A}{\partial t} + \text{ constant} \tag{A.18}$$

where the constant is any vector whose curl is zero. If the electrostatic potential is V, then we can combine eqn $A.18$ with eqn $A.7$ by writing

$$\boldsymbol{\varepsilon} = -\frac{\partial \mathbf{A}}{\partial t} - \nabla V \tag{A.19}$$

This works because $\nabla \times \nabla V = 0$. By taking the divergence of eqn A.19, we can recover Poisson's equation $(A.5)$ if we satisfy eqn $A.16$, that is, if we are in the Coulomb gauge. The more general definition of ε given in eqn A.19 reduces to eqn A. 7 when the magnetic field does not change with time, and to

$$\varepsilon = -\frac{\partial A}{\partial t} \tag{A.20}$$

when the static potential is constant throughout space. The vector potential in the Coulomb gauge is used in the semiclassical treatment of the interaction of light with atoms.

For the electromagnetic wave, Maxwell was able to show that eqns A.10-A.13 were congruent with wavelike solutions in a medium with no free charges or currents. To see this we first simplify eqns A. 12 and A. 13 by setting $\mathbf{j} = 0$ and eliminating B and D using eqns A. 3 and A.9. This gives:

$$\nabla \times \boldsymbol{\varepsilon} = -\mu_0 \mu_r \frac{\partial \mathbf{H}}{\partial t}, \tag{A.21}$$

$$\nabla \times \mathbf{H} = \epsilon_0 \epsilon_r \frac{\partial \boldsymbol{\varepsilon}}{\partial t} \tag{A.22}$$

We then take the curl of eqn A.21 and eliminate $\nabla \times \mathbf{H}$ using eqn A.22. This gives:

$$\nabla \times (\nabla \times \boldsymbol{\varepsilon}) = -\mu_0 \mu_r \epsilon_0 \epsilon_r \frac{\partial^2 \boldsymbol{\varepsilon}}{\partial t^2}. \tag{A.23}$$

The left hand side can be simplified by using the vector identity

$$\nabla \times (\nabla \times \varepsilon) = \nabla(\nabla \cdot \varepsilon) - \nabla^2 \varepsilon. \tag{A.24}$$

Equation A.6 with $Q = 0$ tells us that $\nabla \cdot \varepsilon = 0$. Therefore we obtain the final result:

$$\nabla^2 \boldsymbol{\varepsilon} = \mu_0 \mu_r \epsilon_0 \epsilon_r \frac{\partial^2 \boldsymbol{\varepsilon}}{\partial t^2} \tag{A.25}$$

Equation A. 25 is of the same form as the wave equation:

$$\frac{\partial^2 y}{\partial x^2} = \frac{1}{v^2} \frac{\partial^2 y}{\partial t^2} \tag{A.26}$$

where v is the velocity of the wave. We therefore identify eqn A. 25 as describing clectromagnetic waves with a phase velocity v given by

$$\frac{1}{v^2} = \mu 0 \mu, \epsilon_0 \epsilon_r. \tag{A.27}$$

In free space $\epsilon_r = \mu_r = 1$ and the velocity of the wave is c, so we have:

$$c = \frac{1}{\sqrt{\mu_0 \epsilon_0}} = 2.998 \times 10^8 \text{ m s}^{-1}. \tag{A.28}$$

At the same time, we see from eqns A.27 and A. 28 that the velocity in a medium is given by

$$v = \frac{1}{\sqrt{\epsilon_r \mu_r}} c. \tag{A.29}$$

We define the refractive index n of the medium as the ratio of the velocity of light in free space to the velocity in the medium:

$$n = \frac{c}{v}, \tag{A.30}$$

At optical frequencies we can set $\mu_r = 1$, and thus conclude:

$$n = \sqrt{\epsilon_r}. \tag{A.31}$$

This allows us to relate the propagation constants of electromagnetic waves in a medium to the dielectric constant. The solutions to eqn A. 25 are of the form

$$\varepsilon(z,l) = \varepsilon_0 \mathrm{e}^{i(kz-\omega N)} \tag{A.32}$$

where E_0 is the amplitude of the wave, z is the dir he wave vector, and ω is the angular frequency. The

$$k = \frac{2\pi}{\lambda} = \frac{\omega}{v} = \frac{n\omega}{c} \tag{A.33}$$

$\varepsilon(z,l) = \varepsilon_0 \mathrm{e}^{i(kz-\omega)}$, (A. 32) of the wave, z is the direction of propagation, k is ics and is used extensively throughout this book. Physically measurable quantities are obtained by taking the real part of the complex wave. where λ, is the wavelength inside the medium. The first equality is the definition of k, the second follows by substitution of eqn A. 32 into eqn A. 25 with v given by eqn A.27, and the third follows from the definition of n given in eqn A.30. The energy flow in an electromagnetic wave can be calculated from the Poynting vector:

$$\mathbf{I} = \boldsymbol{E} \times \mathbf{H}. \tag{A.34}$$

intensity of the light wave. The intensity is defined as the energy crossing a unit area in unit time, and is therefore given by:

$$I = v u_v. \tag{A.35}$$

where v is the velocity of the wave and u_v is the energy density per unit volume of the beam. The Poynting vector given by eqn A. 34 can be evaluated easily for the case of plane waves. Consider a wave polarized along the x axis of angular frequency ω propagating in the z direction. From eqn A.21 or A.22 we see that the magnetic field is perpendicular to the electric field. $\boldsymbol{E}$ and $\mathbf{H}$ therefore form a right handed system as depicted in Fig. A.1. Hence the components of the wave must satisfy:

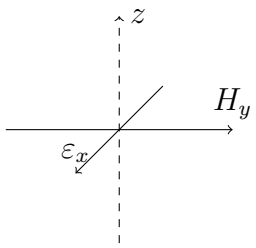

Figure A.1: *The electric and magnetic fields of an electromagnetic wave from a right handed system. The figure shows the directions of the fields in a wave polarized along the x axis and propagating in the z direction*

$$\begin{aligned} \varepsilon_x(z,t) &= \varepsilon_{x0}\mathrm{e}^{(kz-\omega t)} \\ \varepsilon_y(z,t) &= 0 \\ H_x(z,t) &= 0 \\ H_y(z,t) &= H_{y0}\mathrm{e}^{i(kz-\omega t)} \end{aligned} \tag{A.36}$$

On substituting these fields into eqn A.21, we find that:

$$k\varepsilon_{x0} = \mu_o\mu_r\omega H_{y0} \tag{A.37}$$

and hence that

$$H_{y0} = \frac{\varepsilon_{x0}}{Z} \tag{A.38}$$

where

$$Z = \frac{k}{\mu_0\mu_r\omega} = \sqrt{\frac{\mu_0\mu_r}{\epsilon_0\epsilon_r}} = \frac{1}{c\epsilon_0 n}. \tag{A.39}$$

The second equality in eqn A. 39 follows from eqns A.33 and A.27, while the third follows from Eq. A. 28 and A.31 with $\mu_r = 1$. The quantity Z is called the wave impedance. On substituting eqns A. 36− A. 39 into eqn A. 34 , we obtain:

$$I = \frac{\langle\varepsilon(t)^2\rangle_{\mathrm{ms}}}{Z} = \frac{1}{2}c\epsilon_0 n\varepsilon_0^2 \tag{A.40}$$

where $\langle\varepsilon(t)^2\rangle_{\mathrm{ms}}$ represents the root-mean-square time average. This shows that

the intensity of a light wave is proportional to the square of the amplitude of the electric field. The relationship can be generalized for all light waves irrespective of the particular polarization of the beam.

In many topics covered in this book, it will be necessary to treat the refractive index as a complex number. A well-known example of how such a situation arises occurs when treating the propagation of electromagnetic waves through a conducting medium such as a metal. In a conductor, the current density is related to the electric field through the electrical conductivity σ according to:

$$\mathrm{j} = \sigma\varepsilon \tag{A.41}$$

Using this relationship to substitute for j in eqn A.13, and eliminating $\mathbf{D}, \mathbf{B}$ and H in the same way that led to eqn A.25, we obtain:

$$\nabla^2\boldsymbol{\varepsilon} = \sigma\mu_0\mu_r\frac{\partial \boldsymbol{E}}{\partial t} + \mu_0\mu_r\epsilon_0\epsilon_r\frac{\partial^2\boldsymbol{\varepsilon}}{\partial t^2} \tag{A.42}$$

We now look for plane wave solutions of the type given by eqn A.32. Substitution of eqn A. 32 into eqn A. 42 gives:

$$k^2 = i\sigma\mu_0\mu_r\omega + \mu_0\mu_r\epsilon_0\epsilon_r\omega^2 \tag{A.43}$$

This can be made compatible with the usual relationship between ω and k given in eqn A. 33 by allowing n to be a complex number. The complex refractive index is usually written $\tilde{n}$, and is defined by

$$k = n\frac{\omega}{c} \tag{A.44}$$

By combining eqns A.43 and A.44 we obtain:

$$\tilde{n}^2 = \frac{\mu_r\sigma}{\epsilon_0\omega}i + \mu_r\epsilon_r \tag{A.45}$$

Let the electric field for incident, reflected and transmitted electromagnetic beam is ε_x^i,ε_x^r,ε_x^t and simultaneously for magnetic filed the expression is H_y^i,H_y^r,H_y^t.

where we have made use of eqn A.28. This of course reduces to eqn A. 31 if we set $\sigma = 0$ and $\mu_r = 1$. The physical significance of the complex refractive index implied by eqn A.45. The Maxwell equations also allow us to treat the transmission and reflection of light at an interface between two materials. Consider a light ray is incident on dielectric material. Part of the beam is transmitted into the medium and the rest is reflected. The solution for an arbitrary angle of incidence was treated by Fresnel, and the resulting formula are known as Fresnel's equations. We restrict ourselves here to the simpler case when the angle of incidence is zero: that is, normal incidence. We consider again an x-polarized light beam propagating in the z direction, with the field directions as shown in Fig. A.1. The electric and magnetic fields are given by eqn A.36. The beam is incident on a medium with complex refractive index $\tilde{n}$. The fields are related to each other through eqn A.38, with Z given by eqn A.39, although we now have to allow for the possibility that n may be complex. The boundary conditions at the interface between two dielectrics tell us that the tangential components of the electric and magnetic fields are conserved. Applying this to this case, we must have that both ε_x and H_y are conserved across the boundary. Hence we can write:

$$\varepsilon_x^i + \varepsilon_x^r = \varepsilon_{x'}^t \tag{A.46}$$

and

$$H_y^i - H_y^r = H_{y'}^t \tag{A.47}$$

where the superscripts i, r and t refer to the incident, reflected and transmitted beams respectively. By making use of the relationship between the magnetic and electric fields given in eqns A.38-A.39, we can rewrite eqn A.47 as:

$$\varepsilon_x^l - \varepsilon_x' = \bar{n}\varepsilon_x^t \tag{A.48}$$

where we have assumed that the light is incident from air with $\tilde{n} = 1$ and that $\mu_r = 1$ at the optical frequencies of interest here. Equations A.46 and A.48 can be solved together to obtain

$$\frac{\varepsilon_x^r}{\varepsilon_x'} = \frac{\tilde{n}-1}{\bar{n}+1} \tag{A.49}$$

This can be rearranged to obtain the required result for the reflectivity R :

$$R = \left|\frac{\varepsilon_x^r}{\varepsilon_x^i}\right|^2 = \left|\frac{\tilde{n}-1}{\tilde{n}+1}\right|^2 \tag{A.50}$$

Appendix B

Kramers–Kronig relations and dielectric function

The imaginary part of the complex dielectric function ignoring all intra-band transitions would be obtained as [122]

$$\begin{aligned} \mathrm{Im}\,\varepsilon_{\mathrm{ij}}^{\mathrm{inter}}(\omega) = \frac{\mathrm{h}^2\mathrm{e}^2}{\pi \mathrm{m}_\mathrm{e}^2 \omega^2} \sum_{\mathrm{n}} \int \mathrm{dk} \left\langle \Psi_\mathrm{k}^{\mathrm{c_n}} \left| \mathrm{p}^{\mathrm{i}} \right| \Psi_\mathrm{k}^{\mathrm{v_n}} \right\rangle \left\langle \Psi_\mathrm{k}^{\mathrm{v_n}} \left| \mathrm{p}^{\beta} \right| \Psi_\mathrm{k}^{\mathrm{c_n}} \right\rangle \\ \sigma\left(\mathrm{E}_\mathrm{k}^{\mathrm{c_n}} - \mathrm{E}_\mathrm{k}^{\mathrm{v_n}} - \omega\right) \end{aligned} \tag{B.1}$$

It includes the summation of inter-band transitions from occupied valence levels with agent-state $|\Psi_\mathrm{k}^{\mathrm{v}}\rangle$ and agent-value $E_\mathrm{k}^{\mathrm{v}n}$ to unoccupied conduction levels with agent-state $|\Psi_\mathrm{k}^{\mathrm{c}n}\rangle$ and agent-value $E_\mathrm{k}^{\mathrm{c}n}$ where p expressed for momentum operator. The other quantities such as the refraction, absorption, reflection indexes and etc. can be derived using the real or imaginary parts of the dielectric function. With the help of the imaginary part of dielectric function, one can determine the corresponding real part via the Kramers–Kronig relations:

$$\mathrm{Re}\,\varepsilon_{\mathrm{ij}}^{[\mathrm{inter}]}(\omega) = \sigma_{\mathrm{ij}} \frac{2}{\pi} \mathrm{P} \int_0^\infty \frac{\omega\,\mathrm{Im}\,\varepsilon_{\mathrm{ij}(\omega)}}{\omega^2 - \omega^2} \tag{B.2}$$

$$\epsilon_{ij}(\omega) = \epsilon'_{ij}(\omega) + \epsilon''_{ij}(\omega) \tag{B.3}$$

As the equation is mentioned earlier for metallic system. ϵ'_{ij} is the real part of complex dielectric constant function.ϵ''_{ij} is the imaginary part of complex dielectric constant function which is associated with energy loss for passing the wave into the medium.

In which, P demonstrate the principal value of integral. On the other hand, the contribution of metallic intera-band transitions is obtained as follows

$$\mathrm{Im}\,\varepsilon_{\mathrm{ij}}^{[\mathrm{intra}]}(\omega)=\frac{\Gamma\omega_{\mathrm{pl,ij}}^{2}}{\omega\left(\omega^{2}+\Gamma^{2}\right)},\mathrm{Re}\,\varepsilon_{\mathrm{ij}}^{[\mathrm{intra}]}(\omega)=\frac{\omega_{\mathrm{pl,ij}}^{2}}{\omega\left(\omega^{2}+\Gamma^{2}\right)}\omega_{\mathrm{pl}}^{2} \tag{B.4}$$

In this equation,Γ symbolizes the lifetime broadening in Drude model,ω_{pl} implies plasma frequency and n signify electron den-sity. The total dielectric constant function including all interband and intra-band transitions is obtained as follows:

This type of equation is also given before

$$\varepsilon(\omega)=\varepsilon_{\mathrm{ij}}^{[\mathrm{inter}]}(\omega)+\varepsilon_{\mathrm{ij}}^{[\mathrm{in}tra]}(\omega) \tag{B.5}$$

Moreover, the tensor $\epsilon_{ij}(\omega,K)$ determines the energy loss a particle is subject to when moving through matter, the molecular forces between bodies, and the fluctuations of the electromagnetie field. Thus, it characterizes the medium qualitatively. The energy loss of electron through a rapid moving throughout the crystal is described by Eloss function which related to dielec-tric function as follows:

$$(\text{ Eloss }):\mathrm{L}_{\mathrm{ij}}(\omega)=-\,\mathrm{Im}\left\{\frac{1}{\varepsilon_{\mathrm{ij}}(\omega)}\right\}=\frac{\mathrm{Im}\,\varepsilon_{\mathrm{ij}}}{\left(\mathrm{Re}\,\varepsilon_{\mathrm{ij}}\right)^{2}+\left(\mathrm{Im}\,\varepsilon_{\mathrm{ij}}\right)^{2}} \tag{B.6}$$

These interactions include intraband and interband transitions, free electron oscillations, phonon excitations, inner shell ionization and etc. The energy region where the curve transfers from negative to positive values in the diagram of real part of dielectric function corresponds to the plasmon energy. Another calculated optical parameter is coefficient:

$$\mathrm{R}(\omega):\mathrm{R}_{\mathrm{ij}}(\omega)=\left[\frac{\left(\mathrm{Re}\,\varepsilon_{\mathrm{ij}}+\mathrm{i}\,\mathrm{Im}\,\varepsilon_{\mathrm{ij}}\right)^{2}-1}{\left(\mathrm{Re}\,\varepsilon_{\mathrm{ij}}+\mathrm{iIm}\varepsilon_{\mathrm{ij}}\right)^{2}+1}\right] \tag{B.7}$$

Optical absorption coefficient $A(\omega)$ is deduced as follows in terms of real and imaginary parts of dielectric function

$$\mathrm{A_{ij}}(\omega) = \frac{\sqrt{2}\omega}{\mathrm{c}} \left[\left(\mathrm{Re}\, \varepsilon_{\mathrm{ij}}^2 + \mathrm{Im}\, \varepsilon_{\mathrm{ij}}^2 \right)^{1/2} - \mathrm{Re}\, \varepsilon_{\mathrm{ij}} \right]^{1/2} \tag{B.8}$$

Absorption is related to transition between occupied and unoc-cupied bands in consequence of light and electron interaction. Optical conduc-tivity is also a quantity which depends on the interband and intraband transitions. Optical conductivity is calculated in terms of $\mathrm{Im}\, \varepsilon(\omega)$ as follows:

$$\delta_{\mathrm{ij}}(\omega) = \frac{\omega_{\mathrm{ij}}}{4\pi} \mathrm{Im}\, \varepsilon_{\mathrm{ij}}(\omega) \tag{B.9}$$